UNIVERSITY OF OKLAHOMA

GRADUATE COLLEGE

THE CASEINOLYTIC PROTEASE P SYSTEM IN *CLOSTRIDIUM DIFFICILE*

A DISSERTATION

SUBMITTED TO THE GRADUATE FACULTY

in partial fulfillment of the requirements for the

Degree of

DOCTOR OF PHILOSOPHY

By

NATHAN PAUL LAVEY
Norman, Oklahoma
2019

THE CASEINOLYTIC PROTEASE P SYSTEM IN *CLOSTRIDIUM DIFFICILE*

A DISSERTATION APPROVED FOR THE
DEPARTMENT OF CHEMISTRY AND BIOCHEMISTRY

BY

Dr. Adam S. Duerfeldt, Chair

Dr. Ann H. West

Dr. Charles V. Rice III

Dr. Christina R. Bourne

Dr. Laura E. Bartley

Acknowledgements

It is difficult to put into words how grateful I am to my mentor Adam Duerfeldt for his guidance, wisdom, and thoughtfulness. His unwavering support was paramount to completing this body of work, and I acknowledge the unique honor of being his first doctoral graduate student. I will always cherish the time I spent in the Duerfeldt laboratory, alongside a wonderful cast of supportive colleagues that I was honored to work amongst. Thank you all for your encouragement and support over the years, and I look forward to witnessing your success in the future.

I also want to thank my committee of whom were incredibly helpful and kind. Their thoughtful contributions to experiments and attention to detail always left me looking forward to presenting our research to them. I cannot emphasize how much this positively contributed to my graduate experience. Thank you all immensely.

Dr. Jimmy Ballard's laboratory generously provided space, materials, and expertise particularly from the incredibly kind Tyler Shadid, who taught me everything I know about culturing *Clostridium difficile*.

I am incredibly fortunate to have wonderful friends who helped me throughout this journey, and had the opportunity to work alongside some truly amazing people. I am very thankful to Dr. Ryan Finethy who initially persuaded me to pursue a doctoral degree. Also, to my colleague Matt Houck, who was routinely subjected to long-winded rants and was often too nice to tell me when to give it a rest. I also thank the undergraduate students that I was given the opportunity to mentor, particularly Jessie Knobbe who commiserated with

me during our struggles with X-ray crystallography. And of course, my first colleague Jesse Coker, who probably taught me more than I taught him.

I am also very thankful to my mother and father, who always supported and believed in me throughout my academic career. I am extremely fortunate have such wonderful parents.

Most importantly, I thank my partner Brittany Ray for putting up with me over the years and for being a truly amazing source of strength and confidence. I look forward to spending many more (profoundly less stressful) years with you.

Table of Contents

List of Tables

List of Figures

List of Abbreviations

Abz	Aminobenzoic Acid Fluorophore
ACP	Activators of Cylindrical Proteases
ADEP	Acyldepsipeptides
ADP	Adenosine Phosphate
ASE	Apparent Sporulation Efficiency
ATP	Adenosine Triphosphate
BCAA	Branched Chain Amino Acid
BHIS	Supplemented Brain Heart Infusion
BLAST	Basic local alignment search tool
*Bs*ClpP	*Bacillus subtilis* Caseinolytic Protease P
CCK-8	Cell Counting Kit-8
CDC	Centers for Disease Control
CDI	*Clostridium difficile* infection
CDTloc	CDT locus
CFU	Colony Forming Units
CHO	Chinese Hampster Ovary
CHY	Chymotrypsin
ClpP	Caseinolytic Protease P
CRISPR	Clustered Regularly Interspaced Short Palindromic Repeats
CROP	Combined Repetitive Peptides
CSPG4	Chondroitin Sulfate Proteoglycan 4
DFAP	Abz-DFAPKMALVPY^{NO2}
DLS	Dynamic Light Scattering
DMSO	Dimethylsulfoxide
DNA	Deoxyribonucleic Acid
DTT	Dithiothreitol
EC$_{50}$	Half-Maximal Effective Concentration
*Ec*ClpP	*Escherichia Coli* Caseinolytic Protease P
EMM	Eagles Minimal Essential Media
EMS	Epon/Araldite
FASTA	Fast alignment sequence format
FBS	Fetal Bovine Serum
FDA	US Food and Drug Administration
FITC	Fluorescein isothiocyanate
FMT	Fecal Microbiota Therapy
FPLC	Fast Protein Liquid Chromatography
FZD	Wnt receptor Frizzled
GDP	Guanosine Diphosphate
GFP	Green Fluorescent Protein
gRNA	Guide Ribonucleic Acid
GTP	Guanosine Triphosphate
HK	Histidine Kinase

HR-ESIMS	High-Resolution Electrospray Ionisation Mass Spectrometry
HRP	Horseradish Peroxidase
INPART	Institute for Natural Products Applications and Research Technologies
IPTG	Isopropyl β-D-1-thiogalactopyranoside
K_d	Equilibrium Constant
K_m	One-half V_{max}
L.O.D	Limit of Detection
LB	Luria Bertani media
LSR	Lipoprotein Receptor
MIC	Minimum Inhibitory Concentration
MW	Molecular Weight
NMR	Nuclear Magnetic Resonance
OD	Optical Density
OMRF	Oklahoma Medical Research Foundation
PaLoc	Pathogenicity Locus
PBS	Phosphate Buffered Saline
PCR	Polymerase Chain Reaction
PMB	Polymyxin-nonapeptide B
PMC	Pseudomembranous Colitis
PTS	Phosphotransferase
qRT-PCR	Quantitative Real-Time Polymerase Chain Reaction
RFU	Relative Fluorescence Units
RNA	Ribonucleic Acid
RNAP	Ribonucleic Acid Polymerase
SAR	Structure Activity Relationships
SDS-PAGE	Sodium dodecyl sulfate Polyacrylamide Gel Electrophoresis
SEC	Size Exclusion Chromatography
SLY-AMC	Leu-Tyr-aminomethylcoumarin
SMC	Sporulation Media Culture
Spo	Sporulation Regulatory Proteins
TBST	Tris Buffered Saline with Tween
TEM	Transmission Electron Microscopy
TSA	Thermal Shift Assay
UV	Ultraviolet
WT	Wildtype

Abstract

Clostridium difficile is a Gram-positive, spore-forming, toxin producing pathogen that has rapidly gained resistance to several broad-spectrum antibiotics. *C. difficile* infection (CDI) is a leading cause of hospital-acquired illness and presents a unique challenge to therapeutic development, as it is both caused by and clinically managed with antibiotics that indiscriminately kill bacteria present in gut microbiota. As such, identifying new drug targets that affect novel pathways is urgently required in order to combat the rise of CDI. To address this, we focus on elucidating the caseinolytic protease P (ClpP) system in *C. difficile*, which has emerged as a promising new target for antibacterial development. Herein, we describe the biochemical characterization and phenotypic response to loss of ClpP1 and ClpP2 *in vitro* to establish: 1) proteolytic activity and susceptibility to chemo-activation differ between ClpP1 and ClpP2 and that these two isoforms are capable of functioning in an uncoupled fashion. 2) ClpP1 and ClpP2 together are required for sporulation and thus are viable drug targets. We conclude this work with our initial discovery of a novel ClpP activator, Sclerotiamde, and our work towards the optimization of another class of ClpP activators. The work herein describes the uniqueness of the ClpP system in *C. difficile*, opens new avenues of inquiry, and highlights added impact of additional detailed structural, genetic, and biological characterization of this system.

Chapter 1

Introduction

1.1 *Clostridium difficile* Infection

Clostridium difficile is a Gram-positive, anaerobic, toxin-producing, spore-forming bacteria that causes infection in the lower intestinal tract, capable of producing life-threatening diarrhea and pseudomembranous colitis.[1–5] *C. difficile* infections (CDI) are the predominant cause of nosocomial diarrhea and typically arise due to broad-spectrum antibiotic use that eradicate protective intestinal microflora.[6–8] The Centers of Disease Control (CDC) lists *C. difficile* as one the top three threats to human health. This pathogen caused >29,000 mortalities and produced an estimated $5B in additional healthcare expenditures in 2011.[3,9] Relapse has increased five to ten-fold over the last decade, emphasizing the increased transmission and subsequent recurrence of CDI.[10–12] Reports of antibiotic resistant *C. difficile* hospital outbreaks became more common in the early 2000's, as mortality rates rose sharply.[13,14] Poor antibiotic stewardship is largely cited as the driving force behind *C. difficile* becoming such a deadly pathogen. Continued evolution has now led to hypervirulent strains of *C. difficile* that have begun to outcompete the previously more common less deadly endemic strains.[15–17]

Collectively referred to as the "BI/NAP1/027" group, these hypervirulent strains produce significantly more toxin than former less virulent strains.[14,15,18–23] Gradually, hypervirulent strains have largely replaced endemic strains, especially in communal settings, suggesting that the increase in virulence is advantageous to the pathogen.[24] Some hypervirulent strains also demonstrate increased sporulation rates (hypersporulating),

which dramatically increases the number of spores shed in fecal matter and results in more efficient transmission of the infection.[15,17,18,23,25] Spores are the metabolically dormant vessel some Gram-positive organisms produce in response to stress. These spores are able to withstand harsh environments for a prolonged time period (some for millions of years)[26] until favorable growth conditions trigger spore germination and outgrowth.[27] Harsh sterilization approaches (e.g., peroxides, radiation, heat, and chemical fixation) often times fail to eradicate spores from surfaces.[28–32] In nosocomial settings, spores have been reported to germinate after a >6-month desiccation period,[33] and in some cases become airborne.[34] These factors sometimes coalesce and recalcitrant spores can broadly inhabit an entire hospital wing, forcing closure.[35] Taken together, hypervirulent strains rapidly shift between heavy toxin and spore producing phenotypes to cause greater damage to the host and ensure future propagation. These features propagate CDI by increasing gastrointestinal destruction and inflammation in the host, which induces severe diarrhea, and thus provides the vehicle for transmission.
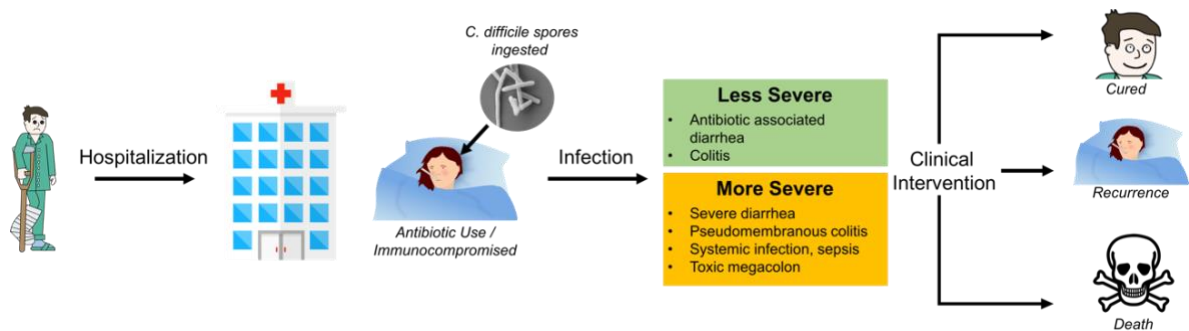
Figure 1.1 The CDI Cycle
The process of *C. difficile* infection from hospitalization to clinical outcome. Clinical interventions include but are not limited to antibiotic treatment, rehydration and/or fecal transplants. Adapted from Hunt and Ballard.[20]

The disease cycle of CDI initiates when spores are ingested via contact with a contaminated source, often facilitated by the close quartered nature of healthcare and community settings (**Figure 1.1**).[36,37] Once ingested, spores pass into the stomach where the acidic environment dissolves the mother cell (the larger body that matures the forespore) and releases the enclosed spore. Upon activation of germination sensors, outgrowth occurs in the lower gastrointestinal tract where the environment is anoxygenic (**Figure 1.2**).[38,39] In an asymptomatic infection, germination is largely inhibited by the low concentration of nutrients, and secreted metabolites from commensal bacteria.[40,41] Lack of a host-defense response may also inhibit germination, as evidence suggests *C. difficile* senses the human antimicrobial peptide LL-37 via the transcriptional regulator ClnR to globally regulate toxin production and sporulation.[25,42] In this manner, asymptomatic carriers shed spores in stool over 1-3 weeks.[43] In this transient model of infection *C. difficile* is not considered pathogenic, because host colonic flora has not been disrupted by antibiotic intervention.[44]
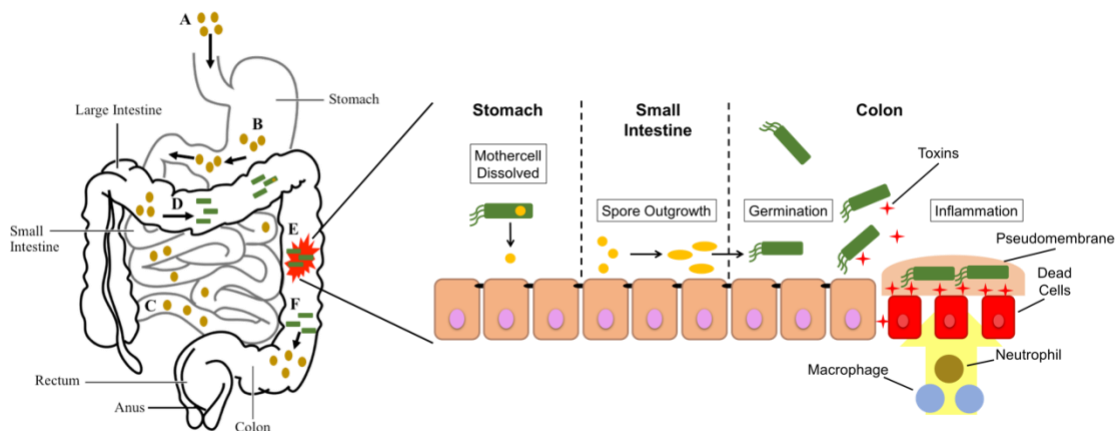
Figure 1.2 Stages of CDI Disease Progression
Shown on the left are the stages of CDI disease progression beginning with (A) the ingestion of *C. difficile* spores. Spores then move from the stomach to the small intestine (B) and migrate through the small intestine (C) before germinating in the large intestine

(D). Germinating *C. difficile* spores release toxins in the colon (E) during outgrowth, before new spores are made (F), which are shed in fecal matter allowing transmission and/or re-infection of the host. The image on the right shows the individual stages leading to, and during the disease state of CDI. Image was adapted and modified from Breitrück *et al*.[45]

In a symptomatic infection, the disease state is proportional to the amount of toxin produced and secreted, which will be more severe with a hypervirulent CDI.[14,46] Toxin production and sporulation are heavily influenced by nutrient availability and carbon catabolite repression.[47–50] Primarily, oligopeptide transferases (Opp/App) and the phosphotransferase system (PTS) uptake nutrients that passively inhibit toxin production and/or sporulation, by influencing CcpA and CodY.[48,51,52] Both CcpA and CodY are known as nutrient sensors and act as global regulatory factors in *C. difficile*.[48,53–55] In the presence of guanosine triphosphate (GTP) and branched-chain amino acids (BCAA) CodY binds DNA to block expression, suppressing sporulation initiation factors and toxin production.[54,56,57] Additionally, in the presence of glucose, CcpA suppresses toxin production, but the mechanism of toxin downregulation in this case is unclear, as *ccpA* mutants also attenuate toxin production.[52] Unlike CodY, which inhibits transcription through binding DNA, CcpA is suggested to bind Spo0A and prevent phosphorylation/activation to reduce sporulation and suppress toxin production.[58] These two global regulators often converge to strictly regulate these two critical processes.

The destruction of the intestinal tissue begins with the glucosylation of Rho proteins by toxins TcdA and TcdB.[59–62] Glucosylation of host Rho proteins stimulates the immune response and triggers inflammation.[63,64] Severe diarrhea occurs as a result of tissue damage, due to water infiltration of the extracellular space. As tissue turns necrotic, macrophages, neutrophils, and macrophils diffuse to the infection site to attack *C. difficile,* resulting in

pseudomembranous colitis (PMC, **Figure 1.2**).[65] Characteristic yellow plaques form on the surface of the inflamed tissue, where toxins have begun to erode the intestinal mucosa. If clinical intervention is delayed or PMC is left untreated, the illness can progress to toxic megacolon.[66] Antibiotic treatment in this case warrants discretion, as the bacterial load is high and some hypervirulent strains increase toxin production in the presence of antibiotics.[2,67] In severe cases, the necrotic section of intestine is removed via colectomy because the damage is too extensive for recovery.[68] *C. difficile* produces toxins for two reasons: 1) limit competition for nutrients by destroying surrounding host-cells, and 2) sufficiently induce diarrhea to shed spores and propagate infection in new hosts.

Both toxin genes, *tcdA* and *tcdB,* are located within the PaLoc, which also contains *tcdR*, *tcdE*, and *tcdC*.[69,70] As *C. difficile* germinates and approaches stationary growth, toxins TcdA and TcdB are produced (**Figure 1.3**). TcdA (308kDa) and TcdB (270kDa) are large clostridial toxins that are responsible for producing the clinical phenotype of CDI. *tcdR* is an RNA sigma factor that promotes PaLoc expression, while *tcdE* is a bacteriophage holin required for toxin secretion.[71,72] *tcdC* is a PaLoc repressor that negatively influences PaLoc expression. Each toxin has four domains with specific functions, from the N-terminus to the C-terminus. The domains are: activity (A), cutting (C), delivery (D), and binding (B).[47] Domain A on the N-terminus is the glucosyltransferase, the enzymatic portion of the toxin that glycosylates Rho proteins. The modification of Rho proteins causes the pathogenic effects of *C. difficile*, and the severity of Rho glycosylation is directly proportional to the intensity of the disease state.[73] Domain B is comprised of a combined repetitive peptides (CROP) motif that is responsible for recognizing and binding cell-surface receptors.[47] The cutting domain C, is an autoproteolytic domain that is

5

activated when exposed to the cytosol, to cleave the toxin and release the N-terminal glucosyltransferase domain A. The toxins share approximately 50% sequence identity, with significant differences in the binding domain.

TcdA binds glycoprotein gp96 in HT29 cells *in vitro*, and several non-human glycan sequences.[74,75] Evidence suggests gp96 is largely a cofactor that enhances binding, as gp96 expression is not required for TcdA internalization or virulence.[76] The required extracellular receptor(s) that induce TcdA internalization remain unknown. Upon receptor binding, internalization via endocytosis proceeds in a syndapin-II and dynamin mediated fashion.[77] TcdB has been shown to bind chondroitin sulfate proteoglycan 4 (CSPG4) and the Wnt receptor Frizzled (FZD), both present on the cell surface.[78,79] However, TcdB is internalized via clathrin mediated endocytosis, which differs from TcdA.[80]
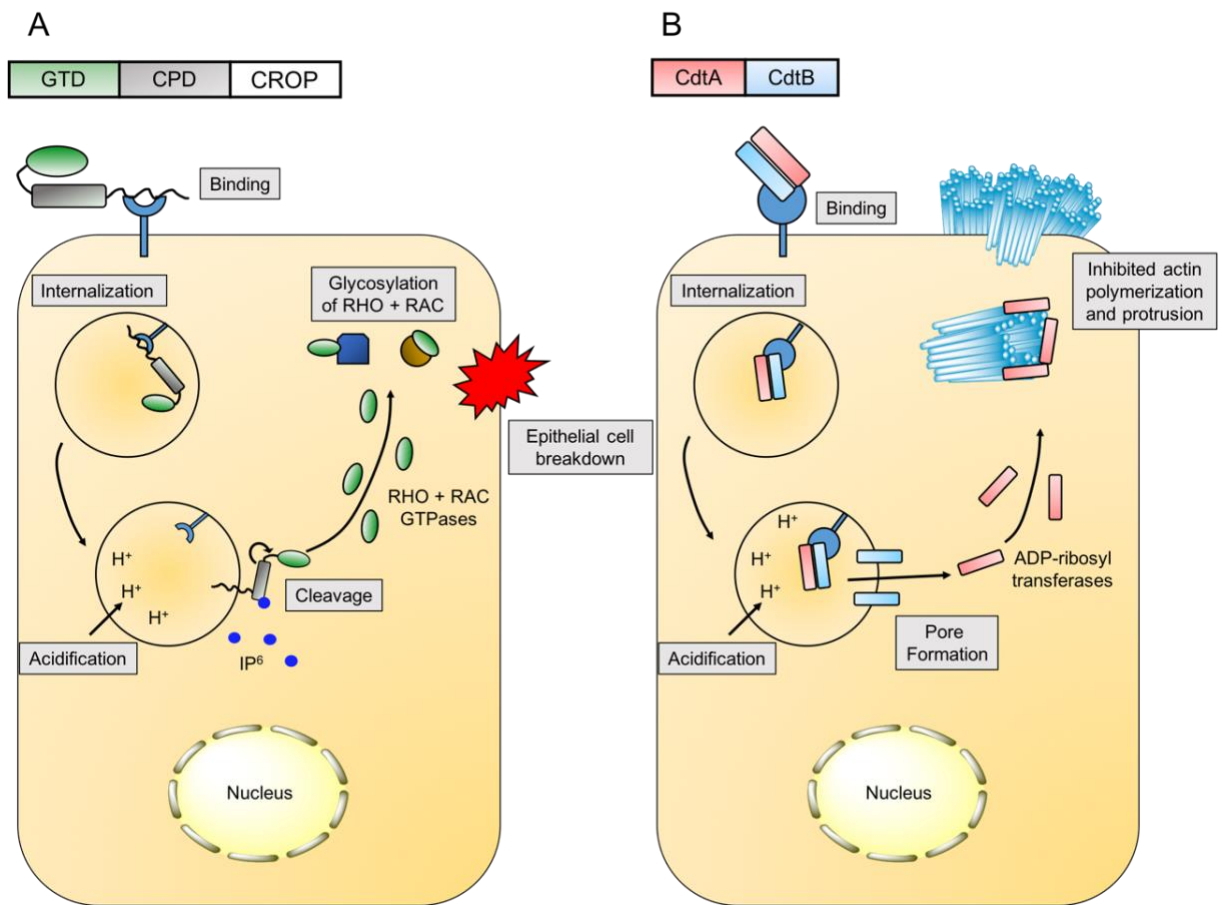
Figure 1.3 Toxin mechanism of action against epithelial cells.
A) TcdA and TcdB: once internalized, each toxin undergoes the same uptake and release process after endosome engulfment. The toxin-receptor complex is enveloped and pinched off at the cell surface, forming the endosome. As the pH inside the endosome becomes acidified the toxin changes conformation and embeds into the endosomal wall using domain B. Once embedded, A and C domains are exposed to the cytosol and inositol hexakisphosphate (IP$_6$) activates CPD (domain C) to autoproteolytically cleave, releasing GTD (domain A). The glucosyltransferase is then free to glycosylate Rho proteins. B) CdtA and CdtB: once expressed, forming a dimer which binds lipoprotein receptor (LSR). CdtAB is then internalized, and as the endosome is acidified CdtB will and embed into the endosomal wall forming a pore that CdtA will diffuse through. CdtA, an ADP-ribosyl transferase, will then bind to uncapped actin to prevent polymerization and cause actin filaments to protrude outside the cellular surface. This image was modified and adapted from Pamer *et al.*[64]

Approximately 5-30% of hypervirulent *C. difficile* strains produce a third toxin known as "CDT" or "binary toxin".[75] CDT is a ADP-ribosyl transferase toxin that primarily

7

affects actin in eukaryotic cells, but the specific function and role of CDT in pathogenesis is poorly understood. The CDT locus (CDTloc) is chromosomally distant from the PaLoc, encoding *cdtA*, *cdtB*, and *cdtR*.[81,82] *cdtA* and *cdtB* are arranged in an operon (*cdtAB*) that is constitutively expressed, and combine to form the heterodimeric toxin CDT (**Figure 1.3**).[82,83] Expression is positively regulated by CdtR, which has also been shown to upregulate PaLoc expression.[56] CdtA is an ADP-ribosyltransferase that ribosylates uncapped actin filaments in eukaryotic cells, while CdtB contains the binding domain and aids CdtA entry.[83–85] The cell surface receptor for CDT is lipolysis-stimulated lipoprotein receptor (LSR), that is primarily involved with low-density lipoprotein clearance/apolipoprotein remodeling.[86–88] LSR also functions to maintain cellular junctions that contribute to cytoskeletal fidelity.[75,89] CDT binds LSR and accumulates at the cell surface on lipid rafts, and is internalized. On the interior of the acidified endosome, CdtB forms a tetradecameric barrel that inserts into the vesicle wall forming a pore.[87,90] CDT then translocates to the cytosol where cochaperones aid refolding, allowing CdtA to ADP-ribosylate immature actin.[87,91,92] The ribosylated actin is unable to polymerize and forms bundles that protrude from the cell surface.[85,93] A recent study suggests that protruding actin filaments from the host cells aid *C. difficile* adherence during infection, offering a potential role for CDT in pathogenesis.[94] CDI caused by a hypervirulent strain that express CDT is more likely to have a fatal outcome, further emphasizing the role of CDT in CDI severity and infectivity.[83]

1.2 Clinical Management of CDI, and Treatments on the Horizon

The clinical management of CDI is complex. Poor antibiotic stewardship is largely responsible for creating multiple-antibiotic resistant *C. difficile* strains and the inability to

effectively treat this pathogen.[95] Historically, CDI has been relegated to nosocomial settings and primarily occurs in elderly populations, and those with reduced immune capacity.[96] Over time, CDI has increased in younger populations, and has infiltrated communal settings.[97–99] To complicate the situation even further, the lack of consensus for a specific treatment protocol has diversified antibiotic resistance in *C. difficile* strains.[100–102] Generally, treatment proceeds over intervals of singular or combinatorial doses of vancomycin, fidaxomycin, and metronidazole, until diagnostic testing no longer detects TcdA/TcdB.[103] Vancomycin and metronidazole share failure rates ranging from 14-27%, while fidaxomicin fails during 12% of treatments.[104] On average, 22.6% and 11.7% of patients will relapse when treated with vancomycin and metronidazole, respectively. In comparison, patients treated with Fidaxomicin exhibit less than a 50% likelihood to relapse.[104] Fecal microbiota transplant (FMT) has showed promising results with a failure rate of approximately 8%, but routine clinical application remains to be established.[105]

Elegant genomic studies have elucidated specific bacterial taxa that are underrepresented in CDI patients, providing further evidence that microflora dysbiosis enhances susceptibility to *C. difficile*.[106] Correcting an imbalanced microflora may impart protective effects. FMT has gained attention in recent years as a method capable of artificially repopulating gut microflora of an infected patient with that from a healthy fecal donor. This replacement restores the balance amongst gut microbiota following antibiotic therapy.[107,108] FMT demonstrates promising initial results in both treating CDI, and reducing patient relapse, boasting a success rate of over 90% in clinical trials.[109] Similarly, diets incorporating prebiotic and probiotic supplements have increased in popularity, as connections between our health and specific commensal taxa are discovered.

As a spore-former, *C. difficile* possesses intrinsic resistance to antibiotics that target an active metabolic pathway. Spores allow *C. difficile* to be transmitted and tolerate oxygenic environments, therefore sporulation is a key step in the infection cycle. Disabling or minimizing sporulation would dramatically reduce the rate of transmission by terminating the infection cycle. So far, no drugs have been approved by the U.S. Food and Drug Administration (FDA) that target *C. difficile* sporulation.[110,111]

Metronidazole, vancomycin, and fidaxomicin are the most commonly used antibiotics to treat CDI (**Figure 1.5**).[102,112] Metronidazole is the preferred first-line drug against perceived CDI when a diagnoses has yet to be confirmed[113] Metronidazole is a small molecule pro-drug that passively diffuses through the cell wall of *C. difficile*, and into the cytoplasm.[114,115] Ferredoxin reduces metronidazole to yield the active form, which creates a nitroso-free-radical that reacts with DNA.[104] This damages DNA and overwhelms *C. difficile*, inducing a DNA damage stress response, which stalls genomic replication and ultimately leads to cell death.[116,117] Resistance to metronidazole has steadily increased in the last 5-10 years, but this drug is still used commonly, as it is selective towards Gram-positive anaerobes.[118] A recent meta-analysis suggests that metronidazole is no longer useful in treating CDI for any case, and fidaxomicin should replace it as a first-line treatment.[119] Though this suggestion is merely an opinion, it suggests that a classically employed drug to treat CDI may soon be out of practice.

Vancomycin is a broad-spectrum hydrophobic macrocyclic peptide that inhibits cell wall synthesis in Gram-positive bacteria (**Figure 1.5**).[120] Specifically, vancomycin binds a precursor component of the cell wall, the dipeptide D-Ala-D-Ala, preventing peptidoglycan cross-linkage.[121] This perforates the cell wall, releasing intracellular

contents into the extracellular space, causing cell death. *C. difficile* is highly susceptible to vancomycin (MIC = 1-2 µg/mL) with only a few resistant mutants known to exist.[104,122] Vancomycin resistant phenotypes that are observed, typically modify the terminal dipeptide residues that vancomycin binds which blocks the mechanism of action.[121] Vancomycin reduces sporulation more than metronidazole and maintains a long-term asymptomatic response.[119]
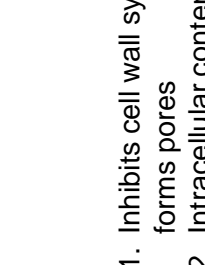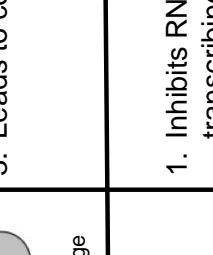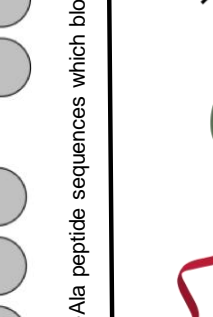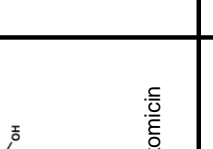
Compound	Mechanism of Action	Consequence
A Vancomycin	Binds d-Ala-Ala peptide sequences which blocks cross-linkage	1. Inhibits cell wall synthesis, forms pores 2. Intracellular content loss 3. Leads to cell death
B Fidaxomicin	Binds RNAP during transcription	1. Inhibits RNA Polymerase from transcribing genes 2. Anchors transcription machinery to the promoter region 3. Blocks future expression of the gene
C Metronidazole	Reduced by ferredoxin to form free radical	1. Free radical damage mostly localized to chromosomal DNA. 2. Leads to cell death

12

Figure 1.4 – A list of common antibiotics prescribed to treat CDI.
A) Vancomycin is a cell permeabilizer of Gram-positive bacteria, which kills bacteria by inhibiting cell wall synthesis, causing pores to form across the cell surface. B) Fidaxomicin is a narrow-spectrum antibiotic that kills Gram-positive anaerobic bacteria by inhibiting RNAP, which stalls transcription at the promoter region of a gene being expressed. C) Metronidazole has broad-spectrum activity across Gram-positive bacteria, which works by damaging chromosomal DNA to overwhelm the bacteria and halt replication.

Fidaxomicin is a macrolide antibacterial that exhibits narrow-spectrum selectivity against *C. difficile* and thus exhibits minimal threat to commensal flora (**Figure 1.4**).[123–127] Furthermore, fidaxomicin's unique mechanism of action has prolonged its clinical use, as only one resistant mutant has been reported.[122] Fidaxomicin kills *C. difficile* by inhibiting RNA polymerase (RNAP) during transcription initiation, locking the RNAP holocomplex to the DNA prior to strand separation.[128] This sequesters the transcription complex to the promoter region of the gene, blocking future expression and prohibiting RNAP from expressing other genes. The cost-effectiveness of fidaxomicin is significantly higher than vancomycin or metronidazole.[119] The primary drawback of treating CDI with fidaxomicin is that almost a third of patients (29%) exhibit no long-term curative effect. This means that a third of patients will have a significantly higher risk of recurrent CDI, experience an extended disease state, and provide the necessary vehicle for the disease to continue to propogate.[124]

Alternative therapies that employ non-small molecule-based strategies are under development or have entered clinical trials and represent a significant departure from the status quo. For example, monoclonal-antibodies that guide the host-immune response to clear CDI has demonstrated proof-of-concept.[129] Vaccination with inactivated toxin to elicit a protective immune response and abrogate virulence by inhibiting toxin activity has also been demonstrated *in vitro*.[130–133] Phage therapy is being revisited as a potential

alternative treatment, despite numerous clinical hurdles.[134] Most alternative therapies attempt to mitigate virulence rather than destroy *C. difficile*, and shape an immune response. This removes the primary drawback of using antibacterials that contribute to gut dysbiosis and CDI recurrence. Though exciting, alternative therapies face an uphill battle, as the new approaches will be expected to not only exhibit efficacy but also be void of problems facing established drugs currently utilized in the clinic.

The development of therapeutics to combat CDI represents an urgent and important endeavor. With no clear "magic bullet" in-hand, the search for novel targets and compounds that act upon these targets will only become more urgent in an increasingly dire situation.

1.3 A Case for Targeting Caseinolytic Protease P

Caseinolytic protease P (ClpP) is a barrel-shaped tetradecameric complex composed of two stacked heptameric rings which form a hollow barrel-shaped cylinder.[135] The core is lined with fourteen Serine-Histidine-Aspartic acid catalytic triads, shielded by N-terminal loops that cover the axial pore (**Figure 1.5A**).[136] Under normal physiologic conditions, ClpP activity is coupled to AAA+ cochaperones (e.g., ClpX and ClpA) that selectively bind degron-tagged proteins for degradation.[136–138] Degrons are phosphorylated arginine residues or ssrA-tags attached to proteins that act as a degradation signal that cochaperones recognize as a substrate.[138,139] After substrate binding, cochaperones bind to ClpP via IGL/F loop motifs that extend from the C-terminal end of each monomer.[140,141] These interact with N-terminal clefts located between monomers.[142] The protein is translocated in an ATP-dependent process into the proteolytic core of ClpP to be degraded

(**Figure 1.5B**). The ClpP protomer can be divided into three domains: 1) N-terminal head, 2) C-terminal end, and 3) handle region (**Figure 1.5A**).[143] ClpP adapts two conformations: 1) the "extended" active form, which interacts with cochaperones and is capable of degrading small polypeptides 5-7aa in length, and 2) an autoproteolytically inactive compressed form.[144,145]
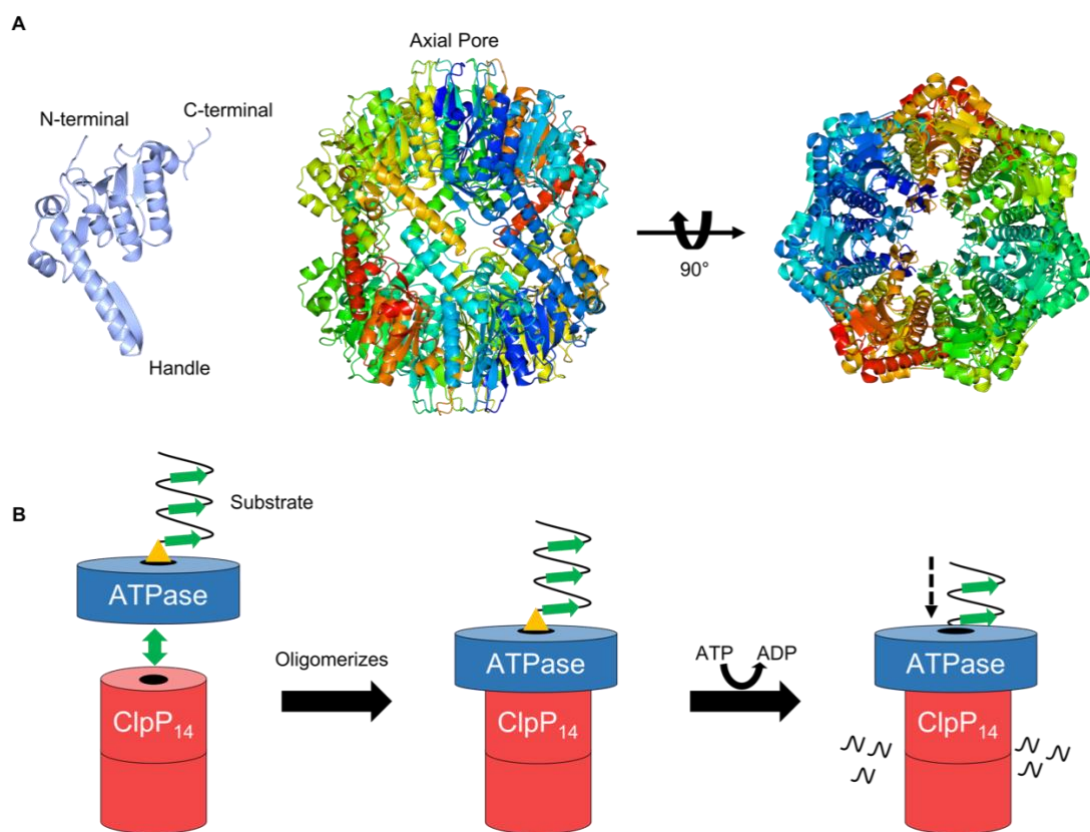
Figure 1.5 – Structural overview of ClpP and cochaperone mediated proteolysis.
A) The extended form of ClpP1 from *C. difficile* (PDB: 6MX2) is shown at the top, with the protomer to the left and the tetradecameric assembly pictured right (side-view = middle, top down view = far right). B) ClpP cochaperones, or unfoldases, recognize the degron (yellow) and bind with or without the assistance of an adaptor protein. This promotes oligomerization of the unfoldase with ClpP via IGL/F motifs located around the axial pore, where each monomer makes contact with another. ATP is then consumed to unfold and translocate the substrate into the proteolytic chamber of ClpP, where the protein will be degraded. Figure 1.5B is reprinted (adapted) with permission from Houry et al.[146] Copyright 2019 American Chemical Society.

As a key regulator of virulence and drug resistance in infectious bacteria, caseinolytic protease P (ClpP) has emerged as a new target for antibacterial development.[146] Aberrant ClpP activity (inhibition or activation) induced by small molecules is detrimental to microbial fitness, reduces virulent phenotypes, and disrupts biofilm formation.[147–149] Specifically, activation of ClpP has been validated and proven safe *in vivo* as an antibacterial strategy against systemic lethal infections of *Enterococcus faecium, E. faecalis* (vancomycin-sensitive and -resistant), *Staphylococcus aureus* (methicillin-resistant and -sensitive), and *Streptococcus pneumonia*. In each case, activation of ClpP with a small molecule acyldepsipeptide (ADEP) outperforms clinically utilized antibiotics, including linezolid and ampicillin.

There are several advantages to targeting ClpP: 1) Both inhibition and activation are possible, with each tactic affecting different aspects of bacterial pathogenicity.[149,150] This provides an opportunity to determine the therapeutic potential of two orthogonal strategies on a single target, a rare phenomenon in antibacterial drug discovery. 2) Due to the diverse regulatory roles of ClpP (e.g., growth, motility, virulence, stress response, sporulation) disruption of its natural activity would have pleotropic effects that may not be easily resolved by compensatory mutations.[146] 3) ClpP activation itself demonstrates efficacy against both actively growing and dormant persister cells,[148] a necessity for improved antibacterial treatments. 4) In organisms investigated thus far, ClpP is essential for pathogenicity, but not survival (with the exception of *Mycobacterium tuberculosis*).[146] Therefore, inhibiting ClpP may provide a means to negatively affect the virulence of pathogens, but preserve the viability of beneficial microbes. 5) Targeting non-essential

virulence regulators like ClpP is likely to impair the organism's infectivity without imparting typical selective pressures that drive resistance.

Despite the advancements in ClpP research, major questions regarding the clinical potential of targeting this protease persist. Although the general involvement of ClpP in bacterial virulence is well-established, the distinct attributes regulated by ClpP are organism dependent. Additionally, while resistance to ADEPs has been generated in laboratory settings (*Escherichia coli*, *Bacillus subtilis*, *E. faecalis*, *S. pneumoniae*, *S. aureus*), all studies have been conducted on single *clpP* containing organisms. While ClpPs from single isoform expressing bacteria have been studied in detail, the function and regulation of systems with more than one *clpP* gene are still poorly understood. Interrogating the behavior of ClpP systems in multi-isoform containing organisms is expected to reveal additional insight into mechanisms of resistance development that should be considered, both during the validation of a target and in its clinical exploitation. In these contexts, we are interested in elucidating the behavior, biological relevance, and therapeutic potential of the ClpP system in *C. difficile*.

1.4 References

1.   Leffler, D. A. & Lamont, J. T. *Clostridium difficile* infection. *N. Engl. J. Med.* **372,** 1539–1548 (2015).

2.   Kelly, C. P. & LaMont, J. T. *Clostridium difficile* — More Difficult Than Ever. *N. Engl. J. Med.* (2008).

3.   Lessa, F. C. *et al.* Burden of *Clostridium difficile* infection in the United States. *N. Engl. J. Med.* **372,** 825–834 (2015).

4.   McDonald, L. C. *Clostridium difficile*: Responding to a New Threat From an Old Enemy. *Infect. Control Hosp. Epidemiol.* **26,** 672–675 (2005).

5.   Kelly, C. P., Pothoulakis, C. & LaMont, J. T. *Clostridium difficile* colitis. *N. Engl. J. Med.* **330,** 257–262 (1994).

6.   Talpaert, M. J., Gopal Rao, G., Cooper, B. S. & Wade, P. Impact of guidelines and enhanced antibiotic stewardship on reducing broad-spectrum antibiotic usage and its effect on incidence of *Clostridium difficile* infection. *J. Antimicrob. Chemother.* **66,** 2168–2174 (2011).

7.   Bartlett, J. G. Antibiotic-associated diarrhea. *New England journal of medicine* (2002).

8.   Nair, S., Yadav, D. & Corpuz, M. *Clostridium difficile* colitis: factors influencing treatment failure and relapse—a prospective evaluation. *The American journal of …* (1998).

9.   Zerey, M. *et al.* The burden of *Clostridium difficile* in surgical patients in the United States. *Surg Infect (Larchmt)* **8,** 557–566 (2007).

10.   Maroo, S. & Lamont, J. T. Recurrent *Clostridium difficile*. *Gastroenterology* **130,** 1311–1316 (2006).

11.   Johnson, S. Meeting the challenge of recurrent *Clostridium difficile* infection. *J Hosp Med* **7 Suppl 3,** S11-3 (2012).

12.   Johnson, S. Recurrent *Clostridium difficile* infection: causality and therapeutic approaches. *Int. J. Antimicrob. Agents* **33 Suppl 1,** S33-6 (2009).

13.   Kuijper, E. J. *et al.* Emergence of *Clostridium difficile*-associated disease in North America and Europe. *Clin. Microbiol. Infect.* **12 Suppl 6,** 2–18 (2006).

14. Warny, M. *et al.* Toxin production by an emerging strain of *Clostridium difficile* associated with outbreaks of severe disease in North America and Europe. *Lancet* **366,** 1079–1084 (2005).

15. Merrigan, M. *et al.* Human hypervirulent *Clostridium difficile* strains exhibit increased sporulation as well as robust toxin production. *J. Bacteriol.* **192,** 4904–4911 (2010).

16. Valiente, E., Dawson, L. F., Cairns, M. D., Stabler, R. A. & Wren, B. W. Emergence of new PCR ribotypes from the hypervirulent *Clostridium difficile* 027 lineage. *J. Med. Microbiol.* **61,** 49–56 (2012).

17. Dawson, L. F., Valiente, E., Donahue, E. H., Birchenough, G. & Wren, B. W. Hypervirulent *Clostridium difficile* PCR-ribotypes exhibit resistance to widely used disinfectants. *PLoS One* **6,** e25754 (2011).

18. Akerlund, T. *et al.* Increased sporulation rate of epidemic *Clostridium difficile* Type 027/NAP1. *J. Clin. Microbiol.* **46,** 1530–1533 (2008).

19. Couturier, J., Davies, K., Gateau, C. & Barbut, F. Ribotypes and new virulent strains across europe. *Adv. Exp. Med. Biol.* **1050,** 45–58 (2018).

20. Hunt, J. J. & Ballard, J. D. Variations in virulence and molecular biology among emerging strains of *Clostridium difficile*. *Microbiol. Mol. Biol. Rev.* **77,** 567–581 (2013).

21. Valiente, E., Dawson, L. F., Cairns, M. D., Stabler, R. A. & Wren, B. W. Emergence of new PCR ribotypes from the hypervirulent *Clostridium difficile* 027 lineage. *J. Med. Microbiol.* **61,** 49–56 (2012).

22. O'Connor, J. R., Johnson, S. & Gerding, D. N. *Clostridium difficile* infection caused

by the epidemic BI/NAP1/027 strain. *Gastroenterology* **136,** 1913–1924 (2009).

23. Vohra, P. & Poxton, I. R. Comparison of toxin and spore production in clinically relevant strains of *Clostridium difficile*. *Microbiology (Reading, Engl.)* **157,** 1343–1353 (2011).

24. Knetsch, C. W. *et al.* Genetic markers for *Clostridium difficile* lineages linked to hypervirulence. *Microbiology (Reading, Engl.)* **157,** 3113–3123 (2011).

25. Edwards, A. N., Nawrocki, K. L. & McBride, S. M. Conserved oligopeptide permeases modulate sporulation initiation in *Clostridium difficile*. *Infect. Immun.* **82,** 4276–4291 (2014).

26. Vreeland, R. H., Rosenzweig, W. D. & Powers, D. W. Isolation of a 250 million-year-old halotolerant bacterium from a primary salt crystal. *Nature* **407,** 897–900 (2000).

27. Gil, F., Lagos-Moraga, S., Calderón-Romero, P., Pizarro-Guajardo, M. & Paredes-Sabja, D. Updates on *Clostridium difficile* spore biology. *Anaerobe* **45,** 3–9 (2017).

28. Wilcox, M. H. & Fawley, W. N. Hospital disinfectants and spore formation by *Clostridium difficile*. *Lancet* **356,** 1324 (2000).

29. Weber, D. J., Rutala, W. A., Miller, M. B., Huslage, K. & Sickbert-Bennett, E. Role of hospital surfaces in the transmission of emerging health care-associated pathogens: norovirus, *Clostridium difficile*, and *Acinetobacter* species. *Am. J. Infect. Control* **38,** S25-33 (2010).

30. Fawley, W. N. *et al.* Efficacy of hospital cleaning agents and germicides against epidemic *Clostridium difficile* strains. *Infect. Control Hosp. Epidemiol.* **28,** 920–925 (2007).

31. Nerandzic, M. M., Cadnum, J. L., Pultz, M. J. & Donskey, C. J. Evaluation of an automated ultraviolet radiation device for decontamination of *Clostridium difficile* and other healthcare-associated pathogens in hospital rooms. *BMC Infect. Dis.* **10,** 197 (2010).

32. Barbut, F., Menuet, D., Verachten, M. & Girou, E. Comparison of the efficacy of a hydrogen peroxide dry-mist disinfection system and sodium hypochlorite solution for eradication of *Clostridium difficile* spores. *Infect. Control Hosp. Epidemiol.* **30,** 507–514 (2009).

33. Setlow, P. Spores of Bacillus subtilis: their resistance to and killing by radiation, heat and chemicals. *J. Appl. Microbiol.* **101,** 514–525 (2006).

34. Roberts, K. *et al.* Aerial dissemination of *Clostridium difficile* spores. *BMC Infect. Dis.* **8,** 7 (2008).

35. Burns, D. A., Heap, J. T. & Minton, N. P. *Clostridium difficile* spore germination: an update. *Res. Microbiol.* **161,** 730–734 (2010).

36. Johnson, S. *et al.* Nosocomial *Clostridium difficile* colonisation and disease. *Lancet* **336,** 97–100 (1990).

37. McFarland, L. V., Mulligan, M. E., Kwok, R. Y. & Stamm, W. E. Nosocomial acquisition of *Clostridium difficile* infection. *N. Engl. J. Med.* **320,** 204–210 (1989).

38. Wilson, K. H. Efficiency of various bile salt preparations for stimulation of *Clostridium difficile* spore germination. *J. Clin. Microbiol.* **18,** 1017–1019 (1983).

39. Sorg, J. A. & Sonenshein, A. L. Bile salts and glycine as cogerminants for *Clostridium difficile* spores. *J. Bacteriol.* **190,** 2505–2512 (2008).

40. Burns, D. A., Heap, J. T. & Minton, N. P. SleC is essential for germination of

Clostridium difficile spores in nutrient-rich medium supplemented with the bile salt taurocholate. *J. Bacteriol.* **192,** 657–664 (2010).

41. Paredes-Sabja, D., Shen, A. & Sorg, J. A. *Clostridium difficile* spore biology: sporulation, germination, and spore structural proteins. *Trends Microbiol.* **22,** 406–416 (2014).

42. Woods, E. C., Edwards, A. N., Childress, K. O., Jones, J. B. & McBride, S. M. The *C. difficile* clnRAB operon initiates adaptations to the host environment in response to LL-37. *PLoS Pathog.* **14,** e1007153 (2018).

43. Paredes-Sabja, D., Shen, A. & Sorg, J. A. *Clostridium difficile* spore biology: sporulation, germination, and spore structural proteins. *Trends Microbiol.* **22,** 406–416 (2014).

44. Freeman, J. & Wilcox, M. H. Antibiotics and *Clostridium difficile*. *Microbes Infect.* **1,** 377–384 (1999).

45. Schäffler, H. & Breitrück, A. *Clostridium difficile* - From Colonization to Infection. *Front. Microbiol.* **9,** 646 (2018).

46. Akerlund, T., Svenungsson, B., Lagergren, A. & Burman, L. G. Correlation of disease severity with fecal toxin levels in patients with *Clostridium difficile*-associated diarrhea and distribution of PCR ribotypes and toxin yields in vitro of corresponding isolates. *J. Clin. Microbiol.* **44,** 353–358 (2006).

47. Voth, D. E. & Ballard, J. D. *Clostridium difficile* toxins: mechanism of action and role in disease. *Clin. Microbiol. Rev.* **18,** 247–263 (2005).

48. Dupuy, B. & Sonenshein, A. L. Regulated transcription of *Clostridium difficile* toxin genes. *Mol. Microbiol.* **27,** 107–120 (1998).

49. Hundsberger, T. *et al.* Transcription analysis of the genes *tcdA-E* of the pathogenicity locus of *Clostridium difficile*. *Eur. J. Biochem.* **244,** 735–742 (1997).

50. Karlsson, S., Burman, L. G. & Akerlund, T. Induction of toxins in *Clostridium difficile* is associated with dramatic changes of its metabolism. *Microbiology (Reading, Engl.)* **154,** 3430–3436 (2008).

51. Kazamias, M. T. & Sperry, J. F. Enhanced fermentation of mannitol and release of cytotoxin by *Clostridium difficile* in alkaline culture media. *Appl. Environ. Microbiol.* **61,** 2425–2427 (1995).

52. Antunes, A., Martin-Verstraete, I. & Dupuy, B. CcpA-mediated repression of *Clostridium difficile* toxin gene expression. *Mol. Microbiol.* **79,** 882–899 (2011).

53. Bouillaut, L., Dubois, T., Sonenshein, A. L. & Dupuy, B. Integration of metabolism and virulence in *Clostridium difficile*. *Res. Microbiol.* **166,** 375–383 (2015).

54. Dineen, S. S., McBride, S. M. & Sonenshein, A. L. Integration of metabolism and virulence by *Clostridium difficile* CodY. *J. Bacteriol.* **192,** 5350–5362 (2010).

55. Karlsson, S., Burman, L. G. & Akerlund, T. Suppression of toxin production in *Clostridium difficile* VPI 10463 by amino acids. *Microbiology (Reading, Engl.)* **145 (Pt 7),** 1683–1693 (1999).

56. Lyon, S. A., Hutton, M. L., Rood, J. I., Cheung, J. K. & Lyras, D. CdtR Regulates TcdA and TcdB Production in *Clostridium difficile*. *PLoS Pathog.* **12,** e1005758 (2016).

57. Nawrocki, K. L., Edwards, A. N., Daou, N., Bouillaut, L. & McBride, S. M. CodY-Dependent Regulation of Sporulation in *Clostridium difficile*. *J. Bacteriol.* **198,** 2113–2130 (2016).

58. Antunes, A. *et al.* Global transcriptional control by glucose and carbon regulator CcpA in *Clostridium difficile*. *Nucleic Acids Res.* **40,** 10701–10718 (2012).

59. Jank, T., Giesemann, T. & Aktories, K. Rho-glucosylating *Clostridium difficile* toxins A and B: new insights into structure and function. *Glycobiology* **17,** 15R–22R (2007).

60. Sullivan, N. M., Pellett, S. & Wilkins, T. D. Purification and characterization of toxins A and B of *Clostridium difficile*. *Infect. Immun.* **35,** 1032–1040 (1982).

61. Lyerly, D. M., Lockwood, D. E., Richardson, S. H. & Wilkins, T. D. Biological activities of toxins A and B of *Clostridium difficile*. *Infect. Immun.* **35,** 1147–1150 (1982).

62. Kuehne, S. A. *et al.* The role of toxin A and toxin B in *Clostridium difficile* infection. *Nature* **467,** 711–713 (2010).

63. Shen, A. *Clostridium difficile* toxins: mediators of inflammation. *J Innate Immun* **4,** 149–158 (2012).

64. Abt, M. C., McKenney, P. T. & Pamer, E. G. *Clostridium difficile* colitis: pathogenesis and host defence. *Nat. Rev. Microbiol.* **14,** 609–620 (2016).

65. Farooq, P. D., Urrunaga, N. H., Tang, D. M. & von Rosenvinge, E. C. Pseudomembranous colitis. *Dis. Mon.* **61,** 181–206 (2015).

66. Dobson, G., Hickey, C. & Trinder, J. *Clostridium difficile* colitis causing toxic megacolon, severe sepsis and multiple organ dysfunction syndrome. *Intensive Care Med.* **29,** 1030 (2003).

67. Drummond, L. J., Smith, D. G. E. & Poxton, I. R. Effects of sub-MIC concentrations of antibiotics on growth of and toxin production by *Clostridium difficile*. *J. Med.*

Microbiol. **52,** 1033–1038 (2003).

68. Lamontagne, F. *et al.* Impact of emergency colectomy on survival of patients with fulminant *Clostridium difficile* colitis during an epidemic caused by a hypervirulent strain. *Ann. Surg.* **245,** 267–272 (2007).

69. Braun, V., Hundsberger, T., Leukel, P., Sauerborn, M. & von Eichel-Streiber, C. Definition of the single integration site of the pathogenicity locus in *Clostridium difficile*. *Gene* **181,** 29–38 (1996).

70. Kachrimanidou, M. & Malisiovas, N. *Clostridium difficile* infection: a comprehensive review. *Crit Rev Microbiol* **37,** 178–187 (2011).

71. Dupuy, B. *et al.* Regulation of toxin and bacteriocin gene expression in *Clostridium* by interchangeable RNA polymerase sigma factors. *Mol. Microbiol.* **60,** 1044–1057 (2006).

72. Govind, R. & Dupuy, B. Secretion of *Clostridium difficile* toxins A and B requires the holin-like protein TcdE. *PLoS Pathog.* **8,** e1002727 (2012).

73. Chen, S., Sun, C., Wang, H. & Wang, J. The Role of Rho GTPases in Toxicity of *Clostridium difficile* Toxins. *Toxins (Basel)* **7,** 5254–5267 (2015).

74. Gerhard, R. Receptors and Binding Structures for *Clostridium difficile* Toxins A and B. *Curr. Top. Microbiol. Immunol.* **406,** 79–96 (2017).

75. Aktories, K., Schwan, C. & Jank, T. *Clostridium difficile* Toxin Biology. *Annu. Rev. Microbiol.* **71,** 281–307 (2017).

76. Lambert, G. S. & Baldwin, M. R. Evidence for dual receptor-binding sites in *Clostridium difficile* toxin A. *FEBS Lett.* **590,** 4550–4563 (2016).

77. Chandrasekaran, R., Kenworthy, A. K. & Lacy, D. B. *Clostridium difficile* Toxin A

Undergoes Clathrin-Independent, PACSIN2-Dependent Endocytosis. *PLoS Pathog.* **12,** e1006070 (2016).

78. Tao, L. *et al.* Frizzled proteins are colonic epithelial receptors for *C. difficile* toxin B. *Nature* **538,** 350–355 (2016).

79. LaFrance, M. E. *et al.* Identification of an epithelial cell receptor responsible for *Clostridium difficile* TcdB-induced cytotoxicity. *Proc. Natl. Acad. Sci. USA* **112,** 7073–7078 (2015).

80. Papatheodorou, P., Zamboglou, C., Genisyuerek, S., Guttenberg, G. & Aktories, K. Clostridial glucosylating toxins enter cells via clathrin-mediated endocytosis. *PLoS One* **5,** e10673 (2010).

81. Carter, G. P. *et al.* Binary toxin production in *Clostridium difficile* is regulated by CdtR, a LytTR family response regulator. *J. Bacteriol.* **189,** 7290–7301 (2007).

82. Perelle, S., Gibert, M., Bourlioux, P., Corthier, G. & Popoff, M. R. Production of a complete binary toxin (actin-specific ADP-ribosyltransferase) by *Clostridium difficile* CD196. *Infect. Immun.* **65,** 1402–1407 (1997).

83. Gerding, D. N., Johnson, S., Rupnik, M. & Aktories, K. *Clostridium difficile* binary toxin CDT: mechanism, epidemiology, and potential clinical importance. *Gut Microbes* **5,** 15–27 (2014).

84. Gülke, I. *et al.* Characterization of the enzymatic component of the ADP-ribosyltransferase toxin CDTa from *Clostridium difficile*. *Infect. Immun.* **69,** 6004–6011 (2001).

85. Schwan, C. *et al. Clostridium difficile* toxin CDT induces formation of microtubule-based protrusions and increases adherence of bacteria. *PLoS Pathog.* **5,** e1000626

(2009).

86. Papatheodorou, P. *et al.* Lipolysis-stimulated lipoprotein receptor (LSR) is the host receptor for the binary toxin *Clostridium difficile* transferase (CDT). *Proc. Natl. Acad. Sci. USA* **108,** 16422–16427 (2011).

87. Hemmasi, S. *et al.* Interaction of the *Clostridium difficile* Binary Toxin CDT and Its Host Cell Receptor, Lipolysis-stimulated Lipoprotein Receptor (LSR). *J. Biol. Chem.* **290,** 14031–14044 (2015).

88. Mann, C. J. *et al.* Inhibitory effects of specific apolipoprotein C-III isoforms on the binding of triglyceride-rich lipoproteins to the lipolysis-stimulated receptor. *J. Biol. Chem.* **272,** 31348–31354 (1997).

89. Masuda, S. *et al.* LSR defines cell corners for tricellular tight junction formation in epithelial cells. *J. Cell Sci.* **124,** 548–555 (2011).

90. Papatheodorou, P. *et al. Clostridium difficile* binary toxin CDT induces clustering of the lipolysis-stimulated lipoprotein receptor into lipid rafts. *MBio* **4,** e00244-13 (2013).

91. Weigt, C., Just, I., Wegner, A. & Aktories, K. Nonmuscle actin ADP-ribosylated by botulinum C2 toxin caps actin filaments. *FEBS Lett.* **246,** 181–184 (1989).

92. Ernst, K. *et al.* Cyclophilin-facilitated membrane translocation as pharmacological target to prevent intoxication of mammalian cells by binary clostridial actin ADP-ribosylated toxins. *J. Mol. Biol.* **427,** 1224–1238 (2015).

93. Lang, A. E. *et al. Photorhabdus luminescens* toxins ADP-ribosylate actin and RhoA to force actin clustering. *Science* **327,** 1139–1142 (2010).

94. Aktories, K., Papatheodorou, P. & Schwan, C. Binary *Clostridium difficile* toxin

(CDT) - A virulence factor disturbing the cytoskeleton. *Anaerobe* **53,** 21–29 (2018).

95. Gross, M. Antibiotics in crisis. *Curr. Biol.* **23,** R1063-5 (2013).

96. Keller, J. M. & Surawicz, C. M. *Clostridium difficile* infection in the elderly. *Clin Geriatr Med* **30,** 79–93 (2014).

97. Dantes, R. *et al.* Investigation of a cluster of *Clostridium difficile* infections in a pediatric oncology setting. *Am. J. Infect. Control* **44,** 138–145 (2016).

98. Miller, R., Simmons, S., Dale, C., Stachowiak, J. & Stibich, M. Utilization and impact of a pulsed-xenon ultraviolet room disinfection system and multidisciplinary care team on *Clostridium difficile* in a long-term acute care facility. *Am. J. Infect. Control* **43,** 1350–1353 (2015).

99. Stokely, J. N. *et al.* Prevalence of human norovirus and *Clostridium difficile* coinfections in adult hospitalized patients. *Clin Epidemiol* **8,** 253–260 (2016).

100. Lauda-Maillen, M. *et al.* Treatment compliance with European guidelines and prognosis of *Clostridium difficile* infection according to age. *Med Mal Infect* (2018). doi:10.1016/j.medmal.2018.08.001

101. Kelly, C. R. *et al.* Fecal microbiota transplant for treatment of *Clostridium difficile* infection in immunocompromised patients. *Am. J. Gastroenterol.* **109,** 1065–1071 (2014).

102. Cohen, S. H. *et al.* Clinical practice guidelines for *Clostridium difficile* infection in adults: 2010 update by the society for healthcare epidemiology of America (SHEA) and the infectious diseases society of America (IDSA). *Infect. Control Hosp. Epidemiol.* **31,** 431–455 (2010).

103. Song, J. H. & Kim, Y. S. Recurrent *Clostridium difficile* Infection: Risk Factors,

Treatment, and Prevention. *Gut Liver* (2018). doi:10.5009/gnl18071

104. Jarrad, A. M., Karoli, T., Blaskovich, M. A. T., Lyras, D. & Cooper, M. A. *Clostridium difficile* drug pipeline: challenges in discovery and development of new agents. *J. Med. Chem.* **58,** 5164–5185 (2015).

105. Ooijevaar, R. E., Terveer, E. M., Verspaget, H. W., Kuijper, E. J. & Keller, J. J. Clinical application and potential of fecal microbiota transplantation. *Annu. Rev. Med.* **70,** (2018).

106. Milani, C. *et al.* Gut microbiota composition and *Clostridium difficile* infection in hospitalized elderly individuals: a metagenomic study. *Sci. Rep.* **6,** 25945 (2016).

107. Bakken, J. S. *et al.* Treating *Clostridium difficile* infection with fecal microbiota transplantation. *Clin. Gastroenterol. Hepatol.* **9,** 1044–1049 (2011).

108. Borody, T. J. & Khoruts, A. Fecal microbiota transplantation and emerging applications. *Nat. Rev. Gastroenterol. Hepatol.* **9,** 88–96 (2011).

109. Reigadas, E. *et al.* Fecal microbiota transplantation for recurrent *Clostridium difficile* infection: Experience, protocol, and results. *Rev Esp Quimioter* **31,** 411–418 (2018).

110. Kochan, T. J. *et al.* Updates to *Clostridium difficile* Spore Germination. *J. Bacteriol.* **200,** (2018).

111. Petrosillo, N., Granata, G. & Cataldo, M. A. Novel Antimicrobials for the Treatment of *Clostridium difficile* Infection. *Front Med (Lausanne)* **5,** 96 (2018).

112. Surawicz, C. M. *et al.* Guidelines for diagnosis, treatment, and prevention of *Clostridium difficile* infections. *Am. J. Gastroenterol.* **108,** 478–98; quiz 499 (2013).

113. Löfmark, S., Edlund, C. & Nord, C. E. Metronidazole is still the drug of choice for treatment of anaerobic infections. *Clin. Infect. Dis.* **50 Suppl 1,** S16-23 (2010).

114. Teasley, D. G. *et al.* Prospective randomised trial of metronidazole versus vancomycin for *Clostridium-difficile*-associated diarrhoea and colitis. *Lancet* **2,** 1043–1046 (1983).

115. Bolton, R. P. & Culshaw, M. A. Faecal metronidazole concentrations during oral and intravenous therapy for antibiotic associated colitis due to *Clostridium difficile*. *Gut* **27,** 1169–1172 (1986).

116. Dale, L. D., Tocher, J. H., Dyson, T. M. & Edwards, D. I. Studies on DNA damage and induction of SOS repair by novel multifunctional bioreducible compounds. II. A metronidazole adduct of a ruthenium-arene compound. *Anti*

117. Menéndez, D., Rojas, E., Herrera, L. A. & López, M. C. DNA breakage due to metronidazole treatment. *Mutation Research …* (2001).

118. Moura, I. *et al.* Multidisciplinary analysis of a nontoxigenic *Clostridium difficile* strain with stable resistance to metronidazole. *Antimicrob. Agents Chemother.* **58,** 4957–4960 (2014).

119. Al Momani, L. A., Abughanimeh, O., Boonpheng, B., Gabriel, J. G. & Young, M. Fidaxomicin vs Vancomycin for the Treatment of a First Episode of *Clostridium difficile* Infection: A Meta-analysis and Systematic Review. *Cureus* **10,** e2778 (2018).

120. Reynolds, P. E. Structure, biochemistry and mechanism of action of glycopeptide antibiotics. *Eur. J. Clin. Microbiol. Infect. Dis.* **8,** 943–950 (1989).

121. Wright, G. D. & Walsh, C. T. D-Alanyl-D-alanine ligases and the molecular mechanism of vancomycin resistance. *Accounts of chemical research* (1992).

122. Leeds, J. A., Sachdeva, M., Mullin, S., Barnes, S. W. & Ruzin, A. In vitro selection,

via serial passage, of *Clostridium difficile* mutants with reduced susceptibility to fidaxomicin or vancomycin. *J. Antimicrob. Chemother.* **69,** 41–44 (2014).

123. Louie, T. J. *et al.* Fidaxomicin versus vancomycin for *Clostridium difficile* infection. *N. Engl. J. Med.* **364,** 422–431 (2011).

124. Cornely, O. A. *et al.* Fidaxomicin versus vancomycin for infection with *Clostridium difficile* in Europe, Canada, and the USA: a double-blind, non-inferiority, randomised controlled trial. *Lancet Infect. Dis.* **12,** 281–289 (2012).

125. Louie, T. J. *et al.* Fidaxomicin preserves the intestinal microbiome during and after treatment of *Clostridium difficile* infection (CDI) and reduces both toxin reexpression and recurrence of CDI. *Clin. Infect. Dis.* **55 Suppl 2,** S132-42 (2012).

126. Miller, M. Fidaxomicin (OPT-80) for the treatment of *Clostridium difficile* infection. *Expert opinion on pharmacotherapy* (2010).

127. Venugopal, A. A. & Johnson, S. Fidaxomicin: a novel macrocyclic antibiotic approved for treatment of *Clostridium difficile* infection. *Clin. Infect. Dis.* **54,** 568–574 (2012).

128. Artsimovitch, I., Seddon, J. & Sears, P. Fidaxomicin is an inhibitor of the initiation of bacterial RNA synthesis. *Clin. Infect. Dis.* **55 Suppl 2,** S127-31 (2012).

129. Roshan, N., Hammer, K. A. & Riley, T. V. Non-conventional antimicrobial and alternative therapies for the treatment of *Clostridium difficile* infection. *Anaerobe* **49,** 103–111 (2018).

130. Wang, S., Wang, Y., Cai, Y., Kelly, C. P. & Sun, X. Novel Chimeric Protein Vaccines Against *Clostridium difficile* Infection. *Front. Immunol.* **9,** 2440 (2018).

131. Gardiner, D. F., Rosenberg, T., Zaharatos, J. & Franco, D. A DNA vaccine targeting

the receptor-binding domain of *Clostridium difficile* toxin A. *Vaccine* (2009).

132. Sougioultzis, S. *et al. Clostridium difficile* toxoid vaccine in recurrent *C. difficile*-associated diarrhea. *Gastroenterology* **128,** 764–770 (2005).

133. Foglia, G., Shah, S., Luxemburger, C. & Pietrobon, P. J. F. *Clostridium difficile*: development of a novel candidate vaccine. *Vaccine* (2012).

134. Meader, E., Mayer, M. J., Steverding, D., Carding, S. R. & Narbad, A. Evaluation of bacteriophage therapy to control *Clostridium difficile* and toxin production in an in vitro human colon model system. *Anaerobe* **22,** 25–30 (2013).

135. Flanagan, J. M., Wall, J. S., Capel, M. S., Schneider, D. K. & Shanklin, J. Scanning transmission electron microscopy and small-angle scattering provide evidence that native *Escherichia coli* ClpP is a tetradecamer with an axial pore. *Biochemistry* **34,** 10910–10917 (1995).

136. Maurizi, M. R., Singh, S. K., Thompson, M. W., Kessel, M. & Ginsburg, A. Molecular properties of ClpAP protease of *Escherichia coli*: ATP-dependent association of ClpA and clpP. *Biochemistry* **37,** 7778–7786 (1998).

137. Gottesman, S., Clark, W. P., de Crecy-Lagard, V. & Maurizi, M. R. ClpX, an alternative subunit for the ATP-dependent Clp protease of *Escherichia coli*. Sequence and in vivo activities. *J. Biol. Chem.* **268,** 22618–22626 (1993).

138. Gottesman, S., Roche, E., Zhou, Y. & Sauer, R. T. The ClpXP and ClpAP proteases degrade proteins with carboxy-terminal peptide tails added by the SsrA-tagging system. *Genes Dev.* **12,** 1338–1347 (1998).

139. Trentini, D. B. *et al.* Arginine phosphorylation marks proteins for degradation by a Clp protease. *Nature* **539,** 48–53 (2016).

140. Kim, Y. I. *et al.* Molecular determinants of complex formation between Clp/Hsp100 ATPases and the ClpP peptidase. *Nat. Struct. Biol.* **8,** 230–233 (2001).

141. Alexopoulos, J. A., Guarné, A. & Ortega, J. ClpP: a structurally dynamic protease regulated by AAA+ proteins. *J. Struct. Biol.* **179,** 202–210 (2012).

142. Joshi, S. A., Hersch, G. L., Baker, T. A. & Sauer, R. T. Communication between ClpX and ClpP during substrate processing and degradation. *Nat. Struct. Mol. Biol.* **11,** 404–411 (2004).

143. Yu, A. Y. H. & Houry, W. A. ClpP: a distinctive family of cylindrical energy-dependent serine proteases. *FEBS Lett.* **581,** 3749–3757 (2007).

144. Lee, B.-G., Kim, M. K. & Song, H. K. Structural insights into the conformational diversity of ClpP from Bacillus subtilis. *Mol. Cells* **32,** 589–595 (2011).

145. Li, D. H. S. *et al.* Acyldepsipeptide antibiotics induce the formation of a structured axial channel in ClpP: A model for the ClpX/ClpA-bound state of ClpP. *Chem. Biol.* **17,** 959–969 (2010).

146. Bhandari, V. *et al.* The role of clpp protease in bacterial pathogenesis and human diseases. *ACS Chem. Biol.* **13,** 1413–1425 (2018).

147. Brötz-Oesterhelt, H. *et al.* Dysregulation of bacterial proteolytic machinery by a new class of antibiotics. *Nat. Med.* **11,** 1082–1087 (2005).

148. Conlon, B. P. *et al.* Activated ClpP kills persisters and eradicates a chronic biofilm infection. *Nature* **503,** 365–370 (2013).

149. Gersch, M. *et al.* The mechanism of caseinolytic protease (ClpP) inhibition. *Angew. Chem. Int. Ed. Engl.* **52,** 3009–3014 (2013).

150. Brötz-Oesterhelt, H. *et al.* Dysregulation of bacterial proteolytic machinery by a new

class of antibiotics. *Nat. Med.* **11,** 1082–1087 (2005).

151. Mikhailov, V. A., Ståhlberg, F., Clarke, A. K. & Robinson, C. V. Dual stoichiometry and subunit organization in the ClpP1/P2 protease from the cyanobacterium *Synechococcus elongatus*. *J. Struct. Biol.* **192,** 519–527 (2015).

152. Stanne, T. M., Pojidaeva, E., Andersson, F. I. & Clarke, A. K. Distinctive types of ATP-dependent Clp proteases in cyanobacteria. *J. Biol. Chem.* **282,** 14394–14402 (2007).

153. Gaillot, O., Bregenholt, S., Jaubert, F., Di Santo, J. P. & Berche, P. Stress-induced ClpP serine protease of *Listeria monocytogenes* is essential for induction of listeriolysin O-dependent protective immunity. *Infect. Immun.* **69,** 4938–4943 (2001).

154. Gaillot, O., Pellegrini, E., Bregenholt, S., Nair, S. & Berche, P. The ClpP serine protease is essential for the intracellular parasitism and virulence of *Listeria monocytogenes*. *Mol. Microbiol.* **35,** 1286–1294 (2000).

155. Zeiler, E. *et al.* Vibralactone as a tool to study the activity and structure of the ClpP1P2 complex from *Listeria monocytogenes*. *Angew. Chem. Int. Ed. Engl.* **50,** 11001–11004 (2011).

156. Zeiler, E. *et al.* Structural and functional insights into caseinolytic proteases reveal an unprecedented regulation principle of their catalytic triad. *Proc. Natl. Acad. Sci. USA* **110,** 11302–11307 (2013).

157. Hall, B. M. *et al.* Two Isoforms of Clp Peptidase in *Pseudomonas aeruginosa* Control Distinct Aspects of Cellular Physiology. *J. Bacteriol.* **199,** (2017).

158. Akopian, T. *et al.* The active ClpP protease from *M. tuberculosis* is a complex

composed of a heptameric ClpP1 and a ClpP2 ring. *EMBO J.* **31,** 1529–1541 (2012).

159. Famulla, K. *et al.* Acyldepsipeptide antibiotics kill mycobacteria by preventing the physiological functions of the ClpP1P2 protease. *Mol. Microbiol.* **101,** 194–209 (2016).

160. Li, M. *et al.* Structure and Functional Properties of the Active Form of the Proteolytic Complex, ClpP1P2, from *Mycobacterium tuberculosis*. *J. Biol. Chem.* **291,** 7465–7476 (2016).

161. Ollinger, J., O'Malley, T., Kesicki, E. A., Odingo, J. & Parish, T. Validation of the essential ClpP protease in *Mycobacterium tuberculosis* as a novel drug target. *J. Bacteriol.* **194,** 663–668 (2012).

162. Raju, R. M. *et al. Mycobacterium tuberculosis* ClpP1 and ClpP2 function together in protein degradation and are required for viability in vitro and during infection. *PLoS Pathog.* **8,** e1002511 (2012).

163. Schmitz, K. R., Carney, D. W., Sello, J. K. & Sauer, R. T. Crystal structure of *Mycobacterium tuberculosis* ClpP1P2 suggests a model for peptidase activation by AAA+ partner binding and substrate delivery. *Proc. Natl. Acad. Sci. USA* **111,** E4587-95 (2014).

164. Personne, Y., Brown, A. C., Schuessler, D. L. & Parish, T. *Mycobacterium tuberculosis* ClpP proteases are co-transcribed but exhibit different substrate specificities. *PLoS One* **8,** e60228 (2013).

165. Jain, S., Graham, C., Graham, R. L. J., McMullan, G. & Ternan, N. G. Quantitative proteomic analysis of the heat stress response in *Clostridium difficile* strain 630. *J. Proteome Res.* **10,** 3880–3890 (2011).

166. Lawley, T. D. *et al.* Proteomic and genomic characterization of highly infectious *Clostridium difficile* 630 spores. *J. Bacteriol.* **191,** 5377–5386 (2009).

167. Emerson, J. E., Stabler, R. A., Wren, B. W. & Fairweather, N. F. Microarray analysis of the transcriptional responses of *Clostridium difficile* to environmental and antibiotic stress. *J. Med. Microbiol.* **57,** 757–764 (2008).

168. Chong, P. M. *et al.* Proteomic analysis of a NAP1 *Clostridium difficile* clinical isolate resistant to metronidazole. *PLoS One* **9,** e82622 (2014).

169. Sekulovic, O. & Fortier, L.-C. Global transcriptional response of *Clostridium difficile* carrying the CD38 prophage. *Appl. Environ. Microbiol.* **81,** 1364–1374 (2015).

Chapter 2

Clostridium difficile ClpP Homologs are Capable of Uncoupled Activity and Exhibit Different Levels of Susceptibility to Acyldepsipeptide Modulation[1]

2.1 Abstract

Caseinolytic protease P (ClpP) has emerged as a promising new target for antibacterial development. While ClpPs from single isoform expressing bacteria have been studied in detail, the function and regulation of systems with more than one ClpP homolog are still poorly understood. Herein, we present fundamental studies toward understanding the ClpP system in *C. difficile*, an anaerobic spore-forming pathogen that contains two chromosomally distant isoforms of ClpP. Examination of proteomic and genomic data suggest that ClpP1 is the primary isoform responsible for normal growth and virulence, but little is known about the function of ClpP2 or the context required for the formation of

functional proteases. For the first time in a pathogenic bacterium, we demonstrate that both isoforms are capable of forming operative proteases. Interestingly, ClpP1 is the only homolog that possesses characteristic response to small molecule acyldepsipeptide activation. On the contrary, both ClpP1 and ClpP2 respond to cochaperone activation to degrade an ssrA-tagged substrate. These observations indicate that ClpP2 is less susceptible to acyldepsipeptide activation but retains the ability to interact with a known cochaperone. Homology models reveal no obvious characteristics that would allow one to predict less efficient acyldepsipeptide binding. The reported findings establish the uniqueness of the ClpP system in *C. difficile*, open new avenues of inquiry, and highlight the importance of more detailed structural, genetic, and biological characterization of the ClpP system in *C. difficile*.

2.2 Introduction

C. difficile infection (CDI) is a leading cause of hospital-acquired illness and presents a unique challenge to therapeutic development, as it is both caused by and clinically managed with traditional antibiotics that indiscriminately eradicate pathogenic and commensal bacteria.[1] Importantly, *C. difficile* is unique from typical beneficial microflora, in that it expresses two isoforms of ClpP (ClpP1 and ClpP2).[2] To date, our understanding of multiple *clpP* gene expressing organisms is based primarily upon four microbes, *Synechococcus elongatus,*[3,4] *Listeria monocytogenes,*[5–9] *Pseudomonas aeruginosa,*[10] and *M. tuberculosis,*[11–17] all of which reveal structural disparities and distinct regulation profiles of ClpP.
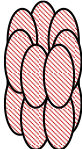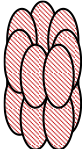
Figure 2.1 Composition and behavior of reported multi-ClpP systems
"Mixing" denotes that this result was obtained by mixing ClpP1 and ClpP2 homotetradecamers.

Gene location and expression characteristics of ClpP1 and ClpP2 in *C. difficile* are not only unique from commensal organisms, but also distinct from any pathogenic system disclosed to date. Of the two ClpP isoforms contained within the *C. difficile* genome, *clpP1*

is located in an apparent operon with the cochaperone *clpX*. Interestingly, *clpP2* is expressed in a chromosomally distant region of the genome without evidence of proximal co-chaperones or adaptors. In previous studies, mass spectrometry-based proteomic evaluation and genomic characterization of sporulated and heat-shocked *C. difficile* 630, revealed the presence of ClpP1 and the cochaperones ClpC and ClpX, but no evidence of ClpP2.[18,19] On the contrary, a microarray analysis completed by Emerson *et al.* detected ClpP1 and ClpP2, with ClpP1 being the only isoform upregulated under pH-induced shock, and antibiotic challenge (Amoxicillin, Clindamycin, and Metronidazole).[20] *clpP2* transcripts have also been detected in NAP1[21] and ϕCD38-2 prophage[22] containing *C. difficile* variants, suggesting that *clpP2* may have involvement in hypervirulent and/or resistant phenotypes. Taken together, ClpP1 has been detected in ribotype 630 and hypervirulent strains, while the presence of ClpP2 expression or protein has only been reported in hypervirulent strains. Nevertheless, these results suggest that contrary to other multi-ClpP organisms, which rely on mixtures of ClpP1 and ClpP2 monomers to form the functionally relevant protease (**Figure 2.1**), *C. difficile* ClpP1 and ClpP2 may operate in an uncoupled fashion and exhibit different biological roles. To evaluate the first portion of this hypothesis and begin to understand the behavior of the *C. difficile* ClpP system, we overexpressed, purified and reconstituted the homomeric ClpP1 and ClpP2 complexes and assessed the activity of these proteases.

Caseinolytic protease P (ClpP) has emerged as a promising new target for antibacterial development. While ClpPs from single isoform expressing bacteria have been studied in detail, the function and regulation of systems with more than one ClpP homologue are still poorly understood. Herein, we present fundamental studies toward

understanding the ClpP system in *C. difficile*, an anaerobic spore-forming pathogen that contains two chromosomally distant isoforms of ClpP. Examination of proteomic and genomic data suggest that ClpP1 is the primary isoform responsible for normal growth and virulence, but little is known about the function of ClpP2 or the context required for the formation of functional proteases. For the first time in a pathogenic bacterium, we demonstrate that both isoforms are capable of forming operative proteases. Interestingly, ClpP1 is the only homologue that possesses characteristic response to small molecule acyldepsipeptide (ADEP) activation. On the contrary, both ClpP1 and ClpP2 respond to cochaperone activation to degrade an ssrA-tagged substrate. These observations indicate that ClpP2 is less susceptible to ADEP activation but retains the ability to interact with a known cochaperone. Homology models reveal no obvious characteristics that would allow one to predict less efficient ADEP binding. The reported findings establish the uniqueness of the ClpP system in *C. difficile*, open new avenues of inquiry, and highlight the importance of more detailed structural, genetic, and biological characterization of the ClpP system in *C. difficile*.

2.3 Results

2.3.1 Significantly higher transcript levels of clpP1 are observed in exponential and stationary growth phases.

To determine the expression profile of *clpP1* and *clpP2* during exponential and stationary growth phases, we quantified transcript levels utilizing quantitative reverse-transcriptase polymerase chain reaction (qRT-PCR). Total RNA extracts were isolated from *C. difficile* 630 cells in biological triplicate from both exponential ($OD_{600} = 0.6$) and stationary ($OD_{600} = 1.2$) growth populations in Brain heart infusion-supplemented (BHIS) media. As shown in **Figure 2.2** (Ct values, **Table A.2**), *clpP1* and *clpP2* transcripts were detected during both phases of growth, albeit with *clpP2* transcripts significantly less prevalent than *clpP1*.

The observed difference in relative mRNA expression levels, paired with previously reported proteomic and transcriptomic data, suggests that *clpP1* is the major contributor to homeostasis in *C. difficile.* The detection of *clpP2,* albeit at a much lower transcript level, indicates that *clpP2* likely carries some function within the organism, but is likely not tied to a large role in general homeostasis. While this speculation is not particularly ground-breaking, it does demonstrate that *clpP2* is transcribed in both phases, a detail that is not obvious from studies described previously. The disparity in transcript levels adds confidence to our original hypothesis that unlike other pathogens investigated to date, ClpP isoforms in *C. difficile* are capable of uncoupled activity and are responsible for disparate biological roles. The qRT-PCR results compelled us to investigate the oligomerization behavior and catalytic profile of reconstituted ClpP1 and ClpP2.
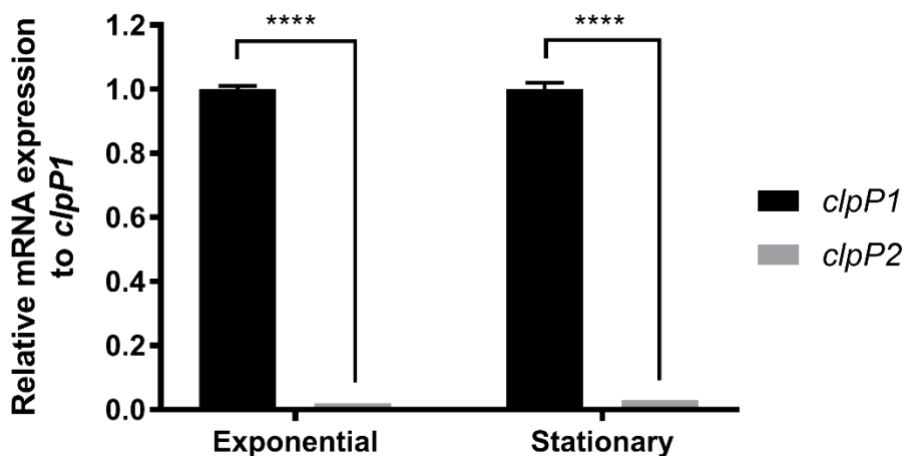
Figure 2.2 Relative quantification of *clpP1* and *clpP2* mRNA expression during exponential and stationary growth phases in BHIS broth.
Transcript levels were normalized to the reference gene *rpoB,* with *clpP2* transcript level reported relative to *clpP1*. The resulting data was analyzed via multiple comparison Two-way ANOVA and corrected by the Sidak method. ****, $P \leq 0.0001$

2.3.2 ClpP1 and ClpP2 share highly conserved sequence homologies and retain key structural motifs.

Within the last 5 years, elegant biophysical studies have revealed ClpP operation to be governed by inter- and intramolecular conformational switches that propagate regulation signals through the complex.[8,23–25] The presence or absence of these hotspots may provide an indicator for how uncharacterized ClpP isoforms can be expected to function. Therefore, to determine if critical motifs are conserved, we aligned the primary sequences of *C. difficile* ClpP1 and ClpP2 to *B. subtilis* ClpP (*Bs*Clp; identity: ClpP1-74% and ClpP2-63%), an evolutionarily related organism with a well-characterized ClpP homolog. As shown in **Figure 2.3**, the primary sequence alignment reveals that key hotspot regions, including the Ser-His-Asp catalytic triad, Tyr63 activation trigger, Asp(Glu)/Arg oligomerization sensor domains, and the Gly-rich heptamer dimerization domain, are

highly conserved in both *C. difficile* ClpP isoforms. Although there seems to be significant variation in the E-helix domain, a motif involved in heptamer dimerization to form the operative tetradecamer, there is no obvious evidence to suggest that either isoform would have difficulty oligomerizing or exhibiting stability in the tetradecameric form as a homomeric complex.
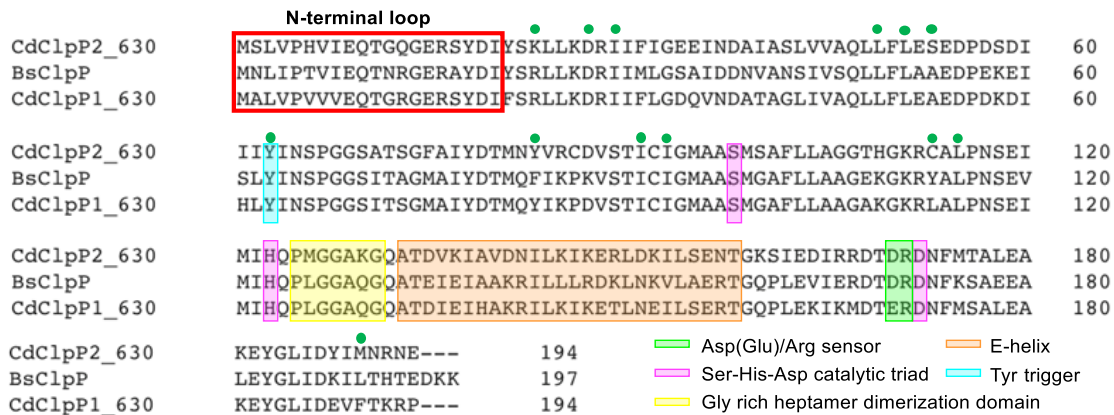
Figure 2.3 Primary sequence alignment of *C. difficile* ClpP isoforms (*Cd*ClpP1 and *Cd*ClpP2) and *Bacillus subtilis* ClpP (*Bs*ClpP).
Alignment and graphic generated with Clustal Omega. Green circles indicate amino acids shown to interact with acyldepsipeptides in *B. subtilis*.

2.3.3 ClpP1 forms a more stable tetradecameric complex.

Because ClpP1 and ClpP2 share high sequence identity (~72%) and retain key structural motifs, we hypothesized that both homologs would form active tetradecameric complexes capable of peptide/protein degradation. This however, cannot be assumed, as has been demonstrated by the *S. elongates, L. monocytogenes*, *P. aeruginosa*, and *M. tuberculosis* studies. To begin the assessment of possible oligomeric configurations of *C. difficile* ClpP1 and ClpP2, we separately expressed and purified each isoform to evaluate homogeneous-oligomeric reconstitution. Initially, *C. difficile* ClpP1 and ClpP2 were expressed with C-terminal 6x His-tags in *E. coli* Rosetta cells, and purified via affinity

chromatography before size exclusion chromatography (SEC) was performed to buffer exchange and confirm oligomeric status.

Assessment of purified fractions by SDS-PAGE and SEC suggested pure, completely tetradecameric ClpP complexes Identity of ClpP1 and ClpP2 were confirmed by high-resolution electrospray mass spectrometry (HR-ESIMS) and peptide digest and sequencing experiments. To our surprise, however, *E. coli* ClpP (*Ec*ClpP) was detected in ~10-30% relative abundance within our purified ClpP1 and ClpP2 preparations. We suspect that endogenous *Ec*ClpP from the expression cell line co-purified with the *C. difficile* ClpPs and was incorporated into the isolated tetradecameric complex. Given the high sequence homology of *Ec*ClpP and *C. difficile* ClpPs, this seems plausible and should not be overlooked when reconstituting other complexes prepared from recombinant techniques. One might assume that such an impurity would be evident by SDS-PAGE analysis, however, no such contamination was evident in our experiments, probably due to very similar molecular weights and suboptimal protein loading concentrations and/or gel-gradients. Unless one is specifically looking for a host-ClpP band and varying experimental conditions in attempts to reveal this, it will not likely be evident in typical preparations. As such we suggest utilizing a variety of methods to verify a pure and monodisperse preparation. To ensure that subsequent biochemical evaluations of these complexes were not influenced by contaminating *Ec*ClpP, each *C. difficile* ClpP isoform was overexpressed and purified from cells lacking *Ec*ClpP (Δ*Ec*ClpP, graciously provided by Dr. Robert Sauer's group, MIT).[26] Unless otherwise noted, all data presented herein utilizes *C. difficile* ClpP prepared from this ΔClpP *E. coli* strain.

ClpP1 rapidly tetradecamerizes prior to SEC purification, as indicated by the single peak corresponding to the molecular weight of tetradecameric ClpP1. (**Figure 2.4A**). The heptameric ClpP1 oligomer was not observed over the course of multiple purifications. ClpP2, however, elutes as a mixture of oligomeric species. If, however, ClpP2 is allowed to equilibrate ≥48 h, nearly complete oligomerization to the tetradecameric complex occurs (**Figure 2.4B**). HR-ESIMS confirmed the identity of both isoforms (**Appendix A.1**) and the absence of any contaminating *Ec*ClpP. Dynamic light scattering (DLS) experiments confirmed tetradecameric assembly for each isoform after purification (**Appendix A.2 - A.3**).
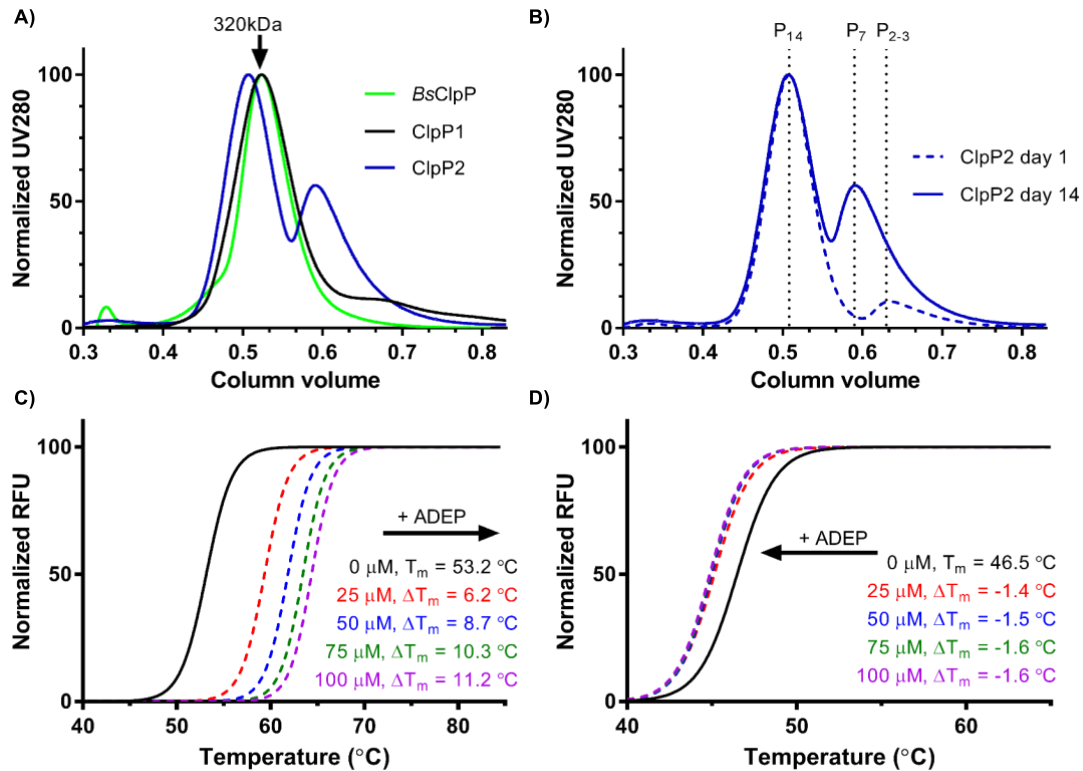
Figure 2.4 Tetradecameric assembly and thermal stability of ClpP1 and ClpP2 homomeric complexes.
A) Size exclusion chromatograph of purified recombinant ClpP1 and ClpP2 following Ni-affinity purification. *Bs*ClpP is included for comparison. B) time-dependent

oligomerization of ClpP2. An aliquot of ClpP2 was injected onto a S-300 SEC (blue, solid), and again 14-days later (blue, dashed). C) and D) SYPRO Orange thermal shift analysis (TSA) of tetradecameric ClpP1 (C) and ClpP2 (D) in the presence and absence of varying concentrations of an ADEP activator.

To evaluate the relative stability of ClpP1 and ClpP2, both were exposed to thermal shift analysis (TSA). As shown in **Figure 2.4C**, ClpP1 exhibits a T_m=53.2 °C and thus is significantly more stable to thermal denaturation than ClpP2 (T_m=46.5 °C). Additionally, the presence of a synthetic acyldepsipeptide (100 μM, ADEP, **Figure 2.7A**) known to stabilize other ClpP homologs, results in stabilization of ClpP1 (ΔT_m = +11.2 °C, **Figure 2.4C**), but an apparent destabilization of ClpP2 (ΔT_m = -1.6 °C, **Figure 2.4D**). ADEP destabilization of tetradecameric ClpP complexes has been reported previously,[27] and is attributed to substoichiometric occupation of ligand binding sites, which leads to disruption of the tetradecameric complex. These results hint at a rather drastic difference in ADEP interactions between the two isoforms. Nonetheless, both isoforms are capable of forming stable homotetradecamers, a feature only observed thus far in *M. tuberculosis* but has recently been disputed.[28]

2.3.4 ClpP1 exhibits prototypical peptidolysis.

When in an extended conformation, the catalytic triad of ClpP is aligned and capable of degrading small peptides (<5–6 amino acids) without the requirement of a cochaperone or ATP.[29] As exemplified by studies on *M. tuberculosis* ClpP isoforms, formation of a stable tetradecamer does not signify catalytic competency. To determine whether or not the assembled homo-oligomeric ClpP1 and ClpP2 complexes exist in the extended confirmation and have active (i.e., aligned) catalytic triads, we evaluated the capability of each ClpP tetradecamer to degrade two fluorescently labeled peptides, Suc-

Leu-Tyr-aminomethylcoumarin (dipeptide, SLY-AMC)[29] and Z-Gly-Gly-Leu-AMC (tripeptide, Z-GGL-AMC).[11] The small peptides freely diffuse into the proteolytic chamber of ClpP, where, in the presence of an active catalytic Ser-His-Asp triad, the peptides are hydrolyzed, releasing quantifiable fluorescence. As shown in **Figure 2.5A**, ClpP1 degrades SLY-AMC in a time dependent manner and exhibits Michaelis-Menten kinetics (**Figure 2.5B**), while ClpP2 fails to induce appreciable degradation. In fact, neither increased time (<24 h) nor alterations in substrate concentration produced measurable ClpP2 mediated degradation of this substrate (data not shown). Both ClpP1 and ClpP2 are, however, able to hydrolyze Z-GGL-AMC, although ClpP2 is not nearly as efficient as ClpP1 and requires extended co-incubation periods (>30 h) with this substrate to see appreciable hydrolysis (**Figures 2.5C** and **2.5D**). Mixing equal concentrations of homomeric ClpP1 and ClpP2 resulted in less peptidolysis for both SLY-AMC and Z-GGL-AMC (**Appendix A.6**) than ClpP1 alone. Native gel assessment of the mixture revealed no evidence of a new heteromeric species (**Appendix A.7**) While this experiment is a rather crude assessment, it provides evidence that disassembly of homomeric complexes and reassembly into more active heteromeric complexes is not thermodynamically favored and does not occur in vitro.

The Z-GGL-AMC results suggest, however, that the catalytic triad for ClpP2 is aligned to some extent under the evaluated conditions, but that experimental (e.g. buffer composition) and/or structural nuances dictating substrate specificity may exist for each ClpP isoform. Further evidence supporting that both complexes exhibit an aligned catalytic triad, arises upon incubation of each with ActivX TAMRA-FP, a fluorescent probe that selectively tags active serine hydrolases.[30] As shown in **Figure 2.5E**, TAMRA-FP labels

ClpP1 efficiently, while reacting to a lower extent with ClpP2. It is worth noting that in all three of these experiments *C. difficile* ClpP samples prepared from Rosetta DE3 cells (contaminated with *Ec*ClpP) were assessed in parallel with samples prepared from the Δ*Ec*ClpP strain and no significant differences in behavior were observed. Likewise, we failed to notice any difference in thermal stability of ClpP complexes prepared from either strain. So, while *Ec*ClpP contamination exists in the Rosetta DE3 preparations, its presence does not seem to affect the activity of either complex. We imagine this may not be the case for other ClpP homologs, especially those that exhibit lower homology, and caution others utilizing endogenous ClpP expressing cell lines for the characterization of recombinant ClpP complexes.

SLY-AMC Degradation

A) [graph: RFU vs Time (min), 0–40 min, y-axis 0–60000]

B) [graph: ΔRFU/min vs [SLY-AMC] mM, 0–6, y-axis 0–1500]

Key for A-C
- ClpP1 (Rosetta DE3)
- ClpP1 (ΔEcClpP)
- ClpP2 (Rosetta DE3)
- ClpP2 (ΔEcClpP)

Z-GGL-AMC Degradation

C) [graph: Relative fluorescence vs Time (min), 0–30, y-axis 0–15000]

D) [graph: Relative fluorescence vs Time (h), 30 and 46, y-axis 0–30000]
- ClpP1
- ClpP2
- DMSO

TAMRA Labeling

E) [gel image]

ClpP1 (DE3) ClpP1 ΔEcClpP ClpP2 (DE3) ClpP2 ΔEcClpP CHY

Figure 2.5 Peptidolytic activity of ClpP1 and ClpP2

A) time-dependent degradation of SLY-AMC by ClpP1 expressed from ΔEcClpP cells (black, solid, solid triangle), ClpP1 from Rosetta DE3 (black, dashed, hollow triangle), ClpP2 from ΔEcClpP (blue, solid, solid square), ClpP2 from Rosetta DE3 (blue, dashed, hollow square). Experiments conducted with 1 µM ClpP tetradecamer and 0.5 mM SLY-AMC. B) Michaelis-Menten analysis of ClpP1 and ClpP2 degradation of SLY-AMC. ClpP1 (DE3) $V_{max} = 1213 \pm 38.0$; ClpP1 (ΔEcClpP) $V_{max} = 1357 \pm 39.9$. ClpP2 V_{max} values were not determined due to relatively negligible cleavage of the substrate. C) time-dependent (0-30 min) degradation of Z-GGL-AMC by ClpP isoforms. Experiments conducted with 1 µM ClpP tetradecamer and 0.1 mM Z-GGL-AMC. D) degradation of Z-GGL-AMC by ClpP isoforms after extended periods (30 h and 46 h) of incubation. Means of each dataset were compared to the control (Z-GGL-AMC alone) at each time point, for statistical significance within a 95% confidence interval by two-way ANOVA analysis, with Dunnett's multiple comparison test. (**, $P < 0.05$). E) serine-protease active site

labeling with ActivX TAMRA-FP visualized in an SDS-PAGE gel with Chymotrypsin (CHY) as a positive control.

While investigating potential reasons for the lack of ClpP2 proteolytic activity, we determined through HR-ESIMS that ClpP2 was capable of forming disulfide bonds (reversible with dithiothreitol (DTT) addition) that may affect enzymatic efficiency. DiANNA, a web server developed by Boston College to define cysteine oxidation states and predict disulfide bond partners, identified two potential disulfide bonds (i.e., Cys86-Cys92, and Cys92-Cys113, **Appendix A.4**) for ClpP2. The algorithm reveals disulfide bond formation to be unique to ClpP2, as ClpP1 contains only a single cysteine. Since the two predicted disulfide bonds in ClpP2 are located in proximity to the catalytic triad, we could not discount that disulfide bond formation may dictate proteolytic activity or cleavage specificity by misshaping the topology around serine catalytic site, or locking ClpP2 in an inactive conformation. Therefore, we also evaluated the activity of ClpP2 in the presence of varying concentrations of DTT, but found that this failed to stimulate proteolytic activity, even at incubation times exceeding 48 h (**Appendix A.5**). It is also worth noting that reduced conditions (expected for an anaerobic environment) had no significant effect on the thermal stability of ClpP1 or ClpP2.

2.3.5 ClpP1 and ClpP2 respond to ClpX activation.

As mentioned previously, ClpP proteolysis of targeted substrates is tightly regulated via coordination between ATP-dependent cochaperones (e.g., ClpX, ClpA, ClpC). These cochaperones recognize degron sequences (e.g., ssrA) that tag proteins for degradation by ClpP.[11] Because *clpP1* and *clpX* are situated in an apparent operon in *C. difficile,* we anticipated that ClpP1 and ClpX would readily combine to form an operative

heteroprotein complex capable of degrading ssrA-tagged substrates. We however, did not know what to expect with ClpP2, as the lack of proteolytic activity in the SLY-AMC assay is not necessarily indicative of the capability to function with natural co-chaperones. To determine the ability of each *C. difficile* ClpP homolog to form the ClpP:ClpX proteolytic machinery and degrade protein substrates we expressed and purified *C. difficile* ClpX and ssrA-tagged green-fluorescent protein (ssrA-GFP) to allow for reconstitution of the "natural" proteolytic machinery.

ClpX and ssrA-GFP were incubated with each ClpP isoform in order to determine if ssrA-GFP degradation could be mediated by ClpX. We observed reductions in GFP gel-band intensity for both ClpP isoforms with ClpX and ATP present (**Figure 2.6A**), with ClpP1 once again outperforming ClpP2. Incubation of ssrA-GFP with each ClpP isoform in the absence of ATP revealed no degradation of the substrate, indicating that the observed degradation is induced by ClpX (**Figure 2.6B**). It is well-known that ClpX ATP hydrolysis is repressed upon engagement with ClpP.[31,32] As such, we determined ATP hydrolysis rates for ClpX in the presence of either ClpP1 or ClpP2. As seen in **Figure 2.6C**, ClpX ATPase hydrolysis decreases when incubated with either ClpP1 (~18% rate reduction) or ClpP2 (~7% rate reduction).
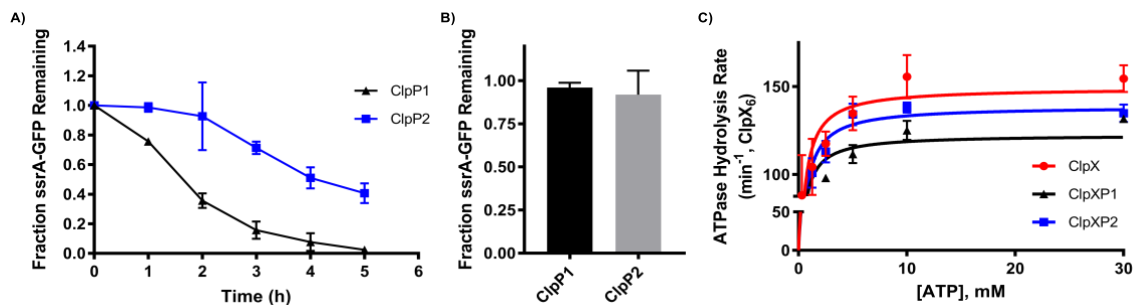
Figure 2.6 ClpXP mediated degradation of ssrA-GFP and ClpP induced reduction in ATP hydrolysis.

A) ClpXP1 and ClpXP2 mediated degradation of ssrA-GFP. Experiment was performed in triplicate and SDS-PAGE results were quantified with ImageJ results (graph). B) Fraction of ssrA-GFP remaining when incubated with ClpP variants in the absence of ClpX. C) the rate of *C. difficile* ClpX ATP hydrolysis in the presence or absence of *C. difficile* ClpP1 or ClpP2. *C. difficile* ClpX hydrolyzed ATP at a rate of 149.2 ± 6.0 min$^{-1} \cdot$ClpX$_6^{-1}$. In the presence of ClpP1 ClpX hydrolyzed ATP at a rate of 122.5 ± 0.3 min$^{-1} \cdot$ClpX$_6^{-1}$. In the presence of ClpP2 ClpX hydrolyzed ATP at a rate of 138.7 ± 0.4 min$^{-1} \cdot$ClpX$_6^{-1}$. Km values for ClpX, ClpP1, and ClpP2 are 375.2 μM, 318.9 μM, and 402.9 μM, respectively.

In an attempt to elicit ClpP2 peptidolytic activity, we added SLY-AMC to an aliquot of the ClpX:ClpP2 reaction. The rationale was that perhaps the ClpX interaction may trigger an autocatalytic-processing, or other maturation event, giving rise to peptidolytic activity. However, no degradation of SLY-AMC was observed.

2.3.6 ClpP1 and ClpP2 exhibit significant differences in susceptibility to chemo-activation.

ADEPs (**Figure 2.7A**) bind and activate bacterial ClpP in a cochaperone and ATP-independent manner, resulting in unselective proteolysis and bacterial cell death.[33] Similar to the natural cochaperones, ADEP binding results in a large conformational shift and a subsequent widening of the proteolytic chamber.[14] In the case of chemo-activation, however, the proteolysis is uncontrolled and unregulated, and thus detrimental to bacterial survival.[34] Analysis of co-crystal structures reveals that the ADEPs mimic the natural isoleucine/leucine-glycine-phenylalanine (I/LGF) loop utilized by AAA+ cochaperones for ClpP binding and thus bind competitively to the same pocket.[34,35] As such, activators of ClpP operate via two mechanisms of action: 1) activating the ClpP protease and inducing unselective degradation; and 2) inhibiting the interaction of AAA+ cochaperones with ClpP, thus disrupting the ability of cochaperones to deliver natural substrates for degradation. Therefore, bacterial cells treated with ClpP activators suffer from simultaneous self-digestion and a build-up of toxic substrates, resulting in a dual attack on

microbes. Recent interest in pursuing ADEPs for CDI treatment has appeared in literature, but no experimental assessment has followed.[36]
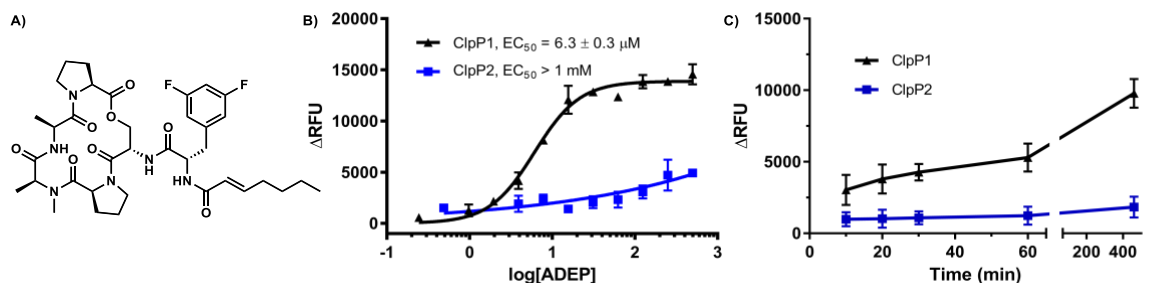
Figure 2.7 Susceptibility of ClpP1 and ClpP2 to ADEP activation.
A) Synthetic ADEP utilized in these experiments. B) dose-dependent ADEP-induced degradation of the decapeptide Abz-DFAPKMALVPY^{NO2}. C) Time-dependent ADEP (100 µM) induced degradation of FITC β-casein; ClpP1 (black, triangles) and ClpP2 (blue, squares).

To determine the susceptibility of homomeric ClpP1 and ClpP2 to ADEP activation, we incubated both isoforms with serially-diluted concentrations of a synthetic ADEP (**Figure 2.7A**) in the presence of a self-quenching decapeptide (Abz-DFAPKMALVPY^{NO2}) or FITC-β-casein. Upon ADEP mediated activation, ClpP will degrade the self-quenching substrate and release quantifiable fluorescence. As shown in **Figure 2.7**, ClpP1 displays a prototypical response to ADEP activation, and efficiently degrades both the decapeptide (**Figure 2.7B**) and protein (**Figure 2.7C**) substrates. ClpP2 on the other hand, demonstrates a much lower susceptibility to ADEP activation and fails to produce significant levels of peptidolysis or proteolysis, even at ADEP concentrations as high as 1 mM.

2.3.7 Homology Models Reveal No Obvious Preclusions in ClpP2 Activating Pocket

Intrigued by the response of ClpP2 to co-chaperone activation while exhibiting significantly less susceptibility to ADEP activation, we generated homology models to aid in visualization of the ADEP binding pocket and elucidate any amino acid substitutions

that may preclude ADEP binding. ClpP from *Bacillus subtilis* exhibits 74% and 63% sequence identity to *C. difficile* ClpP1 and ClpP2, respectively and was thus utilized to generate the models (SWISS-MODEL). Assessment of the primary sequences (**Figure 2.3**) and models (**Figure 2.8**), however, failed to reveal any obvious amino acid substitutions that would allow one to predict less efficient ADEP binding. This leaves us to speculate that alterations in the primary sequence outside of the cochaperone/ADEP binding pocket may lead to subtle perturbations of higher order ClpP structures that result in ADEP insensitivity while maintaining natural function. Adding intrigue to this speculation is an observation that in hypervirulent strains of *C. difficile*, the primary sequence of ClpP1 and ClpP2 retain complete sequence identity to *C. difficile* 630, but include three FT amino acid insertions. Studies are ongoing to determine the effect of those insertions on ClpP1 and ClpP2 functionality. Systematic insertions of this type in other ClpP isoforms has not been previously reported, nor do they occur in characteristic structural motifs relevant to ADEP activation.
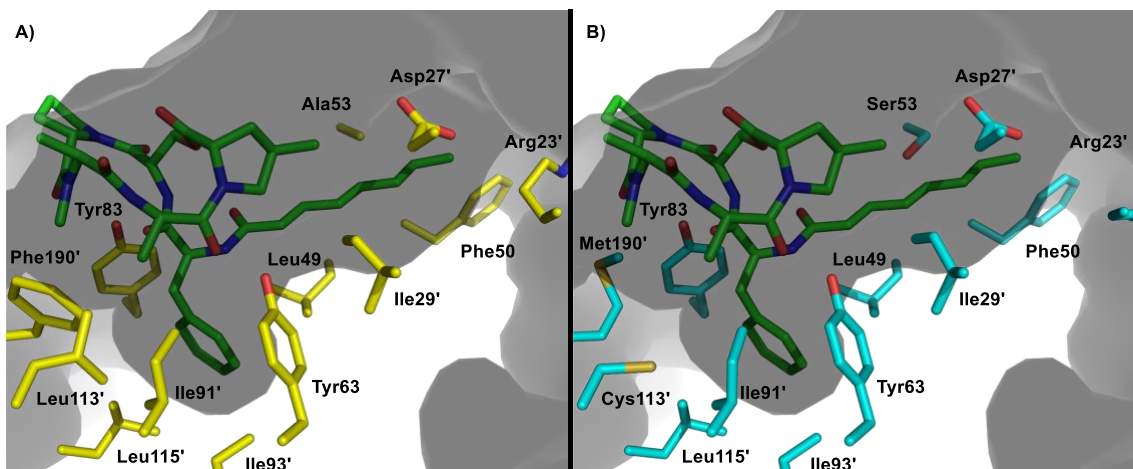
Figure 2.8 Depiction of the A) ClpP1 and B) ClpP2 ADEP binding pockets based on homology modeling with *Bacillus subtilis* ClpP.
Prime numbers indicate one ClpP subunit and non-prime numbers another. Gray indicates the culled surface of ClpP with a solvent radius set to 2.0 Å.

2.3 Conclusion

Reported mechanisms of evolved resistance to ADEP activation include efflux pump upregulation and point mutations close to the active site (e.g., T182A), resulting in impaired proteolytic activity. Both of these observations were obtained from *E. coli*. Unspecified point mutations that eliminate proteolytic activity have also been generated in a laboratory setting at a frequency range of 10^6 in *E. faecalis* and *S. pneumoniae*. All of these studies have been conducted in single ClpP gene containing organisms. We believe that more complex resistance or redundancy mechanisms may exist in multi-ClpP organisms and that studying these systems will reveal new insights into ClpP modulation as a therapeutic strategy and possible resistance evolution. Analysis of previous *C. difficile* genomic and proteomic studies indicated that the ClpP system in this organism may exhibit a behavior distinct from other multi-ClpP organisms interrogated to date and thus inspired us to begin studying this system in *C. difficile*.

The data demonstrate that the proteolytic activity and susceptibility to chemo-activation differ between *C. difficile* ClpP1 and ClpP2 and that these two isoforms are capable of functioning in an uncoupled fashion. This has yet to be observed in other multi-*clpP* organisms (e.g., *M. tuberculosis, L. monocytogenes, S. elongatus*), which require both ClpP1 and ClpP2 to form functionally relevant heterotetradecameric proteolytic complexes. Recently, it was reported that ClpP1 and ClpP2 of *P. aeruginosa* exhibit different expression profiles and disparate biological roles, but reconstitution of an active or fully assembled ClpP2 homomeric complex could not be obtained *in vitro*. Thus, to the best of our knowledge, for the first time in a multi-*clpP* organism, we demonstrate that

57

both isoforms are capable of forming operative proteases. These results clearly differentiate the ClpP system of *C. difficile* and highlight the possibilities of 1) uncoupled function of ClpP isoforms in pathogenic bacteria and 2) selective or specific modulation of one isoform over another.

The studies presented herein lay a foundation for more detailed characterization of the structure, function, and behavior of the ClpP system in *C. difficile,* as many questions remain to be answered. For example, is it possible for ClpP1 and ClpP2 to form operable heterogenous tetradecamers like those exhibited by *S. elongates*, *M. tuberculosis*, and *L. monocytogenes*? If so, how does the activity and susceptibility to chemo-modulation compare to the homogenous complexes? This question is not one that can be answered merely by mixing the two isoforms together. Rather, extensive protein science and analytical work are necessary to assess heteromeric formation and to determine the stoichomeric ratio of each isoform. What are the structural nuances that differentiate operative ClpP complexes and their responses to ADEP activation? This question is particularly interesting because no obvious characteristics emerge during the analysis of the primary sequences. Answering this question will likely require structural characterization of these complexes. While continued biochemical and biophysical evaluation of reconstituted *C. difficile* ClpP complexes will undoubtedly lead to new insights about enzyme kinetics and structure, genetic manipulation of the ClpP system in *C. difficile* is essential to understanding the biological significance and therapeutic potential. These studies are ongoing, and results will be presented in due course.

2.4 Materials and Methods

Unless otherwise noted, all ClpP concentrations are expressed as the

tetradecameric (ClpP$_{14}$) protease.

2.4.1 Expression and Purification of ClpP1 and ClpP2.

clpP1 (YP_001089821.1) and *clpP2* (YP_001089868.1) were synthesized with a

Poly-His(6x) C-terminal tag, codon optimized, and cloned into pET28a by Genscript USA

(Piscataway, NJ). *clpX* (YP_001089820.1) with a TEV-cleavable Poly-His(6x) N-terminal

tag was also synthesized by Genscript USA, codon optimized, and cloned into pET21a. All

plasmids were transformed into Rosetta (DE3) and Δ*Ec*ClpP (DE3) cells (a gracious gift

from Dr. Robert Sauer's laboratory) for expression, through standard techniques. M4100

(DE3) cells (Δ*Ec*ClpX) possessing ssrA-tagged (LAA)-GFP with a Poly-His(6x) N-

terminal tag was provided as a gracious gift from Dr. Tania A. Baker's laboratory, and was

expressed and purified as previously described.[17] All purified proteins were flash frozen in

liquid N$_2$ and stored at -80 °C until needed.

To express ClpP1, ClpP2, and ClpX, a 4L culture was inoculated with an overnight

stock (1:100) and grown to an OD$_{600}$ of $0.5 - 0.7$, shaking at 250rpm at 37 °C. Prior to

induction with 1 mM IPTG, the temperature was decreased to 18 °C and shaking was

reduced to 180 rpm. Overexpression was carried out over 16-18 h at 18 °C, shaking at 180

rpm. The bacteria were pelleted via centrifugation (5000 *g*, 4 °C, 15 min). The pellet was

washed with ice-cold lysis buffer, and stored at -80 °C until lysis. For isolation and

purification of ClpP1 and ClpP2, the pellet was resuspended in ice-cold lysis buffer (50

mM Tris pH 8.0, 200 mM NaCl, 10% glycerol), before being loaded into an Emulsiflex

cell-disruption system, for four-rounds of lysis at ~15000 psi while being cooled on ice.

The lysate was clarified via centrifugation (28500 g, 4 °C, 45 min) and loaded onto a 5 mL HF His-Trap column (GE Healthcare) via an NGC Explorer FPLC (Bio-Rad) at 4 °C. The column was washed with 5% His-elution buffer (Tris pH 8.0, 200 mM NaCl, 10% glycerol, 500 mM imidazole) for 20 column volumes (CV). His-tagged protein was eluted with a step-wise increase of Elution Buffer (10/15/30/70/100%), in reverse-flow. Highly pure fractions were collected in 5 mL intervals and concentrated to ~5 mL before injection onto a HiPrep 16/60 Sephacryl S-300 HR Size Exclusion Column (GE Life Sciences). ClpP was exchanged into activity buffer (25 mM HEPES, 100 mM KCl, 5 mM $MgCl_2$, 1 mM DTT, 10% glycerol) with an NGC Explorer FPLC at 4 °C. ClpP was concentrated with a 50 kDa MW-cutoff concentrator, and flash frozen until needed. All proteins expressed in the ΔEcClpP cell line were purified identically, except for induction of expression was accomplished with 0.5 mM IPTG.

Both isoforms express well in ΔEcClpP cells, and are stable at 4 °C for >1-month. Typical ClpP1 and ClpP2 protein expression yields range from 15-25 mg/mL and 7.5-12.5 mg/mL, respectively. ClpP1 can be concentrated to ~60 mg/mL without any sign of precipitation, while ClpP2 exhibits less stability at concentrations exceeding 12.5 mg/mL. Samples were flash frozen in activity buffer (25 mM HEPES, 100 mM KCl, 5 mM $MgCl_2$, 1 mM DTT, 10% glycerol) and stored at -80 ˚C until further use.

For isolation and purification of ClpX, the pellet was resuspended in ice-cold ClpX lysis buffer (50 mM Tris-Cl pH 8.8, 200 mM NaCl, 100 mM KCl, 20 mM imidazole, 10% glycerol). Cells were lysed, and the lysate was clarified in an identical manner to ClpP1 and ClpP2. The clarified lysate was then loaded onto a 5 mL HF His-Trap column, and washed/eluted similar to ClpP1 and ClpP2, except the concentration of imidazole in the

His-elution buffer was decreased 300 mM. Fractions were pooled and concentrated to ~5 mL, and buffer exchanged via SEC into ClpX activity buffer (50 mM HEPES pH 7.6, 200 mM KCl, 100mM NaCl, 20 mM $MgCl_2$, 1 mM DTT, 10% glycerol). ClpX fractions were concentrated with a 10 kDa MW-cutoff Amicon Ultra concentrator. All assay protein concentrations were obtained via A280 nm readings and are reported as tetradecameric concentrations unless otherwise stated.

2.4.2 RNA extraction, cDNA preparation, Quantitative Reverse-Transcriptase PCR, and Genomic DNA isolation.

Freezer stocks of *C. difficile 630* were struck onto BHIS agar plates and grown at 37 °C in a Coy vinyl anaerobic chamber (85% N_2, 5% H_2, and 10% CO_2). In biological triplicate, single colonies were picked and used to inoculate ~5 mL of BHIS media. When the absorbance reached OD_{600} of ~0.6 (exponential phase) and ~1.2 (stationary phase) the cultures were harvested. Samples were added directly to 2x volume of RNAprotect Bacteria Reagent (Qiagen) centrifuged at 5,000 x G, 25 °C for 10 minutes, decanted then stored at -20°C until further use. RNeasy Mini kit (Qiagen) was used to isolate the total RNA as described by the manufacturer. Contaminating genomic DNA was removed from the total RNA samples by two rounds of treatment using TURBO DNA-free kit (Invitrogen). cDNA was generated with the SuperScript IV VILO cDNA synthesis kit (Thermo) from 1 μg of total RNA, in 20 μL reactions. Appropriate no RT and no template control samples were performed alongside each biological replicate. 1 μL of the cDNA reaction mixture was added to 12.5 μL 2X qPCR iTaq Universal SYBR Green Supermix (Bio-Rad), 10 nM of the forward and reverse primers, and DNAse/RNase free water was added to bring the total PCR reaction volume to 25 μL. A 7500 Fast Real-Time PCR

System (Applied Biosystems) was used to perform qPCR (See **Table A.1** for primers) for 40 cycles of amplification at 51.5 °C. qRT-PCR primers were designed utilizing the PrimerQuest tool by Integrated DNA Technologies. Each primer was then put into the NCBI BLAST program to confirm no off-target hits. Primer efficiencies were calculated for each set of primers and are as follows *rpoB* = 99.1%, *clpP1* = 97.1%, and *clpP2* = 97.8%. Expression of *clpP1* and *clpP2* was normalized to the reference gene *rpoB,* with the results calculated via the comparative cycle threshold method.[18]

As previously stated, freezer stocks of *C. difficile* 630 were struck onto BHIS agar plates and grown at 37°C in anaerobic chamber. Then a single colony was picked and used to inoculate ~5 mL of BHIS media. Genomic DNA was isolated using GenElute Bacterial Genomic DNA kit and purified using Zymo Genomic DNA Clean and Concentrator kit, following manufacturer's protocols.

2.4.3 FITC-β-Casein Proteolysis Assay.

260 nM ClpP in activity buffer was incubated with ADEP (serially diluted from 500 µM) at 37 °C for 15 min in flat bottom, nonbinding, nonsterile, white polystyrene 96-well plates (Corning 3990). After the preincubation period 1 µL 100X FITC-β-casein stock was added to each well to give a final concentration of 4.5 µM FITC-β-casein and final well volume of 100 µL. Assay plates were then incubated at 37 °C, and hydrolysis of the fluorogenic substrate was monitored via an i-TECAN Infinite M200 plate reader (excitation: 485 nm; emission: 538 nm). Readings were taken every 30 min for 6 h.

2.4.4 SLY-AMC & Z-GGL-AMC Peptidolysis Assays.

All reactions were performed in activity buffer. Reactions contained 1 uM ClpP and were performed at 30 °C unless otherwise specified. SLY-AMC was dissolved in

DMSO at a stock concentration of 5 mM that was aliquoted into a 2x SLY-AMC master mix containing nanopure water and 10% DMSO. 200 µL reactions were assembled in 2x concentrations, and three 50 µL 2x reactions were dispensed into black 96-well plates. Reactions were started by adding 50 µL of 2x SLY-AMC, and a 0 hr reading was taken (excitation: 380nm / emission: 440nm) before incubation at 30 ℃. Hydrolysis of the fluorogenic substrate was monitored via an i-TECAN Infinite M200 plate reader and readings were taken at the time points indicated in the reported data.

2.4.5 Decapeptide Degradation Assay.

Assays were performed with 25 nM ClpP in activity buffer supplemented with 5% DMSO. ADEP was serially diluted and pipetted into the plate at 10X concentration, before a ClpP master mix was added, and both were incubated at 30 ℃ for 15 min in flat bottom, nonbinding, nonsterile, black polystyrene 96-well plates (Grenier). After the preincubation period 1 µL of 1.5 mM Abz-DFAPKMALVPY^{-NO2} (Biomatik) solution was added to each assay well to give a final assay concentration of 15 µM fluorogenic decapeptide and final assay volume of 100 µL. Assay plates were incubated at 30 ℃, and hydrolysis of the fluorogenic peptide was monitored via an i-TECAN Infinite M200 plate reader (excitation: 320 nm; emission: 420 nm). Readings were taken at the time points indicated in the reported data. The data was normalized to a 5% DMSO + peptide negative control.

2.4.6 ssrA-GFP Degradation Assay.

ClpP1 and ClpP2 were separately co-incubated with ClpX at 25 ℃ in ATPase buffer for 1 h prior to the start of the assay. An ATP-regeneration system containing 75 µg/mL creatine kinase and 5 mM creatine phosphate was used. All components were freshly prepared prior to addition to the reaction. The final concentration of ClpP and ClpX

were 400 nM, and 100 nM respectively. 2 μM of ssrA-GFP was added prior to the addition of ATP. All controls were incubated for 6 h at 30 °C. The reactions were initiated by addition of ATP in ATPase buffer to a final concentration of 4 mM, into a master reaction mixture which were distributed into 50 uL aliquots, placed onto a 30 °C heat block, and covered in foil. Reactions were then quenched each hour with 95 °C Laemmli buffer. 10 μL of each reaction was loaded into individual wells of a 4-20% SDS-PAGE gel. Experiments were performed in triplicate and intensities were analyzed with ImageJ. The fraction of ssrA-GFP remaining was calculated at each time point by dividing the intensity ssrA-GFP band by the intensity of the ssrA-GFP + ClpP control.

2.4.7 ssrA-GFP ATPase Hydrolysis Assay.

ClpP1 and ClpP2 were separately co-incubated with ClpX at 25 °C in ATPase buffer (50 mM HEPES pH 7.6, 10 mM Tris pH 7.6, 100 mM KCl, 20 mM $MgCl_2$, 1mM DTT, 10% glycerol, 0.032 NP-40, 0.01% Triton X-100) for 1 h prior to the start of the assay. An ATP-regeneration system[19] was utilized to monitor ATP-hydrolysis by ClpX via absorbance measurements taken at 340 nm in clear 96-well plates. Final concentrations of the ATP-regeneration assay were: 1 mM NADH, 20U Lactate dehydrogenase/Pyruvate kinase, 7.5 mM phosphoenolpyruvate. All components were freshly prepared prior to addition to the reaction. The final concentration of ClpP and ClpX were 200 nM, and 50 nM, respectively. The reaction was initiated by addition of ATP in ATPase buffer, and measurements were taken every 2 min over the course of 4 h to ensure assay completion. Initial rates were processed in Microsoft Excel, and transferred to GraphPad Prism for Michaelis-Menten and statistical analysis.

2.4.8 Thermal Shift Assay.

The procedure was performed as previously described[7] with slight modifications. 1 µM of $ClpP_1$ in activity buffer was incubated in the presence or absence of ADEP for 15 min at 37 °C prior to addition of SYPRO Orange (2x final concentration), final reaction volume 200 µL. The reaction was then allowed to equilibrate at room temperature in the dark for 15 min before dispensing 50 µL aliquots into 96-well plates in triplicate, sealed with optically clear microplate tape, and centrifuged briefly to remove bubbles. Thermal shift analysis was carried out on a CFX96 Real-Time System (Bio-Rad), heating from 25 °C to 85 °C in 0.3 °C increments, measuring fluorescence every 1-minute in FRET mode. The data was then processed in GraphPad Prism and fit to a Boltzmann distribution curve after normalization.

2.4.9 Mass Spectrometry Analysis of Oligomeric Species.

ClpP proteins in solution were reduced with DTT, alkylated with iodoacetamide and digested with trypsin according to standard protocols. Liquid chromatography tandem mass spectrometry was performed by coupling a nanoAcquity UPLC (Waters Corp., Manchester, UK) to a Q-TOF SYNAPT G2S instrument (Waters Corp., Manchester, UK). Each protein digest (about 100 ng of peptide) was delivered to a trap column (300 µm × 50 mm nanoAcquity UPLC NanoEase Column 5 µm BEH C18, Waters Corp, Manchester, UK) at a flow rate of 2 µL/min in 99.9% solvent A (10 mM ammonium formate, pH 10, in HPLC grade water). After 3 min of loading and washing, peptides were transferred to another trap column (180 µm × 20 nanoAcquity UPLC 2G-V/MTrap 5 µm Symmetry C18, Waters Corp., Manchester, UK) using a gradient from 1% to 60% solvent B (100% acetonitrile). The peptides were then eluted and separated at a flow rate of 200 nL/min

using a gradient from 1% to 40% solvent B (0.1% formic acid in acetonitrile) for 60 min on an analytical column (7.5 μm × 150 mm nanoAcquity UPLC 1.8 μm HSST3, Waters Corp, Manchester, UK). The eluent was sprayed via PicoTip Emitters (Waters Corp., Manchester, UK) at a spray voltage of 3.0 kV and a sampling cone voltage of 30 V and a source offset of 60 V. The source temperature was set to 70 °C. The cone gas flow was turned off, the nano flow gas pressure was set at 0.3 bar, and the purge gas flow was set at 750 mL/h. The SYNAPT G2S instrument was operated in data-independent mode with ion mobility (HDMSe). Full scan MS and MS2 spectra (m/z 50–2000) were acquired in resolution mode (20 000 resolution fwhm at m/z 400). Tandem mass spectra were generated in the trapping region of the ion mobility cell by using a collisional energy ramp from 20 V (low mass, start/end) to 35 V (high mass, start/end). A variable IMS wave velocity was used. Wave velocity was ramped from 300 to 600 m/s (start to end), and the ramp was applied over the full IMS cycle. A manual release time of 500 μs was set for the mobility trapping and a trap height of 15 V with an extract height of 0 V. The pusher/ion mobility synchronization for the HDMSe method was performed using MassLynx V4.1 and DriftScope v2.4. LockSpray of glufibrinopeptide-B (m/z 785.8427) was acquired every 60 s and lock mass correction was applied post acquisition.

Raw MS data were processed by PLGS (ProteinLynx Global Server, Waters Corp., Manchester, UK) for peptide and protein identification. MS/MS spectra were searched against the Uniprot *E.Coli* database and the *C. difficile* database (4,322 reviewed proteins and 7,753 unreviewed proteins respectively) and with the following search parameters: full tryptic specificity up to two missed cleavage sites, carbamidomethylation of cysteine

residues set as a fixed modification, and N-terminal protein acetylation and methionine oxidation.

2.5 References

1. Jarrad, A. M., Karoli, T., Blaskovich, M. A. T., Lyras, D. & Cooper, M. A. *Clostridium difficile* drug pipeline: challenges in discovery and development of new agents. *J. Med. Chem.* **58,** 5164–5185 (2015).

2. Yu, A. Y. H. & Houry, W. A. ClpP: a distinctive family of cylindrical energy-dependent serine proteases. *FEBS Lett.* **581,** 3749–3757 (2007).

3. Mikhailov, V. A., Ståhlberg, F., Clarke, A. K. & Robinson, C. V. Dual stoichiometry and subunit organization in the ClpP1/P2 protease from the cyanobacterium *Synechococcus elongatus*. *J. Struct. Biol.* **192,** 519–527 (2015).

4. Stanne, T. M., Pojidaeva, E., Andersson, F. I. & Clarke, A. K. Distinctive types of ATP-dependent Clp proteases in cyanobacteria. *J. Biol. Chem.* **282,** 14394–14402 (2007).

5. Gaillot, O., Bregenholt, S., Jaubert, F., Di Santo, J. P. & Berche, P. Stress-induced ClpP serine protease of *Listeria monocytogenes* is essential for induction of listeriolysin O-dependent protective immunity. *Infect. Immun.* **69,** 4938–4943 (2001).

6. Gaillot, O., Pellegrini, E., Bregenholt, S., Nair, S. & Berche, P. The ClpP serine protease is essential for the intracellular parasitism and virulence of *Listeria monocytogenes*. *Mol. Microbiol.* **35,** 1286–1294 (2000).

7. Zeiler, E. *et al.* Vibralactone as a tool to study the activity and structure of the ClpP1P2 complex from *Listeria monocytogenes*. *Angew. Chem. Int. Ed. Engl.* **50,**

11001–11004 (2011).

8. Zeiler, E. *et al.* Structural and functional insights into caseinolytic proteases reveal an unprecedented regulation principle of their catalytic triad. *Proc. Natl. Acad. Sci. USA* **110,** 11302–11307 (2013).

9. Dahmen, M., Vielberg, M.-T., Groll, M. & Sieber, S. A. Structure and mechanism of the caseinolytic protease ClpP1/2 heterocomplex from *Listeria monocytogenes. Angew. Chem. Int. Ed. Engl.* **54,** 3598–3602 (2015).

10. Hall, B. M. *et al.* Two Isoforms of Clp Peptidase in *Pseudomonas aeruginosa* Control Distinct Aspects of Cellular Physiology. *J. Bacteriol.* **199,** (2017).

11. Akopian, T. *et al.* The active ClpP protease from *M. tuberculosis* is a complex composed of a heptameric ClpP1 and a ClpP2 ring. *EMBO J.* **31,** 1529–1541 (2012).

12. Famulla, K. *et al.* Acyldepsipeptide antibiotics kill mycobacteria by preventing the physiological functions of the ClpP1P2 protease. *Mol. Microbiol.* **101,** 194–209 (2016).

13. Li, M. *et al.* Structure and Functional Properties of the Active Form of the Proteolytic Complex, ClpP1P2, from *Mycobacterium tuberculosis*. *J. Biol. Chem.* **291,** 7465–7476 (2016).

14. Ollinger, J., O'Malley, T., Kesicki, E. A., Odingo, J. & Parish, T. Validation of the essential ClpP protease in *Mycobacterium tuberculosis* as a novel drug target. *J. Bacteriol.* **194,** 663–668 (2012).

15. Raju, R. M. *et al. Mycobacterium tuberculosis* ClpP1 and ClpP2 function together in protein degradation and are required for viability in vitro and during infection. *PLoS Pathog.* **8,** e1002511 (2012).

16. Schmitz, K. R., Carney, D. W., Sello, J. K. & Sauer, R. T. Crystal structure of *Mycobacterium tuberculosis* ClpP1P2 suggests a model for peptidase activation by AAA+ partner binding and substrate delivery. *Proc. Natl. Acad. Sci. USA* **111,** E4587-95 (2014).

17. Personne, Y., Brown, A. C., Schuessler, D. L. & Parish, T. *Mycobacterium tuberculosis* ClpP proteases are co-transcribed but exhibit different substrate specificities. *PLoS One* **8,** e60228 (2013).

18. Jain, S., Graham, C., Graham, R. L. J., McMullan, G. & Ternan, N. G. Quantitative proteomic analysis of the heat stress response in *Clostridium difficile* strain 630. *J. Proteome Res.* **10,** 3880–3890 (2011).

19. Lawley, T. D. *et al.* Proteomic and genomic characterization of highly infectious *Clostridium difficile* 630 spores. *J. Bacteriol.* **191,** 5377–5386 (2009).

20. Emerson, J. E., Stabler, R. A., Wren, B. W. & Fairweather, N. F. Microarray analysis of the transcriptional responses of *Clostridium difficile* to environmental and antibiotic stress. *J. Med. Microbiol.* **57,** 757–764 (2008).

21. Chong, P. M. *et al.* Proteomic analysis of a NAP1 *Clostridium difficile* clinical isolate resistant to metronidazole. *PLoS One* **9,** e82622 (2014).

22. Sekulovic, O. & Fortier, L.-C. Global transcriptional response of *Clostridium difficile* carrying the CD38 prophage. *Appl. Environ. Microbiol.* **81,** 1364–1374 (2015).

23. Gersch, M., List, A., Groll, M. & Sieber, S. A. Insights into structural network responsible for oligomerization and activity of bacterial virulence regulator caseinolytic protease P (ClpP) protein. *J. Biol. Chem.* **287,** 9484–9494 (2012).

24. Ni, T. *et al.* Characterization of Gain-of-Function Mutant Provides New Insights into

ClpP Structure. *ACS Chem. Biol.* **11,** 1964–1972 (2016).

25. Stahl, M. & Sieber, S. A. An amino acid domino effect orchestrates ClpP's conformational states. *Curr. Opin. Chem. Biol.* **40,** 102–110 (2017).

26. Kenniston, J. A., Baker, T. A., Fernandez, J. M. & Sauer, R. T. Linkage between ATP consumption and mechanical unfolding during the protein processing reactions of an AAA+ degradation machine. *Cell* **114,** 511–520 (2003).

27. Gersch, M. *et al.* AAA+ chaperones and acyldepsipeptides activate the ClpP protease via conformational control. *Nat. Commun.* **6,** 6320 (2015).

28. Leodolter, J., Warweg, J. & Weber-Ban, E. The *Mycobacterium tuberculosi*s ClpP1P2 Protease Interacts Asymmetrically with Its ATPase Partners ClpX and ClpC1. *PLoS One* **10,** e0125345 (2015).

29. Woo, K. M., Chung, W. J., Ha, D. B., Goldberg, A. L. & Chung, C. H. Protease Ti from *Escherichia coli* requires ATP hydrolysis for protein breakdown but not for hydrolysis of small peptides. *J. Biol. Chem.* **264,** 2088–2091 (1989).

30. Liu, Y., Patricelli, M. P. & Cravatt, B. F. Activity-based protein profiling: the serine hydrolases. *Proc. Natl. Acad. Sci. USA* **96,** 14694–14699 (1999).

31. Martin, A., Baker, T. A. & Sauer, R. T. Distinct static and dynamic interactions control ATPase-peptidase communication in a AAA+ protease. *Mol. Cell* **27,** 41–52 (2007).

32. Kim, Y. I. *et al.* Molecular determinants of complex formation between Clp/Hsp100 ATPases and the ClpP peptidase. *Nat. Struct. Biol.* **8,** 230–233 (2001).

33. Brötz-Oesterhelt, H. *et al.* Dysregulation of bacterial proteolytic machinery by a new class of antibiotics. *Nat. Med.* **11,** 1082–1087 (2005).

34. Lee, B.-G. *et al.* Structures of ClpP in complex with acyldepsipeptide antibiotics reveal its activation mechanism. *Nat. Struct. Mol. Biol.* **17,** 471–478 (2010).

35. Li, D. H. S. *et al.* Acyldepsipeptide antibiotics induce the formation of a structured axial channel in ClpP: A model for the ClpX/ClpA-bound state of ClpP. *Chem. Biol.* **17,** 959–969 (2010).

36. Gil, F. & Paredes-Sabja, D. Acyldepsipeptide antibiotics as a potential therapeutic agent against *Clostridium difficile* recurrent infections. *Future Microbiol* **11,** 1179–1189 (2016).

37. Bolon, D. N., Grant, R. A., Baker, T. A. & Sauer, R. T. Nucleotide-dependent substrate handoff from the SspB adaptor to the AAA+ ClpXP protease. *Mol. Cell* **16,** 343–350 (2004).

38. Pfaffl, M. W. A new mathematical model for relative quantification in real-time RT-PCR. *Nucleic Acids Res.* **29,** e45 (2001).

39. Nørby, J. G. in *Biomembranes Part P: ATP-Driven Pumps and Related Transport: The Na,K-Pump* **156,** 116–119 (Elsevier, 1988).

Chapter 3

Phenotypic Response from the

Loss of ClpP Function in *Clostridium difficile*[2]

3.1 Abstract

Multiple antibiotic resistant *Clostridium difficile* has continued to plague hospitals and long-term care facilities for the last few decades, and represents a massive burden to the global healthcare community. *C. difficile* is an anaerobic pathogen that produces aerotolerant spores, which enables transmission to other hosts. Despite this, the process of sporulation is not well understood in *C. difficile*. However, sporulation has been researched extensively in a similar Gram-positive organism, *Bacillus subtilis*, where it was shown that loss of caseinolytic protease P (ClpP) function resulted in an asporogenic phenotype. Herein we demonstrate that each ClpP homolog maintains both distinct and shared roles in regulating sporulation in *C. difficile*. The loss of ClpP1 function appears to lead to stalled engulfment while loss of ClpP2 function may accelerate the production of small compartments. The total loss of ClpP function abolishes engulfment which precludes

---

[2] This chapter is adapted from a manuscript currently under preparation. The authors are: Nathan P. Lavey, Tyler Shadid, Jimmy D. Ballard, and Adam S. Duerfeldt. N.P.L. conducted all experiments described herein except CRISPR/Cas9 mutagenesis experiments conducted solely by T.S. which produced the ClpP mutants, and where specifically mentioned. N.P.L. and A.S.D. designed the research studies, analyzed and interpreted the data, and wrote and reviewed the manuscript. J.D.B. provided critical insight, expertise, personnel, and facilities and reviewed the manuscript.

sporulation, demonstrating the therapeutic potential for disrupting the ClpP system in *C. difficile*.

3.2 Introduction

C. difficile transmission hinges upon the production of aerotolerant spores, which spread via the fecal-oral route and propagate infection.[1–4] Despite this knowledge, strategic targeting and inhibition of sporulation to obviate the transmission cycle remains underexplored.[5–7] Major reasons for the lack of anti-sporulating approaches are that the regulatory machinery surrounding sporulation in *C. difficile* remains poorly understood and tractable targets affecting this process are limited.[8] Recently, several drugs have entered clinical trials aiming to reduce transmission through the disruption of sporulation or germination; however, none of these leads demonstrate a unique mode of action, or directly interfere with known sporulation mechanisms.[8] Vancomycin, metronidazole, and fidaxomicin are the most commonly prescribed drugs for CDI, however, their use promotes microfloral imbalance and predisposes patients to infection and/or recurrence.[7,9] Identifying new drug targets involved with sporulation is important and successful drugging of these targets would be transformative to CDI treatment, as halting sporulation would break the transmission cycle and thus simultaneously address the pathological and transmissive features of CDI.

Caseinolytic protease P (ClpP) has emerged as an attractive antibacterial target due to its global regulatory roles in cell developmental and stress response.[10,11] Although the general roles of ClpP in bacterial virulence are evolutionarily conserved, the distinct attributes regulated by ClpP are organism dependent and have not been defined in *C difficile*. In the closely related Gram-positive organism *Bacillus subtilis*, ClpP and its

74

cognate chaperones (e.g., ClpX and ClpC) regulate key pathways that influence sporulation and virulence. For example, ClpXP regulates early-stage sporulation by degrading the checkpoint polypeptide Sda, which inhibits sporulation in response to DNA damage.[12,13] On the other hand, ClpCP initiates early forespore maturation by indirectly activating σ^F through the degradation of SpoIIAB.[14,15] No ortholog of Sda is present in *C. difficile* but the RNA polymerase sigma factors (σ) and sporulation regulatory proteins (Spo-) are highly conserved.[16]

The ClpP system in *C. difficile* expresses two ClpP isoforms, ClpP1 and ClpP2, while *B. subtilis* expresses a single isoform. Sustained expression of both isoforms during vegetative and stationary growth suggests that both maintain active roles over the life cycle of *C. difficile*. Similar to *B. subtilis*, *C. difficile* expresses the ClpX and ClpC cochaperones, both of which exhibit high sequence identity to the *B. subtilis* variants (ClpX: 72% and ClpC: 60%). Comparatively, both ClpP1 and ClpP2 are highly similar to *B. subtilis* ClpP and there are no obvious differences between known regulatory domains (ClpP1: 74% and ClpP2: 63%). Interestingly, proteomic and transcriptomic studies suggest ClpP1, ClpX, and ClpC are present in purified *C. difficile* spores, while ClpP2 is absent. This suggests that ClpP1 plays an essential role in sporulation or germination and may interact with ClpX or ClpC. Given the parallels between sporulation in both organisms, we hypothesized that ClpP1 and ClpP2 influence sporulation in *C. difficile*, but that each isoform exhibits disparate roles.

This chapter describes our initial phenotypic studies with *clpP1*, *clpP2*, and *clpP1/clpP2* knockout mutants produced in collaboration with Dr. Jim Ballard's laboratory. These mutants were generated using a novel CRISPR-Cas9 nickase system, and

these results represent the first application of this methodology. Each *clpP* mutant has been genomically sequenced to ensure no off-target mutations occurred, and that no significant mutations exist in laboratory-maintained strain of *C. difficile* 630. The data presented herein demonstrate that 1) ΔP1 mutants have lower sporulation efficiency, and severe morphological abnormalities during forespore engulfment; 2) ΔP2 mutants hypersporulate but have little morphological differences overall; 3) ΔP1P2 mutants fail to sporulate; and 4) all three mutants exhibit decreased levels of cytotoxicity. Bright-field, fluorescence, and transmission electron microscopy reveals the ΔP1P2 mutant to form multiple small-compartments that are engulfed to begin the forespore lifecycle, yet fail to mature or become viable. Lastly, we propose a working model of sporulation that incorporates overlapping and distinctive roles for ClpP1 and ClpP2 in regulating sporulation.

3.3 Results

3.3.1 clpP mutants are less cytotoxic, ΔP1 is sensitive to heat-shock
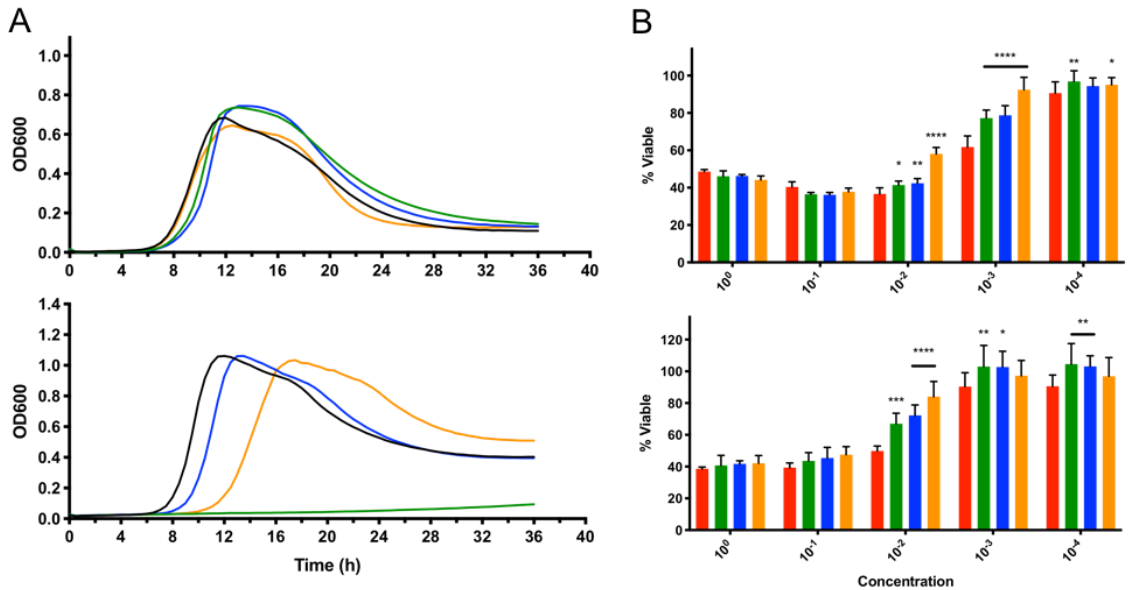
Figure 3.1 Growth profiles for *clpP* mutants and cytotoxicity TcdB titer assay
(A) *C. difficile* were grown anaerobically at 37 °C (top) and 42 °C (bottom) and OD600 was continually monitored over 36h. (B) Natively purified TcdB from *C. difficile* 630 was used to titer relative TcdB toxin levels against CHO (top) and Caco-2 (bottom) mammalian cells (WT *red*, ΔP1 *green*, ΔP2 *blue*, ΔP1P2 *orange*, for all figures).

WT and mutant *clpP* strains exhibit similar growth profiles in supplemented Brain Heart Infusion (BHIS) media at 37 °C (**Figure 3.1A**, top). The ΔP1 mutant was unable to replicate under heat-shock conditions at 42 °C, while ΔP2 grew similarly to the WT (**Figure 3.1A**, below). Despite ΔP1 growth inhibition at the elevated temperature, the ΔP1P2 mutant was able to replicate under heat-shock conditions, albeit at a substantially slower growth-rate. In minimal-defined media, all mutants deviated from WT growth under heat-shock conditions (**Appendix B.1**). ΔP1 replicates minimally before entering stationary growth, while ΔP2 and ΔP1P2 grow exponentially before shifting to the

77

stationary phase at different time points. None of the mutants significantly differed in motility (**Appendix B.2**).

The uncoupled activity of ClpP1 and ClpP2 described in Chapter 2 led us to anticipate disparate roles in biology, manifesting phenotypes linked to their respective regulatory function. In a recent study, Baker *et al.* suggest *Pseudomonas aeruginosa* ClpP1 and ClpP2 exhibit separate roles in virulence.[17] Though a Gram-negative organism, the results demonstrate that each ClpP isoform maintains specialized functionality and are differentially expressed between exponential and stationary growth. ClpP1 plays an important role in toxin production, while ClpP2 influences late-stage adhesion and microcolony formation. We anticipated a similar outcome in *C. difficile* and began by examining cytotoxicity in the *clpP* mutants. In a TcdB toxin titer assay using Chinese Hampster Ovarian (CHO) (**Figure 3.1A**, top) and Caco-2 endothelial cells (**Figure 3.1A**, bottom), all mutants exhibited one to two-fold lower cytotoxicity in comparison to the WT. ΔP1 and ΔP2 exhibit similarly reduced cytotoxicity levels, while ΔP1P2 is the least toxic mutant. Here we observed equal contributions to cytotoxicity from each isoform deletion, with an additive effect being observed in the ΔP1P2 mutant. Therefore, either ClpP isoform is likely sufficient to rescue toxin production and/or secretion.

3.3.2 Sporulation phenotypes differ significantly between mutants
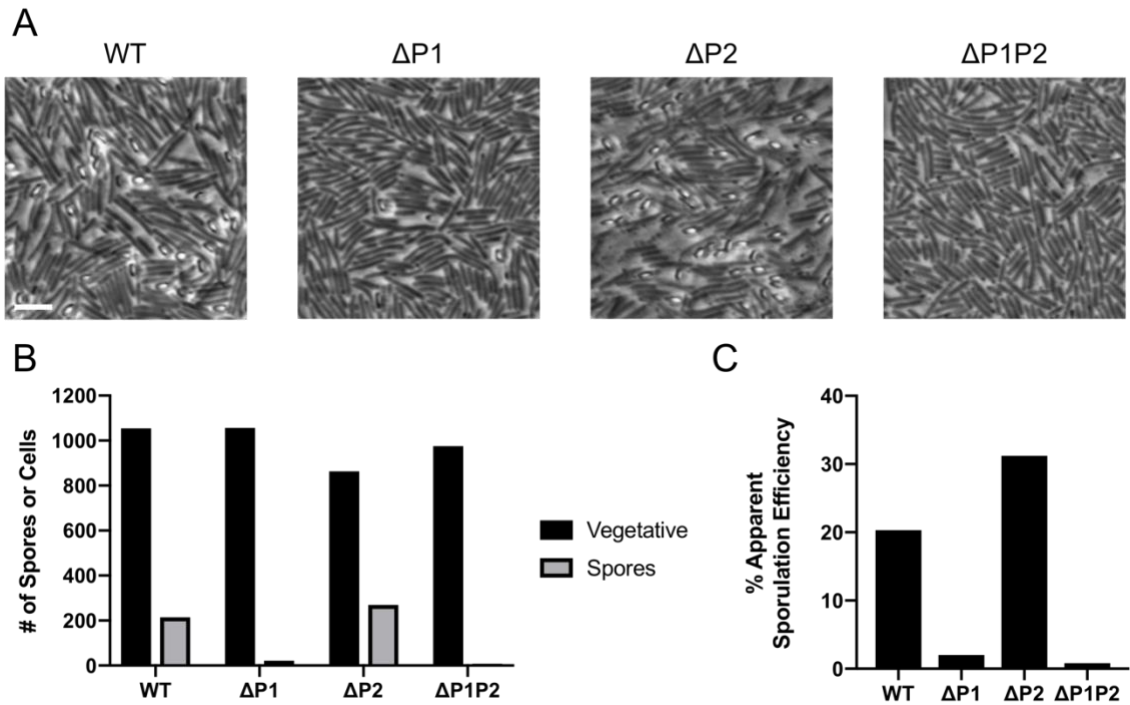
Figure 3.2 Bright field microscopy and semi-quantitative analysis shows varied sporulation in ΔP1 and ΔP2

(A) Bright field microscopy images were taken with a DP8 Olympus Camera (Ph3, 100x), of each strain after 20-23 h of growth on 70:30 plate media. Cells were embedded into 1% agarose and sealed with a coverslip surrounded in vacuum grease. Vegetative *C. difficile* are phase-dark rods, while spores appear phase-bright. Scale bar = 5 μm. (B) Areas of significantly high cell density were counted under high phase-contrast, which show vegetative cells as phase-dark rods, and spores as small phase-bright ovals. Apparent sporulation efficiency was calculated by (# phase-bright spores / # vegetative cell) x 100%.

Cultures of each mutant entering exponential growth were plated on 70:30 (70% BHIS and 30% sporulation media culture (SMC)) media and incubated for ~20 h prior to examination via phase microscopy. 70:30 plate media is generally believed to enhance *C. difficile* sporulation, and yields more reproducible spore counts.[18] Samples were examined via bright field microscopy to assess apparent sporulation efficiencies (ASE) for each mutant, calculated by dividing the total number of phase-bright spores by the total number

of vegetative cells (**Figure 3.2A and B**). This is a qualitative method, which makes broad conclusions about the sporulation efficiency being observed and is simply suggestive as entities other than spores can appear phase-bright. ΔP1 produced phase-bright spores with approximately 2.0% ASE, while ΔP2 exhibited hypersporulation, and was 10.3% more efficient than the WT. Surprisingly, we found the ASE for ΔP1P2 was <0.10%, significantly lower than the WT (**Figure 3.2C**).

To qualitatively measure *clpP* mutant sporulation, samples were taken after ~22 h incubation from 70:30 plates. Half of the sample is initially struck out on BHIS media supplemented with taurocholate to enumerate vegetative cells and spores[19–21] to get a total cell count. The other half is heat-treated to kill vegetative cells, while retaining mature spores that are heat-tolerant. Dividing the number of spores enumerated by the total number of cells provides the sporulation efficiency. This method provides more robust results that are highly repeatable, as it excludes counting immature spores that also appear phase-bright. After heat-treatment, ΔP1 sporulation efficiency was found to be 69% lower than the WT, suggesting that spores produced in ΔP1 are more susceptible to heat-inactivation (**Figure 3.3A**). ΔP2 sporulation efficiency did not significantly differ from WT (**Figure 3.3A**), despite apparent hypersporulation when quantified via bright field microscopy. Spores were not observed in ΔP1P2 after heat-treatment, which suggests any spores observed via bright field microscopy were immature. From these results, we determined that sporulation was severely inhibited in ΔP1 and ΔP1P2, while the ΔP2 mutant produced approximately the same quantity of heat-tolerant spores as the WT.

Interestingly, if sporulation efficiency was assessed in BHIS broth rather than 70:30 plate media, ΔP1 and ΔP2 fail to produce spores above the limit of detection (1 x 10^2 CFU) after 24 h of incubation. As such, ΔP1 and ΔP2 initially produce less spores than the WT in BHIS broth (**Figure 3.3B**). However, both mutants will produce similar quantities of mature spores as the WT, given >72 h incubation, which suggests the rate of sporulation lags in *clpP* mutants. ΔP1P2 was not found to sporulate in BHIS broth, despite incubation to endpoint sporulation at 6 d. It is generally believed that *C. difficile* sporulation is complete at the 6 d timepoint (>144 h).[22] ΔP1P2 spore enumeration at 6 d was performed via heat-treatment and ethanol treatment to differentiate between heat and ethanol susceptibility. Spore outgrowth was not observed in either method at endpoint incubation for ΔP1P2.
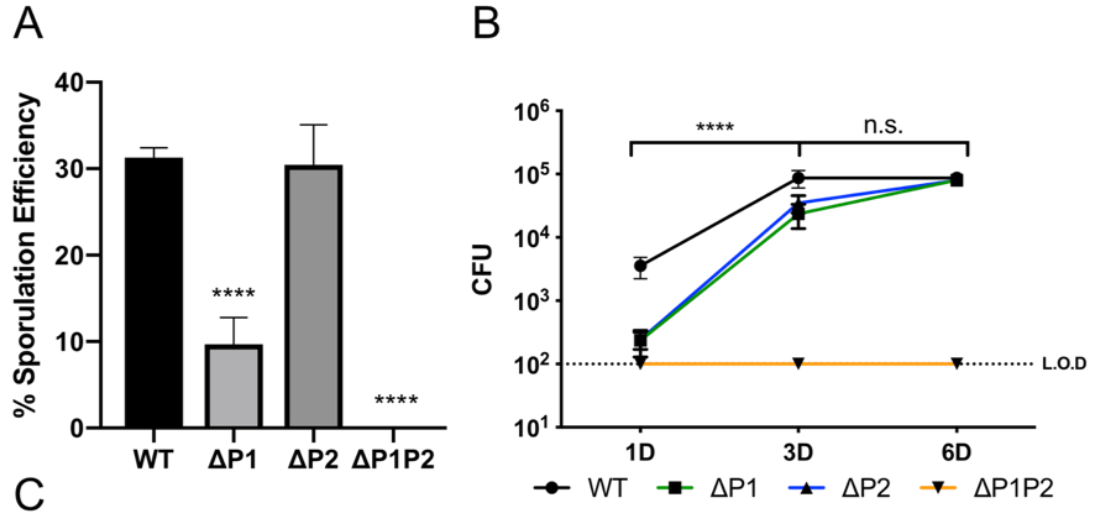
Figure 3.3 Sporulation efficiency and rate aberrations in *clpP* mutants
(A) Sporulation efficiency was measured after sporangia heat-inactivation on 70:30 plate media. (B) Rates of sporulation in BHIS broth for WT and *clpP* mutants. (L.O.D. Limit of detection, 1×10^2 CFU) (C) Table of sporulation efficiency experimental results. (n.d. not determined)

Notably, bright field microscopy analysis of ΔP1P2 revealed frequent elongated cell phenotypes, with multiple phase-bright spore-like structures populating the length of the cell (**Appendix B.3**). These elongated cells were significantly longer, averaging approximately 521 µm while normal vegetative *C. difficile* cells are 4-5 µm. It should be noted that while elongated cells were observed frequently, not all exhibited multiple phase bright regions. Of those that did, phase-bright spore-like structures were present asymmetrically, and stochastically spaced. These observations indicate that ΔP1P2 may be

able to initiate sporulation but fails to coordinate the initial forespore development or engulfment.

To vividly illustrate differences in forespore development and sporulation, we performed fluorescence microscopy with samples of sporulating cultures. Samples were propagated in SMC media for ~23 h to sufficiently induce sporulation prior to harvesting.[23] Hoescht 33342 (referred to hereafter as Hoescht), which penetrates vegetative cells and immature spores, was used to stain nuclear DNA (blue). Samples were harvested and immobilized on 1% agarose pads on glass slides mixed with the lipophilic dye FM 4-64 (red), which stains bacterial cell walls and spore coats bright red. Mature spores are expected to appear red, as they exclude Hoescht and only retain FM 4-64, providing significant contrast between forespores and mature spores.[24]
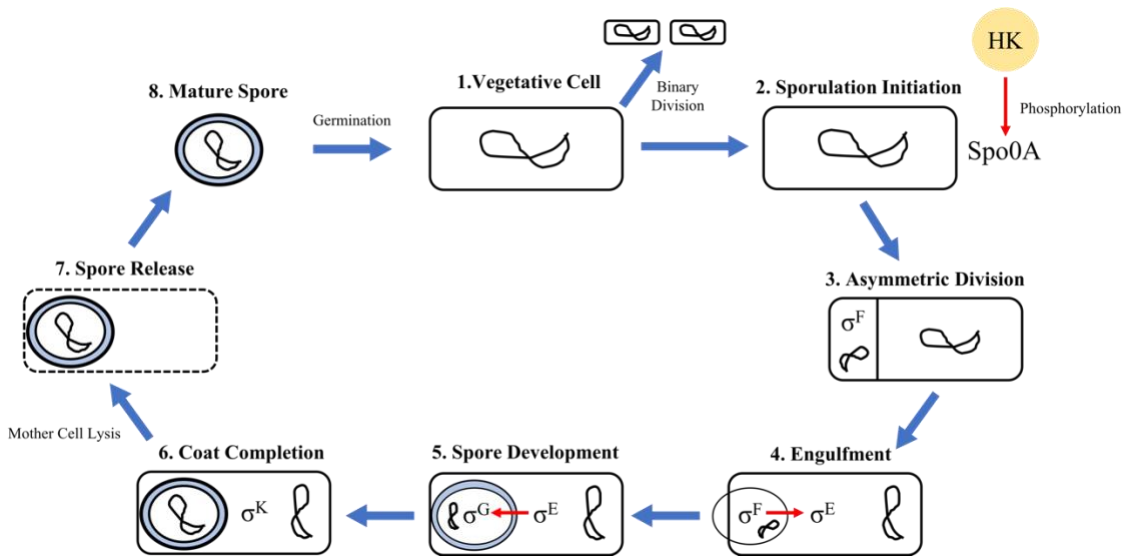
Figure 3.4 Sporulation in *C. difficile*
Sporulation in *C. difficile* occurs via a highly conserved process across spore-forming bacteria, that generally begins with the activation of Spo0A to initiate asymmetric division and begin sporulation. A small compartment containing compacted genomic material will be shed, then rapidly engulfed in a phagocytic-like mechanism. Activation of Spo0A will

83

inhibit SpoIIAB (anti-σ^F), leading to σ^F activation that localizes to the pre-forespore prior to engulfment completion. σ^F coordinates initial forespore development, which will then activate σ^E upon engulfment to begin forespore development and activate σ^G when the forespore has been fully engulfed. Image adapted and modified with permission.

In WT cells, the mature forespore is localized to one pole and brightly fluoresces with FM 4-64 stain. ΔP1 forespore engulfment is delocalized and overlaps the outer membrane, which may indicate defective or delayed engulfment (**Figure 3.5**, ΔP1). The intracellular location of ΔP2 forespores are varied, which may result in premature spore release (**Figure 3.5**, ΔP2). Elongated ΔP1P2 mutants formed multiple lipid-dense particles throughout the length of the cell which appeared spore-like (**Figure 3.5,** merged ΔP1P2). The abnormal forespores in ΔP1P2 were also found to delocalize across the cell wall, suggesting deficient or stalled engulfment. Overall, ΔP1P2 appears to lack coordinated asymmetric division during the initial stages of sporulation, resulting in: 1) abnormal septation, 2) multiple apparent forespores throughout the elongated cell, 3) unsuccessful engulfment. To structurally interrogate sporulation and the spores themselves, we decided to perform transmission electron microscopy (TEM) on sporulated cultures.
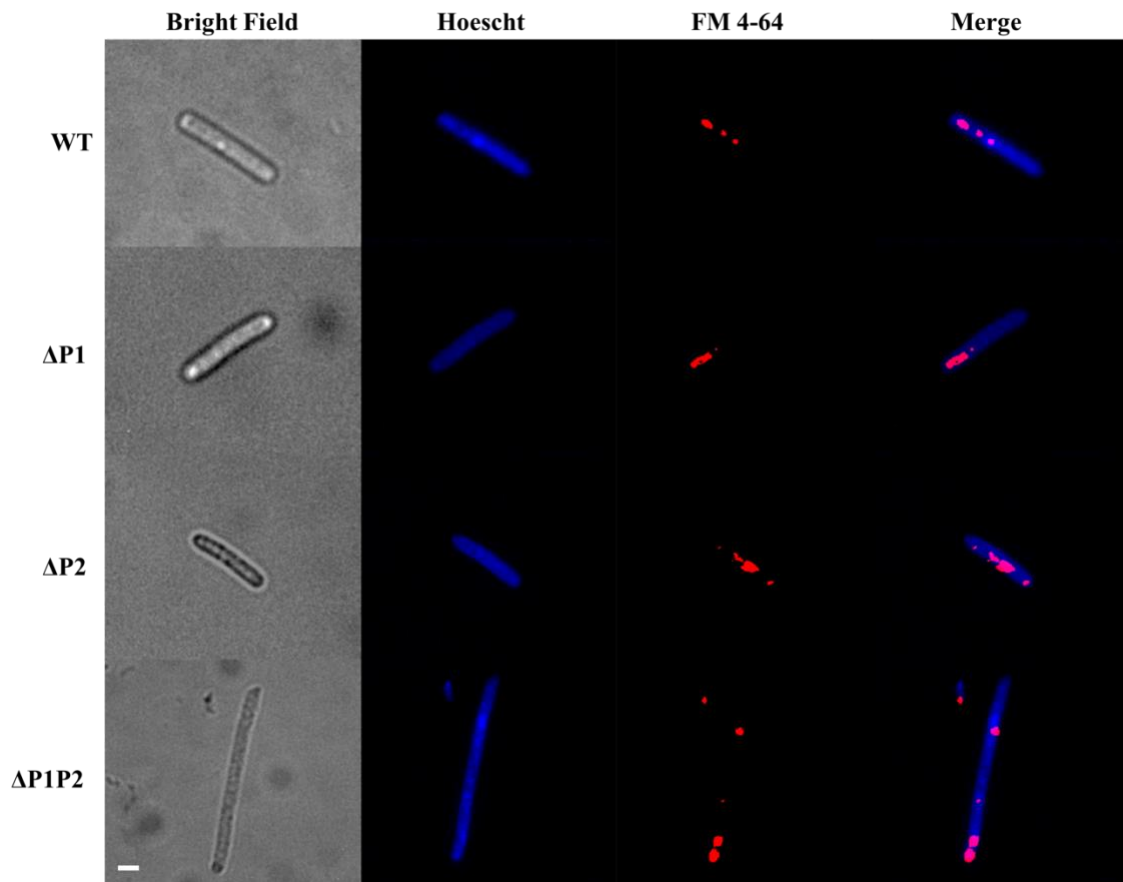
Figure 3.5 Forespore development in sporulating cultures imaged with fluorescent microscopy

Sporulating cultures of *C. difficile* and *clpP* mutants were obtained with a Zeiss Axiovert 200m at 63x magnification under oil-immersion. A differential contrast filter was used to obtain phased bright-field images. Cells were stained with Hoescht (blue channel) and FM 4-64 (red channel) to differentiate between DNA and bacterial cell wall, respectively. 0.1 µm Z-stacked images were obtained in red and blue channels to aid focusing and reduce the background noise. Individual color channels were merged into a composite and normalized with ImageJ.[25] Scale bar represents 1 µm.

3.3.3 Loss of ClpP function results in morphological distortions during spore development

Successfully engulfed forespores were observed in the ΔP1 mutant that were morphologically similar to WT and absent of obvious structural abnormalities (**Figure 3.6**). However, ΔP1 also exhibited severe morphological abnormalities during what appears to be forespore engulfment (**Figure 3.7A**). Nearly half (47.9%) of sporulating cells appeared

to have stalled during forespore engulfment, and of those that were successfully engulfed 30.9% displayed distorted phenotypes (**Figure 3.7B**). Though we cannot state this definitively in thin-section TEM without Z-stack analysis, as cells are oriented over one another. Interestingly, some possessed phase-dark spots flanking the forespore (**Figure 3.7A**). Perhaps this is compressed outer cell membrane or an aggregation of the engulfment machinery, but this is purely speculative. Together, these results hint towards ΔP1 possibly generating a stalled engulfment phenotype, but this evidence alone is not enough to conclusively suggest so.
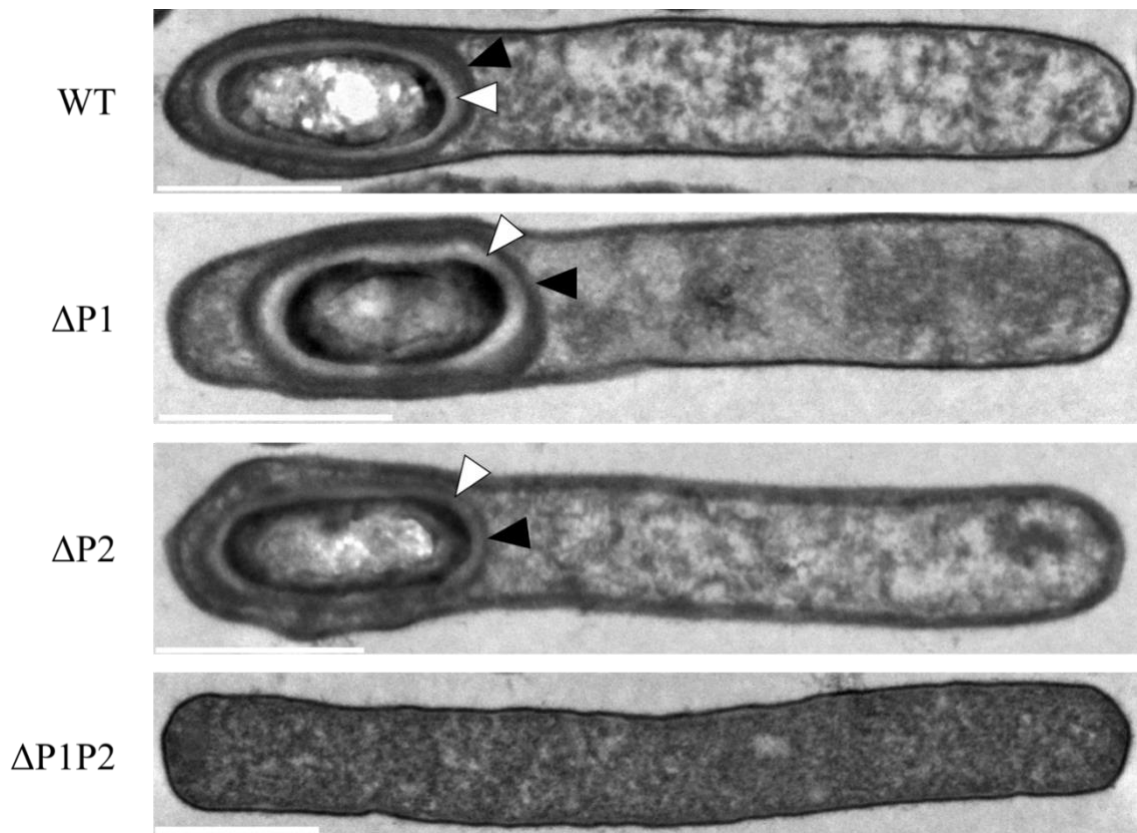
Figure 3.6 Typical cellular morphology of each strain in sporulating cultures

ΔP1 and ΔP2 produced characteristic forespore morphologies, while no spores were observed in ΔP1P2 cells. White arrows denote light-colored areas between the spore coats, which appear to be the cortex. Black triangles indicate forespore coat proteins. Scale bars represent 1 µm. See **Appendix B.4-B.11** for overview TEM images.

Loss of ClpP2 function did not correlate with an increased frequency of apparent sporulation errors when compared to the WT (**Figure 3.6**). However, ΔP2 mutants produced an abundance of small vesicles that are regularly dispersed throughout each thin section sample that was analyzed (**Appendix B.8**). These appear to be small compartments that are released coinciding with the initiation of sporulation, which are subsequently engulfed to form the forespore. Similarly, an abundance of small compartments was observed throughout ΔP1P2 in TEM analysis. ΔP1P2 mutants attempted engulfment though no spores or intracellular structures containing a forespore were observed, suggesting loss of both ClpP1 and ClpP2 function renders *C. difficile* unable to complete engulfment.
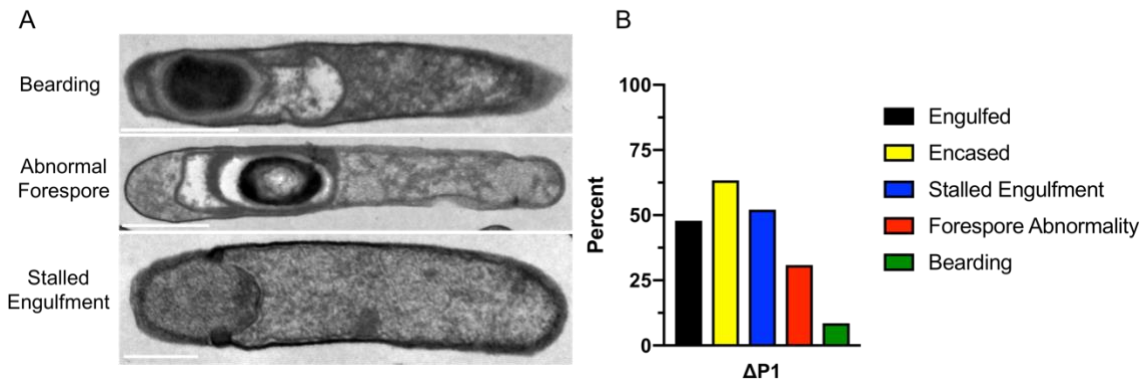
Figure 3.7 Representative TEM images of apparent ΔP1 morphological abnormalities (A) TEM images of ΔP1 depict irregular morphologies related to sporulation. Scale bars represent 1 µm (B) Morphological abnormalities were quantified by counting at least 100 cells per biological replicate.

In order to determine whether the spore ultrastructure was impacted by loss of ClpP function, spores were isolated and purified from sporulating cultures.[26] Mature *C. difficile*

spores are composed of several distinct layers as shown in **Figure 3.8A**. No attached exosporium was observed in ΔP1 and ΔP2 spores, which rarely remain intact during spore purification and TEM preparation.[27] ΔP1 and ΔP2 spores were not found to significantly differ in overall spore ultrastructure, forming characteristic spore coat layers and dense cortex (**Figure 3.8B**). ΔP1P2 formed circular structures similar in shape and size to spores isolated in the WT but lacked any structural features of a typical spore (**Figure 3.8A** and **B**).
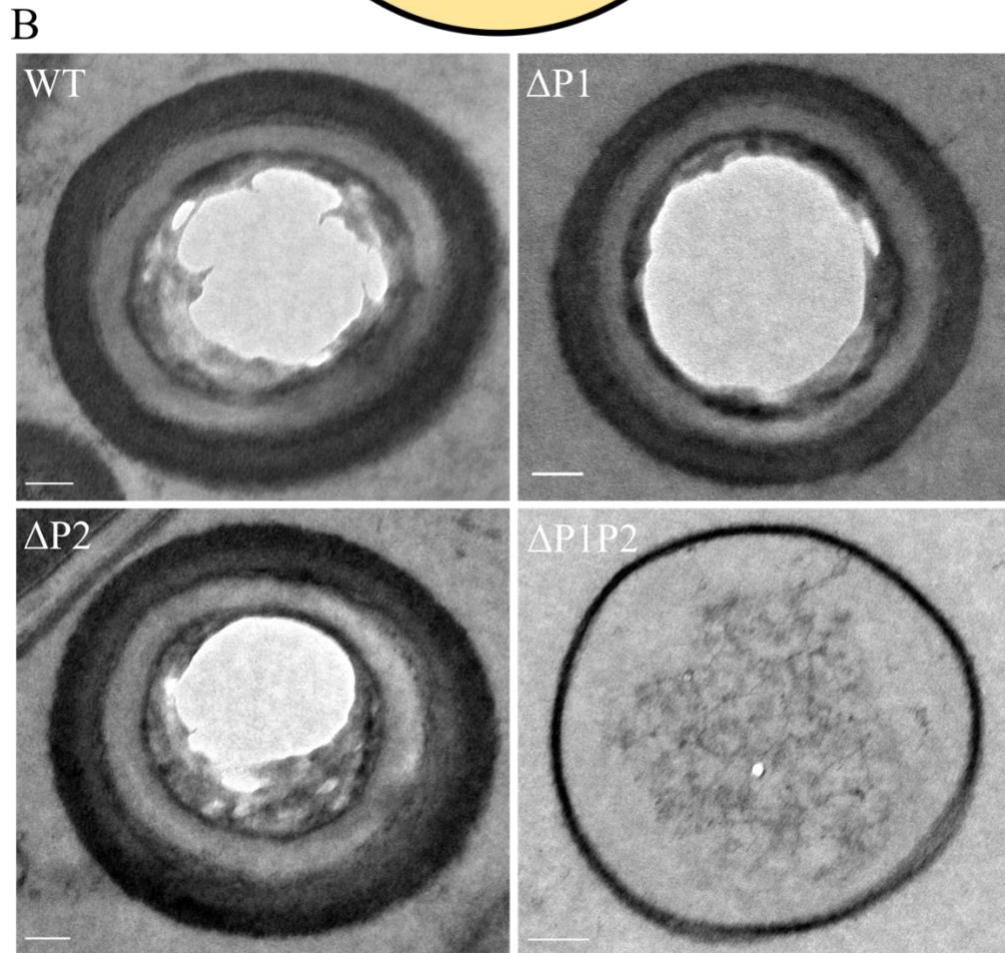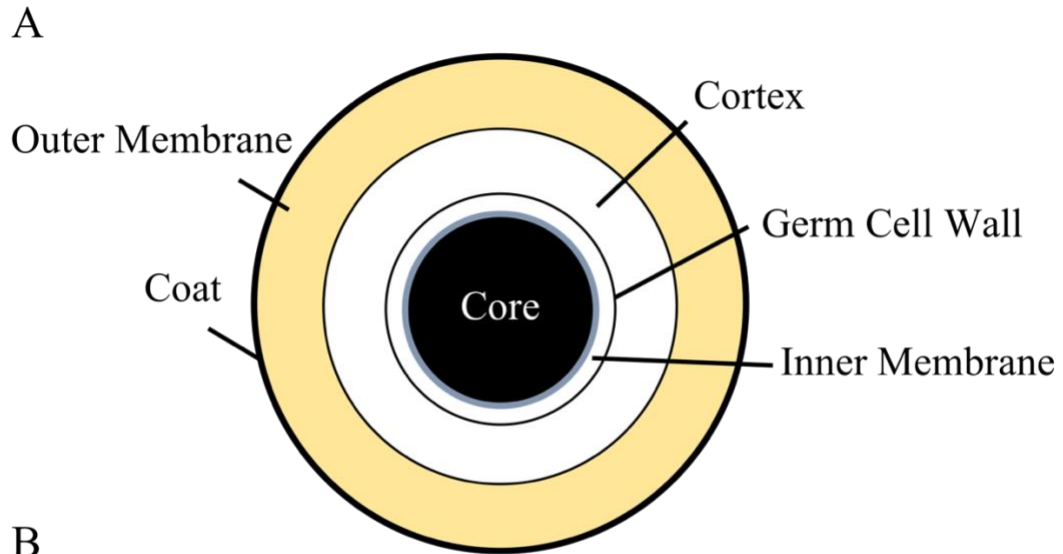
Figure 3.8 ΔP1 and ΔP2 produce mature spores, ΔP1P2 spores are immature
(A) Mature spore structure (B) TEM analysis of purified spores from each strain. The coat proteins and denseness of the core itself in mature spores will often prohibit total resin

penetration, causing the core to appear hollow. ΔP1 and ΔP2 are able to produce mature spores, while ΔP1P2 produces porous vesicles. Scale bar represents 100 nm.

ΔP1P2 appears to be unable to complete engulfment to produce a forespore, which precludes spore formation. ΔP1P2 sporulation efficiency at endpoint sporulation was 0%, failing to produce mature spores which could be enumerated after heat-treatment. Taken together with the results from our TEM analysis, it appears total loss of ClpP function in *C. difficile* generates an asporogenic phenotype. ΔP1 also struggles to complete engulfment, while ΔP2 appears to produce mature spores similarly to WT. Although ΔP1 can eventually complete engulfment, ΔP1P2 is unable to do so. Taken together this suggests that ClpP2 may regulate engulfment directly or indirectly through an unknown mechanism. ΔP2 mutants produce an abundance of small vesicles similar to ΔP1P2, otherwise they are phenotypically similar to WT. This suggests differentiated roles for each ClpP isoform at the initiation of engulfment, which overlaps with engulfment completion. To determine a possible reason for the errors during engulfment we examined the relative expression of known sporulation regulators in *C. difficile*.
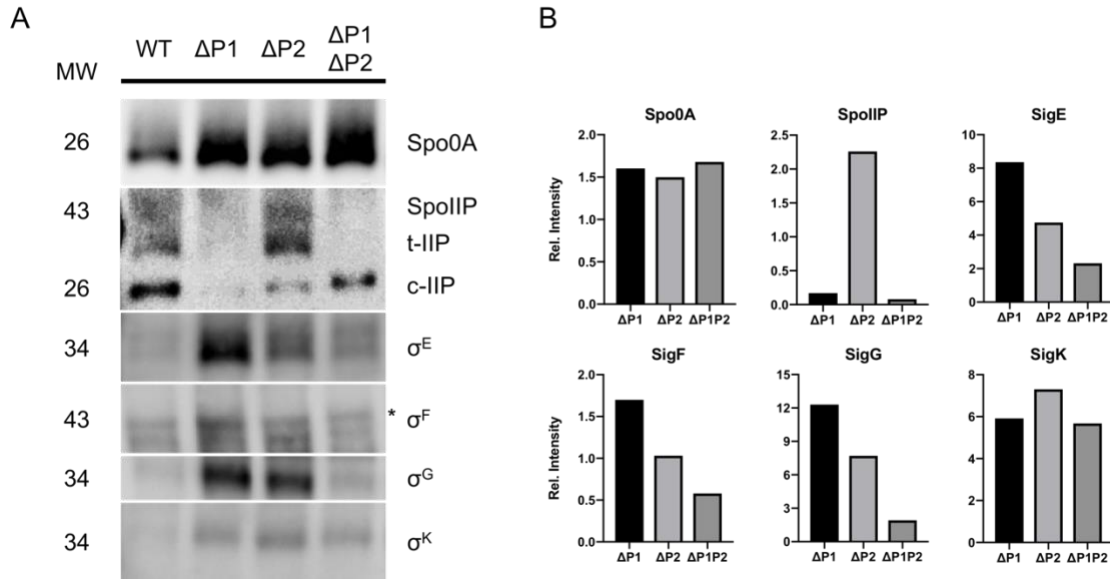
Figure 3.9 Western blot analysis of sigma-factors that control sporulation in *C. difficile*
(A) Samples at exponential phase were plated onto 70:30 media to induce sporulation over 44 h. Molecular weights (MW) are shown to the left (kDa) while each corresponding sporulation factor is to the right. Asterisk indicates an off-target band which has previously been observed.[28] (B) Relative intensities of individual bands when compared against WT.

Spo0A is the master sporulation regulator in *C. difficile* and is highly conserved across spore-forming Gram-positive organisms.[1,29–31] Spo0A regulates ~75% of the sporulation-related genes in *C. difficile*, and ultimately controls the initiation of the sporulation cascade.[8] Loss of Spo0A function renders *C. difficile* unable to express any of the σ-factors necessary to orchestrate sporulation, precluding sporulation.[28] Spo0A is overexpressed in all mutants, which may be indicative an attempt to rescue sporulation or a general stress response. Alternatively, ClpP may regulate systems that inhibit or promote sporulation (e.g., CodY is a known substrate of ClpCP), thus ClpP may indirectly participate in sporulation regulation. σ-factors present in the mother cell and forespore are

activated during specific phases of sporulation after Spo0A is activated by phosphorylation (**Figure 3.4**). σ^F and σ^G, which are confined to the forespore, are activated following asymmetric division. σ^E and σ^K reside in the mother cell and coordinate expression with other forespore σ-factors via cell-cell communication. Upon phosphorylation, Spo0A activates σ^F immediately following asymmetric division to coordinate early stages of sporulation. The ΔP1 and ΔP2 mutants exhibit slightly elevated levels of σ^F to the WT, while ΔP1P2 σ^F expression is lower than WT expression (**Figure 3.9**). σ^E activation follows soon after σ^F to direct forespore development in the mother cell. The ΔP1 mutant significantly overexpresses σ^E, while ΔP2 exhibits increased expression compared to the ΔP1P2 mutant but less than ΔP1, and displays a similar phenotype as previously reported in *sigG* mutants.[28] σ^G expression is upregulated following the completion of engulfment, and both ΔP1 and ΔP2 mutants overexpressed σ^G, while the ΔP1P2 expression is similar to the WT. σ^G activates σ^K, concluding engulfment, and only occurs in the presence of expressed SpoIIIA-operon proteins. All three mutants express similar levels of σ^K, whose expression does not rely upon activation of a former σ-factor.
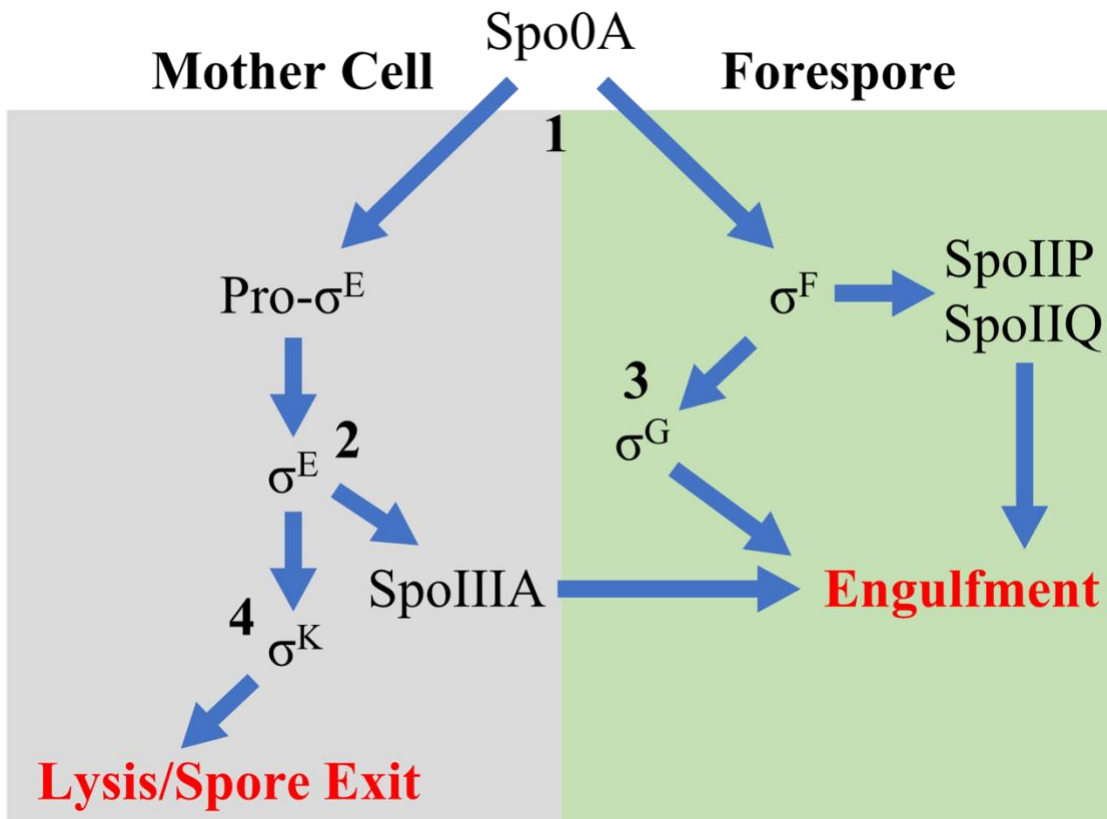
Figure 3.10 Sequence of sigma factor activations and sporulation processes
Sigma factors are activated following Spo0A phosphorylation which initiates sporulation
1) σ^F is activated and upregulates SpoIIP and SpoIIQ which signals the start of engulfment.
Simultaneously Pro-σ^E is processed to σ^E in the mother cell, which starts organizing initial
forespore development factors 2) σ^E upregulates SpoIIIA which also signals engulfment 3)
σ^G activity is stimulated by σ^F, which typically coincides with completion of engulfment
4) σ^K activity is stimulated by σ^E, which then upregulates expression of coat proteins and
coincides with mother cell lysis and subsequent spore release.

SpoIIP is part of the "DPM" complex comprised of SpoII**D**, SpoII**P**, and SpoII**M**,
which functions to initiate and complete engulfment during sporulation.[32–34] Successful
engulfment requires the steady degradation of mother cell wall composed of peptidoglycan
and proceeds via a "zipper-like" mechanism.[32] SpoIID engulfment machinery "pulls" the
mother cell around the forespore, while SpoIIP degrades peptidoglycan coordinated by the
scaffolding protein SpoIIM, to enclose the forespore within the germ cell wall and form a

layer of the outer spore coat. Loss of SpoIID, SpoIIP, or SpoIIM will trigger the engulfment vesicle to collapse, and push the small compartment outward. ΔP1 and ΔP1P2 lack SpoIIP expression, offering a possible explanation as to why the possibly defective forespore engulfment occurs in the former, and inhibited in the latter.

3.4 Discussion
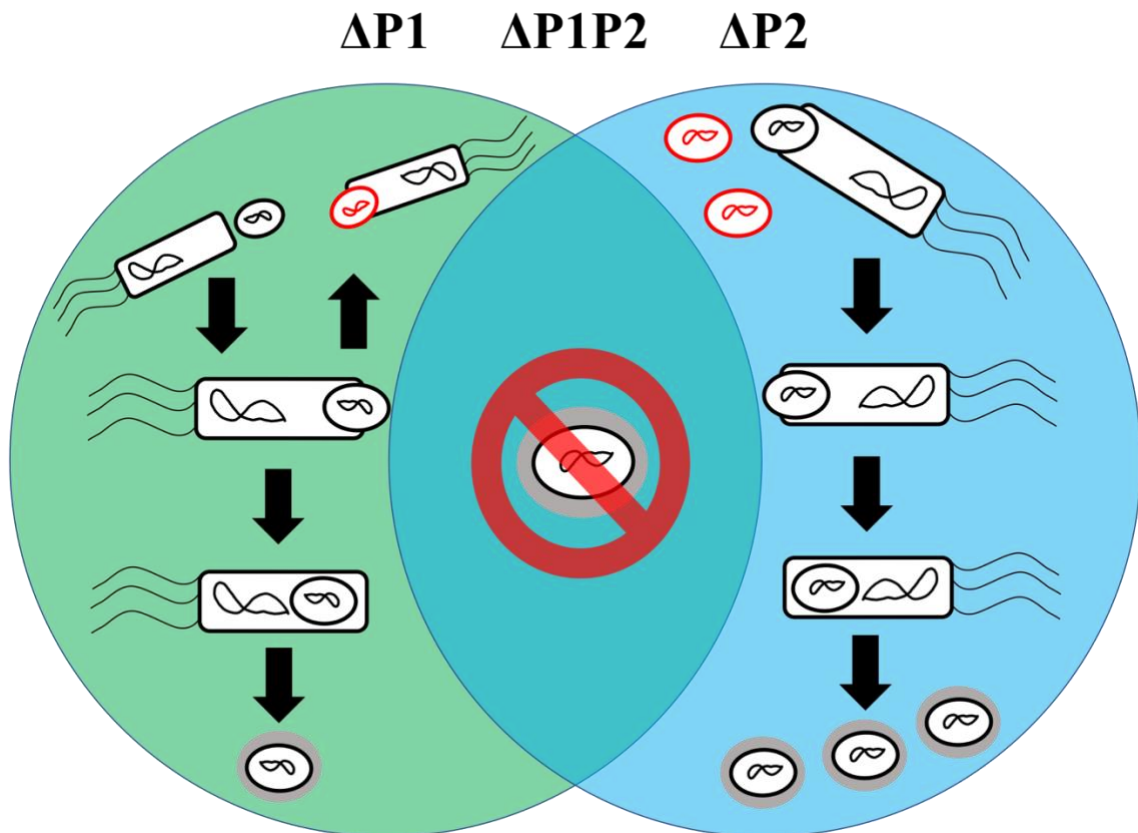
Figure 3.11 Venn-diagram summary conclusion
Summary of the overall conclusion drawn from this work. ΔP1 frequently fails to engulf the forespore, producing less spores overall. ΔP2 Is similar to WT in spore efficiency, but appears to make more pre-spore structures. ΔP1P2 is unable to produce mature spores.

The work described in this chapter builds upon work described in Chapter 2, which describes the biochemical characterization of recombinant ClpP1 and ClpP2 *in vitro*. Our

results from this study broadly reveal differences in sporulation and cytotoxicity phenotypes for all of the ClpP mutants generated. We to successfully produced knockout mutants of *clpP1*, *clpP2*, and the dual *clpP1/clpP2*. Our attempts at ΔP1P2 complementation have failed thus far due to the inherent design of the CRISPR/Cas9 mutagenesis system employed. Complements have been produced for both *clpP1* and *clpP2*, but we have had difficulty replicating experimental results to demonstrate reversion to WT behavior. We believe this is likely due to the requirement of thiamphenicol within the culture media during complementation growth. This is needed to select for *C. difficile* that retains the complement plasmid encoding thiamphenicol resistance. Thiamphenicol degrades rapidly at elevated temperatures and we speculate that as the concentration decreases, *C. difficile* rejects the plasmid and reverts back to the mutant phenotype.[35]

To address this issue, we have pivoted to a new strategy, which will incorporate the CRISPR/Cas9 machinery into the *C. difficile* chromosome, allowing tunable genetic silencing via the introduction of targeting vectors. The targeting vectors will contain our guide sequence (gRNA) and be integrated chromosomally via homologous recombination. In this manner, the CRISPR/Cas9 machinery will be natively expressed at a basal rate and integration of the targeting vector to the CRISPR/Cas9 operon will ensure our gRNA will be produced. Therefore, it is not necessary to retain the targeting vector as the point mutation will be permanent. Our current vector contains the CRIPSR/Cas9 machinery, thiamphenicol resistance, gRNA, and homologous recombination region resulting in a >10kb plasmid. This reduces the likelihood it is retained during normal binary division. Integration to the chromosome will lower the size of the plasmid to 2 kb, significantly increasing the likelihood complementation will be successful. As stated earlier, whole

genome sequencing was performed on our WT strain of *C. difficile* 630 along with biological triplicates of each mutant. No off-target mutations were observed, and no mutations were present in any gene known to impact sporulation or virulence prior to or after CRISPR/Cas9 mutagenesis. Thus, we are confident that an alteration in experimental approach will provide a means to overcome the short-comings of the previous strategy.

Loss of either ClpP1 or ClpP2 equally decreases cytotoxicity and loss of both homologs additively reduce cytotoxicity against both CHO and Caco-2 cell lines. Growth profiles for all mutants vary in response to elevated temperature, with significant differences observed when grown in a defined minimal medium,[37,38] particularly under heat-shock. Heat-treating cells reveals a reduced sporulation efficiency for ΔP1, 69% lower than the WT. Spores produced by ΔP1 are more susceptible to heat-inactivation, in contrast to ΔP2 which possess a sporulation efficiency similar to the WT. This differs from spore quantitation results produced via bright field microscopy that suggest ΔP2 may produce spores that are immature and therefore heat-intolerant. We failed to observe any ΔP1P2 spores post heat-treatment, indicating that any spores observed via bright field microscopy were immature or were phase-bright artifacts. From these results, we determined that sporulation is substantially inhibited in ΔP1, and unlikely to occur in ΔP1P2. ΔP2 maintained similar levels of sporulation to the WT.

ΔP1 forespore engulfment overlaps between the forespore and cell wall, which was not frequently observed in WT, which may be indicative of defective engulfment. The intracellular location of ΔP2 forespores varies, which may allow for the forespore to disengage or prematurely release from the mother cell. The elongated ΔP1P2 mutant

commonly forms multiple brightly staining spore-like structures throughout the length of the cell. The brightly stained vesicles could also be septa, repetitively forming and dividing, and so on to elongate the cell. Hoescht stain trails one of the lipid-dense areas, suggesting DNA condensation towards that point which is a precursor to asymmetric division. These results demonstrate a lack of coordinated asymmetric division, and irregular sporulation initiation occurring towards the cell poles.

TEM results demonstrated the ability of ΔP1 and ΔP2 to sporulate, while ΔP1P2 failed to produce spores or forespores. ΔP1 is able to overcome what appears to be delayed or stalled engulfment, though phenotypic abnormalities seem to arise during sporulation, to produce mature spores that are morphologically similar to WT. ΔP2 mutants do not show an abnormal sporulation phenotype. Instead, loss of ClpP2 function leads to overproduction of small vesicles also apparent in ΔP1P2 mutants. ΔP1P2 produces circular vesicles similar in size to mature spores, though no characteristic spore layers form. Purified spore samples analyzed via TEM also show fully mature spores produce by ΔP1 and ΔP2 mutants, whereas the ΔP1P2 mutant produces only the pseudo-spore husks.

Western blot results reveal that ΔP1 and ΔP2 overexpress σ^F, which has previously been observed in σ^E mutants that exhibit a stalled sporulation phenotype.[16,28] σ^E is highly overexpressed in ΔP1, and slightly less so in ΔP2, signaling activation of sporulation factors present in the mother cell that coincide with successful engulfment. In this manner, σ^E is more strongly overexpressed in ΔP1, which may indicate an attempt to rescue engulfment. Recent studies have demonstrated that σ^E is required for engulfment machinery expression, offering an explanation for the ΔP1 mutant exhibiting increased

evidence of stalling during this phase of sporulation.[34,36] However, σ^E is dispensable in σ^G activation, and σ^G can be activated without the presence of σ^E or σ^F,[28] suggesting that ClpP1 and ClpP2 both play a role in indirectly regulating σ^G expression.

SpoIIP expression is abolished in ΔP1 mutants, but significantly overexpressed in ΔP2. σ^F has been shown to positively regulate SpoIIP expression and subsequent SpoIIP processing, which is absent in ΔP1 despite increased SigF expression. ΔP2 processes SpoIIP and exhibits sporulation efficiency similar to the WT, agreeing with previous reports that SpoIIP is required for engulfment and sporulation.[32] SpoIIP is processed to the cleaved form in the ΔP1P2 mutant, which cannot form mature spores. This is contrary to ΔP1 mutants, which express virtually no forms of SpoIIP but still form viable spores. From this, it seems ClpP1 function is necessary for efficient SpoIIP processing, though loss of ClpP1 function does not always arrest sporulation. Loss of ClpP1 and ClpP2 function restores SpoIIP processing to form cleaved SpoIIP but cannot form mature spores suggesting alternate regulatory roles for ClpP1 and ClpP2.

No spores or engulfed forespores are observed in ΔP1P2 mutants, which suggests that cooperativity may exist between ClpP1 and ClpP2 in order to complete sporulation. Perhaps *in vivo*, a heteromeric ClpP1/ClpP2 complex is formed that cooperates with sporulation regulatory factors. Previously, we were unable to produce a heteromeric ClpP1/ClpP2 complex *in vitro* using recombinant protein, but we are cognizant that recombinant approaches fail to accurately mimic the complex nature of the cell and thus does not rule out heterocomplex formation *in vivo*. Other intracellular factors may be involved with altering ClpP1 or ClpP2 *in vivo* to promote heterocomplex formation.

However, our results point to ClpP1 and ClpP2 maintaining distinct roles in regulating sporulation, with loss of both isoforms resulting in the inhibition of spore formation. In this manner, this work shows the therapeutic potential and biological significance for inhibition of ClpP in *C. difficile*. Inhibiting ClpP could reduce or even abolish sporulation, which would halt the transmission cycle, disabling CDI transmission. It follows that ClpP is a potentially druggable target in *C. difficile* that offers new inroads for developing drugs that act on novel pathways.

3.5 Materials and Methods

3.5.1 Bacterial strains and growth conditions

630 was used as the model strain of *Clostridium difficile* in all experiments described herein (ATCC: BAA-1382-FZ). Frozen stocks were grown anaerobically at 37 °C in a COY vinyl anaerobic chamber which maintained an atmosphere of 85% N_2, 10% H_2, and 5% CO_2. *C. difficile* was routinely cultured in Brain Heart Infusion media, supplemented with yeast extract (BHIS). Cefoxitin (8 μg/mL), thiamphenicol (20 μg/mL), taurocholate (0.1% w/v), and kanamycin (50 μg/mL) were used as needed in conjugation complementation experiments during CRISPR/Cas9 mutagenesis.

3.5.2 clpP mutant generation

The methodology describing the generation of *clpP* mutants in *C. difficile* is novel and currently unpublished, and as such some specific details will be omitted or described vaguely on purpose. The pMTL84151 plasmid was utilized as the vector to introduce the CRISPR/Cas9 machinery along with guide sequence for the ClpP1 and ClpP2 mutants (**Appendix B.13**). The ClpP1 and ClpP2 serine proteases of *Clostridium difficile* 630 were targeted for genetic alteration via CRISPR/Cas9 mutagenesis, in a manner similar to

previously described methodologies.[37] Both involved the addition of an *NheI* restriction site upon homology directed repair from the donor template sequence on the vector. This change resulted in a stop codon being formed at the 13th residue of ClpP1 (GGA → TGA) and the 12th of ClpP2 (CAA → TAA). After vector construction, conjugation with donor *E. coli*, and five passages under selective pressure the respective cultures were plated and screened via PCR followed by *NheI* restriction digestion. Sanger sequencing further confirmed the accuracy of the desired genetic alteration. Additionally, whole genome resequencing was conducted to confirm that no off-target mutations occurred.

Single complement mutants were constructed by inserting the pMTL84151 plasmid back into each ClpP mutant. Each complement was constructed by inserting *clpP1* + 100bp upstream, or *clpP2* + 100bp upstream into the *lacZ* operon in the pMTL84151 plasmid. To ensure the promoter region was maintained, the entire gene plus 100bp upstream of *clpP1* or *clpP2* was performed. In this manner, both of the single complementation vectors were made and then introduced into *C. difficile* 630 via conjugation.

3.5.3 Genomic sequencing

Frozen stocks of *C. difficile* maintained by the Ballard laboratory were struck onto BHIS agar plates supplemented with taurocholate along with the ATCC reference strain and *clpP* mutants. Individual colonies were picked for each strain to inoculate ~5 mL of BHIS broth and allowed to grow for 12 h. Genomic DNA was isolated from each culture using the GenElute Bacterial Genomic DNA kit (Thermo) and purified with the Zymo Genomic DNA Clean and Concentrator kit (Zymo). DNA samples were sent to the Oklahoma Medical Research Foundation for DNA library preparation and Next Generation sequencing performed with a MiSeqV1. Data was processed in Geneous.

3.5.4 Growth curves

~5mL of BHIS was inoculated with freezer stocks of WT and the *clpP* mutants, and allowed to grow overnight. Overnight cultures were back diluted 1:1,000 and allowed to reach exponential growth (OD600 = 0.4 – 0.5) before 1:10,000 dilution in BHIS, with 10 300 µL aliquots of each strain distributed into Bioscreen C honeycomb plates. The plates were sealed with vacuum grease and placed into a Bioscreener C plate reader, and OD600 measurements were taken every 30 minutes for 36 – 48 h at 37 °C with no shaking. All readings have been normalized to the media control (background subtracted).

3.5.5 Cytotoxicity titer assay

72 h cultures of the WT and *clpP* mutants were pelleted (3000x rcf, 15 minutes) in order to extract the supernatant. The supernatants were 0.2 µm syringe filtered and serially diluted in the appropriate mammalian cell medium accordingly. Filtering the supernatant removed the bacteria, but retains the toxins TcdA and TcdB.

All mammalian cell cultures were grown in cell culture treated plastics, in a humidified incubator at 37 °C with 5% CO_2. Caco-2 and CHO cells were cultured as recommended by ATCC, with Eagles Defined Medium (EMM) and F-12K medium, both supplemented with 10% Fetal bovine serum (FBS). Cell cultures were trypsinized once they had reached ~80% confluency, and equal volumes of media were added to neutralize the trypsin. Detached cells were then harvested by centrifugation (100x rcf, 15 minutes) and resuspended in appropriate media. 100 µL aliquots (5×10^5 cell density) were used to seed 96-well plates and were allowed to grow overnight. Once cells had reached 60-70% confluency, the media was aspirated and serially diluted supernatant from each strain was

added across triplicate wells to the seeded 96-well plates. Plates were then incubated with the supernatant for 18h before cell viability was assessed via Cell Counting Kit-8 (CCK-8, Dojindo) according to the manufacturer.

3.5.6 Plate-based sporulation

Plate-based sporulation was performed as previously described,[38] but will be discussed here briefly. Frozen glycerol stocks of WT and *clpP* mutants were used to inoculate starter cultures of ~5 mL BHIS and allowed to grow overnight. Overnight culture was back-diluted 1:20 into ~2 mL of BHIS and allowed to reach exponential phase growth at ~0.4 OD600. 100 µL of exponential phase culture was used to inoculate 70:30 plates (70% BHIS, 30% SMC) to lawn the bacteria. Sporulation was induced for ~20 − 22 h, before harvesting and resuspending in PBS. These samples were then used for downstream applications.

3.5.7 Liquid-culture sporulation

Frozen glycerol stocks were used to inoculate ~5 mL of BHIS, and allowed to grow overnight before 1:200 back-dilution into SMC broth.[38] Sporulation was allowed to continue for 20 - 24 h before they were prepared for fluorescent microscopy analysis.

3.5.8 Sporulation efficiency assay

Sporulation efficiency was determined as previously described.[39] Plate-based spore samples were thoroughly resuspended in PBS with 10 µL of each sample was then serially diluted and plated on BHIS supplemented with 0.1% taurocholate in triplicate for total cell count. The original resuspended samples were then incubated at 70 °C for 30 minutes, briefly vortexed every 10 minutes, and then 10 µL of each sample was plated onto BHIS media in triplicate to quantify mature spores. By comparing the quantity of spores to the

total cell count, the sporulation efficiency can be calculated. Statistical significance was obtained by One-way ANOVA and Tukey test.

Otherwise, ASE can be quantified by visually counting spores and vegetative cells via differential contrast or phase contrast microscopy. Comparing vegetative cell counts to spore counts yields the ASE.

3.5.9 Microscopy analysis

Liquid-based spore samples from each strain were back-diluted 1:10 in BHIS media and incubated with 3 - 4 drops of Hoescht 33342 (15 µg/mL) for 1 h at 37 °C anaerobically. 6 µL of Hoescht stained samples were then immobilized microscope slides with 1% agarose pads that contained 1% (w/v) FM 4-64. The agarose pads were then sealed with coverslips. Bright field and fluorescence microscopy were then performed using a Zeiss Axiovert 200m at 63x magnification under oil-immersion, imaged with a CCD AxioCam. Some phased images were obtained with a DP8 Olympus Camera (Ph3, 100x) where described. A differential contrast filter was used to obtain phased bright-field images. 0.1 µm Z-stacked images were obtained in red and blue channels to aid focusing and reduce background noise. Individual color channels were merged into a composite image and normalized with ImageJ.[25]

3.5.10 Transmission Electron Microscopy

TEM sample preparation was performed by OMRF personnel, as described herein. Spores were fixed with 4% Paraformaldehyde (EM grade), 2.5% Gluteraldehyde (EM grade), in 0.2M Sodium Cacodylate buffer for 1 day at 4 ^{0}C. Samples were then post fixed for 60 minutes in 1% Osmium tetroxide (OsO_4) in 0.2M Sodium Cacodylate, and rinsed three times for five minutes each in 0.2M Sodium Cacodylate buffer. The samples were

stored in 0.2M Sodium Cacodylate buffer overnight on a rocker at room temperature. The spores were then dehydrated in a graded ethanol series. The ethanol gradient was as follows; 50%, 60%, 75%, 85%, 95%, 100%. The spores were in each concentration for 15 minutes on a rocker. Then the samples had two 15-minute treatments in 100% Propylene Oxide. Following dehydration, the samples were infiltrated in a graded Epon/Araldite (EMS) resin/Propylene Oxide series (1:3, 1:1, 3:1) for 60 minutes, overnight, and 120 minutes the next day respectfully. The spores were further infiltrated with pure resin for 45 minutes, 90 minutes, and then overnight. The samples were then embedded in resin plus BDMA (accelerator) and polymerized at 60 °C for 48 hours. Ultrathin sections were stained with Sato's Lead and Saturated Uranyl Acetate in 50% methanol before viewing on a Hitachi H7600 Transmission Electron Microscope. At least 200 cells were counted for quantification.

3.5.11 Western blot analysis

Plate-based spore samples (~40 h sporulation) were pelleted and resuspended in 1 mL of Western Blot buffer (8M Urea, 10mM β-mercaptoethanol). Samples were then mixed 1:1 with 2x SDS-PAGE loading buffer (Bio-Rad), and heated at 100 ^{0}C for 10 minutes before centrifugation at 15,000x rcf for 8 minutes. 5 µL of each sample was then loaded onto 4-20% TGX Bis-Tris SDS-PAGE gradient gels (Bio-Rad) and resolved via electrophoresis until the dye front had migrated off the gel-front. The samples were then transferred onto Turbo-Blot PVDF membranes (Bio-Rad) and blocked with 5% non-fat milk in Tris-Buffered Saline with 0.1% (v/v) Tween-20 (TBST) for 1 h at room temperature. All antibodies were provided by Dr. Aimee Shen (Tufts) as a generous gift, and were obtained as described elsewhere.[32] The primary antibodies were diluted 1:2000

in 5% non-fat milk in TBST and used to blot the membranes for each protein for 18-20 h at 4 ^{0}C while rocked. The membranes were washed and then incubated with anti-rabbit and anti-mouse (Spo0A primary antibody was mouse derived, all others are rabbit-derived) horseradish peroxide (HRP) secondary antibodies, and were then diluted 1:2000 in 5% non-fat milk in TBST. Membranes were then incubated with secondary antibody for 1 h, washed, and treated with ECL Clarity substrate (Bio-Rad) as per the manufacturer description. Blots were then imaged with a Bio-Rad ChemiDoc MP Imaging System with automatic image correction applied.

3.7 References

1. Deakin, L. J. *et al.* The *Clostridium difficile* spo0A gene is a persistence and transmission factor. *Infect. Immun.* **80,** 2704–2711 (2012).

2. Abt, M. C., McKenney, P. T. & Pamer, E. G. *Clostridium difficile* colitis: pathogenesis and host defence. *Nat. Rev. Microbiol.* **14,** 609–620 (2016).

3. Gil, F., Lagos-Moraga, S., Calderón-Romero, P., Pizarro-Guajardo, M. & Paredes-Sabja, D. Updates on *Clostridium difficile* spore biology. *Anaerobe* **45,** 3–9 (2017).

4. Swick, M. C., Koehler, T. M. & Driks, A. Surviving between hosts: sporulation and transmission. *Microbiol. Spectr.* **4,** (2016).

5. Lo Vecchio, A. & Zacur, G. M. *Clostridium difficile* infection: an update on epidemiology, risk factors, and therapeutic options. *Curr. Opin. Gastroenterol.* **28,** 1–9 (2012).

6. Ofosu, A. *Clostridium difficile* infection: a review of current and emerging therapies. *Ann Gastroenterol* **29,** 147–154 (2016).

7. Jarrad, A. M., Karoli, T., Blaskovich, M. A. T., Lyras, D. & Cooper, M. A. *Clostridium difficile* drug pipeline: challenges in discovery and development of new agents. *J. Med. Chem.* **58,** 5164–5185 (2015).

8. Zhu, D., Sorg, J. A. & Sun, X. *Clostridioides difficile* Biology: Sporulation, Germination, and Corresponding Therapies for *C. difficile* Infection. *Front. Cell Infect. Microbiol.* **8,** 29 (2018).

9. Venugopal, A. A. & Johnson, S. Current state of *Clostridium difficile* treatment options. *Clin. Infect. Dis.* **55 Suppl 2,** S71-6 (2012).

10. Brötz-Oesterhelt, H. & Sass, P. Bacterial caseinolytic proteases as novel targets for antibacterial treatment. *Int. J. Med. Microbiol.* **304,** 23–30 (2014).

11. Bhandari, V. *et al.* The role of ClpP protease in bacterial pathogenesis and human diseases. *ACS Chem. Biol.* **13,** 1413–1425 (2018).

12. Ruvolo, M. V., Mach, K. E. & Burkholder, W. F. Proteolysis of the replication checkpoint protein Sda is necessary for the efficient initiation of sporulation after transient replication stress in Bacillus subtilis. *Mol. Microbiol.* **60,** 1490–1508 (2006).

13. Ruvolo, M. V. The role and regulation of a checkpoint pathway that coordinatesspore development with chromosome replication in *Bacillus subtilis*. (2008).

14. Pan, Q. & Losick, R. Unique degradation signal for ClpCP in *Bacillus subtilis*. *J. Bacteriol.* **185,** 5275–5278 (2003).

15. Pan, Q., Garsin, D. A. & Losick, R. Self-Reinforcing Activation of a Cell-Specific Transcription Factor by Proteolysis of an Anti-σ Factor in *B. subtilis*. *Mol. Cell* **8,** 873–883 (2001).

16. Edwards, A. N. & McBride, S. M. Initiation of sporulation in *Clostridium difficile*: a twist on the classic model. *FEMS Microbiol. Lett.* **358,** 110–118 (2014).

17. Hall, B. M. *et al.* Two Isoforms of Clp Peptidase in *Pseudomonas aeruginosa* Control Distinct Aspects of Cellular Physiology. *J. Bacteriol.* **199,** (2017).

18. Edwards, A. N. & McBride, S. M. Isolating and Purifying *Clostridium difficile* Spores. *Methods Mol. Biol.* **1476,** 117–128 (2016).

19. Wilson, K. H., Kennedy, M. J. & Fekety, F. R. Use of sodium taurocholate to enhance spore recovery on a medium selective for *Clostridium difficile*. *J. Clin. Microbiol.* **15,** 443–446 (1982).

20. Wilson, K. H. Efficiency of various bile salt preparations for stimulation of *Clostridium difficile* spore germination. *J. Clin. Microbiol.* **18,** 1017–1019 (1983).

21. Edwards, A. N. & McBride, S. M. Isolating and Purifying *Clostridium difficile* Spores. *Methods Mol. Biol.* **1476,** 117–128 (2016).

22. Burns, D. A. & Minton, N. P. Sporulation studies in *Clostridium difficile*. *J. Microbiol. Methods* **87,** 133–138 (2011).

23. Permpoonpattana, P. *et al.* Surface layers of *Clostridium difficile* endospores. *J. Bacteriol.* **193,** 6461–6470 (2011).

24. Pishdadian, K., Fimlaid, K. A. & Shen, A. SpoIIID-mediated regulation of σK function during *Clostridium difficile* sporulation. *Mol. Microbiol.* **95,** 189–208 (2015).

25. Collins, T. J. ImageJ for microscopy. *BioTechniques* **43,** 25–30 (2007).

26. Edwards, A. N. & McBride, S. M. Isolating and Purifying *Clostridium difficile* Spores. *Methods Mol. Biol.* **1476,** 117–128 (2016).

27. Pizarro-Guajardo, M., Calderón-Romero, P. & Paredes-Sabja, D. Ultrastructure Variability of the Exosporium Layer of *Clostridium difficile* Spores from Sporulating Cultures and Biofilms. *Appl. Environ. Microbiol.* **82,** 5892–5898 (2016).

28. Fimlaid, K. A. *et al.* Global analysis of the sporulation pathway of *Clostridium difficile*. *PLoS Genet.* **9,** e1003660 (2013).

29. Pettit, L. J. *et al.* Functional genomics reveals that *Clostridium difficile* Spo0A coordinates sporulation, virulence and metabolism. *BMC Genomics* **15,** 160 (2014).

30. Brown, D. P. *et al.* Characterization of *spo0A* homologues in diverse *Bacillus* and *Clostridium* species identifies a probable DNA-binding domain. *Mol. Microbiol.* **14,** 411–426 (1994).

31. Levin, P. A. & Losick, R. Transcription factor Spo0A switches the localization of the cell division protein FtsZ from a medial to a bipolar pattern in *Bacillus subtilis*. *Genes Dev.* **10,** 478–488 (1996).

32. Ribis, J. W., Fimlaid, K. A. & Shen, A. Differential requirements for conserved peptidoglycan remodeling enzymes during *Clostridioides difficile* spore formation. *Mol. Microbiol.* **110,** 370–389 (2018).

33. Dembek, M. *et al.* Peptidoglycan degradation machinery in *Clostridium difficile* forespore engulfment. *Mol. Microbiol.* **110,** 390–410 (2018).

34. Serrano, M. *et al.* The SpoIIQ-SpoIIIAH complex of *Clostridium difficile* controls forespore engulfment and late stages of gene expression and spore morphogenesis. *Mol. Microbiol.* **100,** 204–228 (2016).

35. Tyurin, M. V., Lynd, L. R. & Wiegel, J. in **35,** 309–330 (Elsevier, 2006).

36. Fimlaid, K. A., Jensen, O., Donnelly, M. L., Siegrist, M. S. & Shen, A. Regulation

of *Clostridium difficile* Spore Formation by the SpoIIQ and SpoIIIA Proteins. *PLoS Genet.* **11,** e1005562 (2015).

37. McAllister, K. N., Bouillaut, L., Kahn, J. N., Self, W. T. & Sorg, J. A. Using CRISPR-Cas9-mediated genome editing to generate *C. difficile* mutants defective in selenoproteins synthesis. *Sci. Rep.* **7,** 14672 (2017).

38. Edwards, A. N. & McBride, S. M. Isolating and Purifying *Clostridium difficile* Spores. *Methods Mol. Biol.* **1476,** 117–128 (2016).

39. Permpoonpattana, P. *et al.* Functional characterization of *Clostridium difficile* spore coat proteins. *J. Bacteriol.* **195,** 1492–1503 (2013).

40. Seddon, S. V. & Borriello, S. P. A chemically defined and minimal medium for *Clostridium difficile*. *Lett. Appl. Microbiol.* **9,** 237–239 (1989).

41. Karasawa, T., Ikoma, S., Yamakawa, K. & Nakamura, S. A defined growth medium for *Clostridium difficile*. *Microbiology (Reading, Engl.)* **141 (Pt 2),** 371–375 (1995).

Chapter 4

Addressing ClpP Modulator Inefficiencies

As discussed in Chapter 1 of this dissertation, ClpP represents a unique target for antibacterial discovery, as beneficial activity is observed via inhibition or activation of this protease (**Figure 4.1**). Activators stimulate ClpP and promote ATP-independent hydrolysis of intrinsically disordered intracellular proteins. Known activators of ClpP bind competitively to the cochaperone binding sites and thus operate via two mechanisms of action: 1) activating the ClpP protease and inducing unselective degradation; and 2) inhibiting the interaction of AAA+ cochaperones with ClpP, thus disrupting the ability of cochaperones to deliver natural substrates for degradation.[1] Therefore, bacterial cells treated with ClpP activators suffer from self-digestion and a build-up of toxic substrates, resulting in a dual attack on microbes. Alternatively, inhibitors render ClpP proteolytically inactive by restricting conformational plasticity, or chemically inactivating the Ser-His-Asp catalytic triad. While ClpP modulation has attracted serious interest from the antibacterial research community, little has been done to expand the arsenal of ClpP modulators. Due to the liabilities of known modulators (discussed below), new chemotypes will be required in order to exploit ClpP clinically. In addition to our studies on the ClpP system in *C. difficile*, we have an ongoing interest in identifying new ClpP modulators and working to address the liabilities of known activators and/or inhibitors.
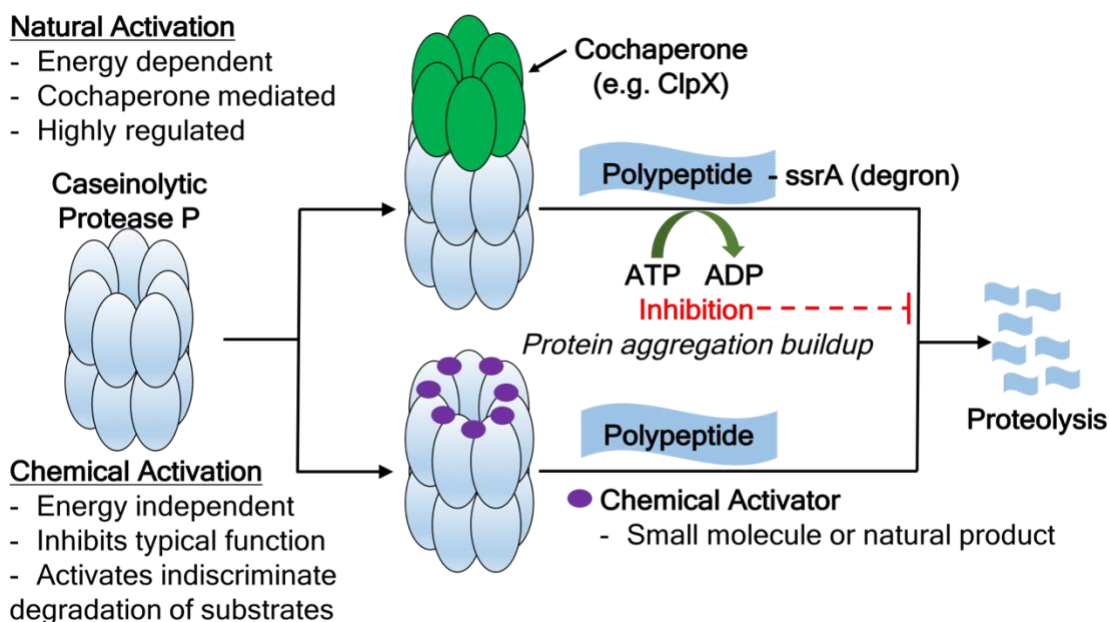
Figure 4.1 Therapeutically relevant orthogonal approaches to targeting ClpP

4.1 Inhibitors

Two classes of ClpP selective inhibitors, β-lactones and phenyl esters, have been identified (**Figure 4.2**).[2] These inhibitors covalently modify the serine within the conserved catalytic triad to irreversibly halt proteolysis.[3,4] β-lactones and phenyl esters exhibit unique activity profiles against different ClpP homologs. The β-lactones were the first ClpP selective inhibitors identified and SAR studies have produced efficacious analogs against *S. aureus* and *M. tuberculosis*.[5–7] Although the β-lactones are effective at clearing *S. aureus* skin infections (sub-cutaneous injection) in mice, the utility of this class is limited by the susceptibility to hydrolysis in plasma (mouse = 3.7 ± 1.5 min, human = 4.7 ± 0.4 min).[8–10] Attempts to increase the stability of β-lactones have failed to provide pharmacological value, as potency suffers dramatically upon β-lactone replacement.[4]

In attempts to identify new ClpP inhibitory chemotypes, Sieber and colleagues screened a small molecule library and discovered the phenyl ester pharmacophore (**Figure 4.1**).[8] While this chemotype exhibits improved stability of the pharmacologically relevant acyl-enzyme complex (β-lactone: $t_{1/2} = 5.0$ h $\pm$ 0.4 h; phenyl ester: $t_{1/2} = 8.2$ h $\pm$ 0.8 h), no evidence of improved plasma stability is presented and translation of this chemotype into therapeutically relevant anti-virulence agents still represents a major hurdle.

4.2 Activators

4.2.1 Acyldepsipeptides (ADEPs)

In 1985, acyldepsipeptide antibiotics (ADEPs) were isolated from *Streptomyces hawaiiensis* culture and were largely ignored until Heiki *et al.* determined that ADEPs bind and activate bacterial ClpP and elicit bacterial cell death.[11,12] In a murine model ADEP1 (A54556A) produced an 80% survival rate when provided as a treatment against a lethal challenge of *S. aureus* and *E. faecalis*, lowering bacterial loads in vital organs two to three-fold versus the control. The mechanism of action was determined through biochemical means and the binding mode was revealed through the characterization of two ClpP:ADEP cocrystal structures, which showed that ADEPs bind to ClpP in a manner that mimics cochaperone binding.[13–15] Cochaperones (e.g., ClpX) bind to ClpP via an I/FGL motif present towards the C-terminal end of each monomer, which interacts with the hydrophobic clefts between ClpP monomers.[16,17] ADEPs bind competitively to the same monomeric interface, and trigger a conformational change that widens the axial pore of ClpP.[1,14,15,18] When activated, disordered proteins are able to diffuse into the proteolytic compartment to be degraded.

Eventually, studies revealed significant ADME drawbacks such as: poor solubility, poor bioavailability, and limited to no activity against Gram-negative bacteria.[3] The first attempt to optimize ADEPs was undertaken by Hinzen *et al.*, where it was found that removing conjugation of the acyl side-chain improved *in vitro* MIC activity assays and stability.[20] Fluorination at the 3,5 positions of the phenyl ring coupled with alteration of the macrocyclic core to instill conformational rigidity were found to significantly improve *in vitro* activity (~160-fold). The resulting compound, ADEP4, was used in combination with rifampicin and erythromycin to eliminate spores, and rescue a mouse from a lethal challenge of MRSA.[21] Further SAR studies on the ADEPs have produced >40 analogs, some of which exhibit impressive efficacy (≤0.0002 µg/mL) against Gram-positive pathogens (*S. pneumoniae* and *E. faecalis*).[20,22–24] Unfortunately, pharmacokinetic (PK) detriments and the inability to surpass bacterial defense mechanisms continues to impede the clinical use of ADEPs.[25]
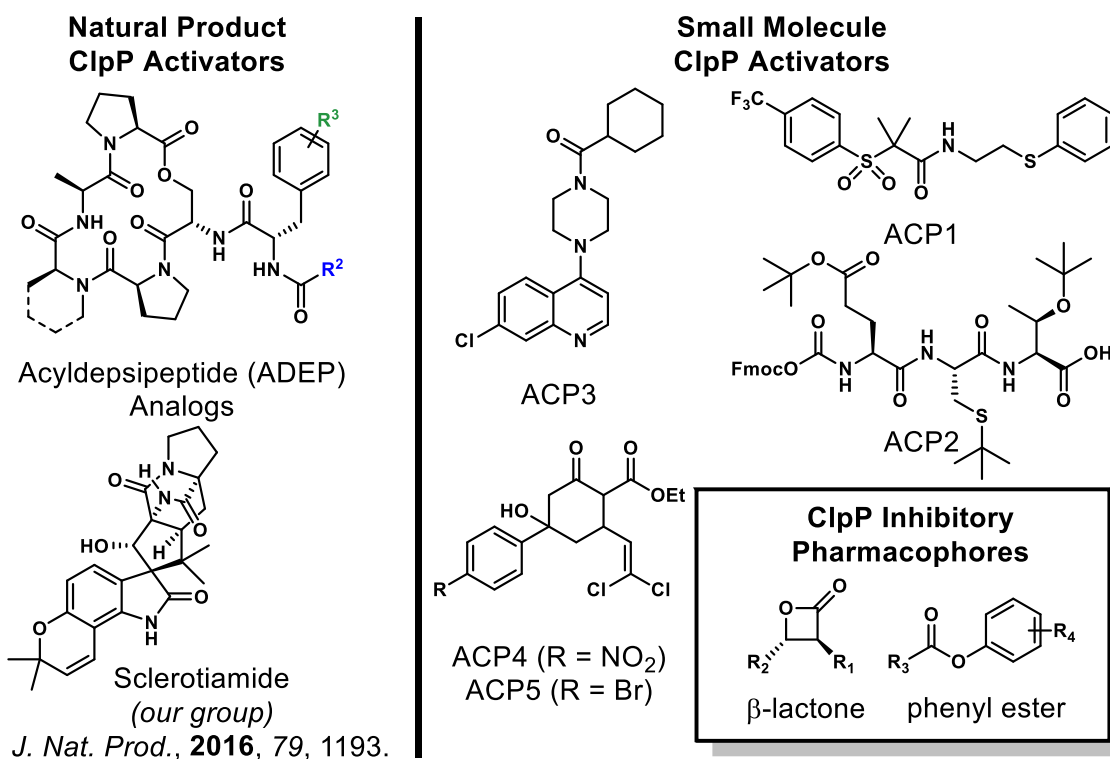
Figure 4.2 Current ClpP chemo-modulating scaffolds.

4.2.2 Activators of Cylindrical Proteases (ACPs)

A separate class of activators known as Activators of Cylindrical Proteases (ACPs) were found in a broad screen of >50,000 small molecules from multiple commercial library sources.[26] Five ACPs (ACP1-ACP5) were found to stimulate *B. subtilis* ClpP to degrade an artificial substrate *in vitro* (i.e., FITC-casein) of which ACP1 was identified as the most potent. Therefore, chemical optimization proceeded with ACP1, resulting in the synthesis of ACP1a and ACP1b, which exhibited improved potency. MIC studies revealed that the chemical modification of this scaffold provided only a modest reduction in MIC between ACP1 and ACP1a/ACP1b of approximately 2-fold against *N. meningitis*. Notably, the combination of polymyxin-nonapeptide B (PMB) and ACP1b significantly lowered the

MIC against *H. influenza*. However, none of the ACPs tested approached MIC values reported for ADEP1 against any pathogen tested.

The binding mode of ACPs has not been determined, but rather suggested through mutational and computational studies and by ACPs' ability to prevent GFP-ssrA degradation in a ClpXP-mediated degradation assay. As observed with ADEPs,[27] when ClpP is pre-treated with ACPs, ClpX is unable to translocate a GFP-ssrA substrate into the ClpP proteolytic chamber, thus inhibiting degradation. This is most likely due to ACP binding in the same clefts that ClpX interacts with in order to associate with ClpP for targeted proteolysis. Physical evidence of ACP binding was provided via isothermal titration calorimetry. *In silico* binding studies suggest that ACPs bind in the northern or southern clefts close to the N-termini of ClpP monomers in a manner similar to ADEP. From these observations, various point mutations were introduced to ClpP in an attempt to reveal the binding pocket, but no definitive conclusion was obtained.

4.3 Sclerotiamide: The First Non-Peptide-Based Natural Product Activator of Bacterial Caseinolytic Protease P[3]

4.3.1 Abstract

Caseinolytic protease P (ClpP) maintains essential roles in bacterial homeostasis. As such, both the inhibition and activation of this enzyme result in bactericidal activity,

---

making ClpP a promising target for antibacterial drug development. Herein, we report the results of a fluorescence-based screen of ~450 structurally diverse fungal and bacterial secondary metabolites. Sclerotiamide (1), a paraherquamide-related indolinone, was identified as the first non-peptide-based natural product activator of ClpP. Structure-activity relationships arising from the initial screen, preliminary biochemical evaluation of 1, and rationale for the exploitation of this chemotype to develop novel ClpP activators are presented.

4.3.2 Results

While ClpP modulation has attracted serious interest from the antibacterial research community, little has been done to identify new ClpP modulating chemotypes. In fact, no natural product screen for ClpP modulators had been reported when our lab entered this space.[28] In efforts to expand the arsenal of ClpP activating chemotypes, we screened a focused but structurally diverse subset of secondary fungal and bacterial metabolites, housed within our Institute for Natural Products Applications and Research Technologies (INPART). The complete library has been established by the Cichewicz laboratory over nearly a decade and is comprised of metabolites isolated from > 180 soil samples and > 80 distinct zip codes across the United States.[29] This continually growing collection includes a rich source of structural diversity (depsipeptides, alkaloids, carbocycles, terpenes,

polyketides, non-ribosomal peptides, etc.) and biological activity, which has provided leads in a number of targeted phenotypic screens and functional assays.[30–33] Thus, we believed this library represented a promising untapped source to screen for novel natural product ClpP activators.

"Hit"	ΔRFU	IF	PA
C	23997	yes	ND
D	23372	yes	ND
E	23404	yes	ND
F	22978	yes	ND
G	23214	yes	ND
H	23122	yes	ND
I	22798	yes	ND
J	22904	yes	ND
1	29909	no	no
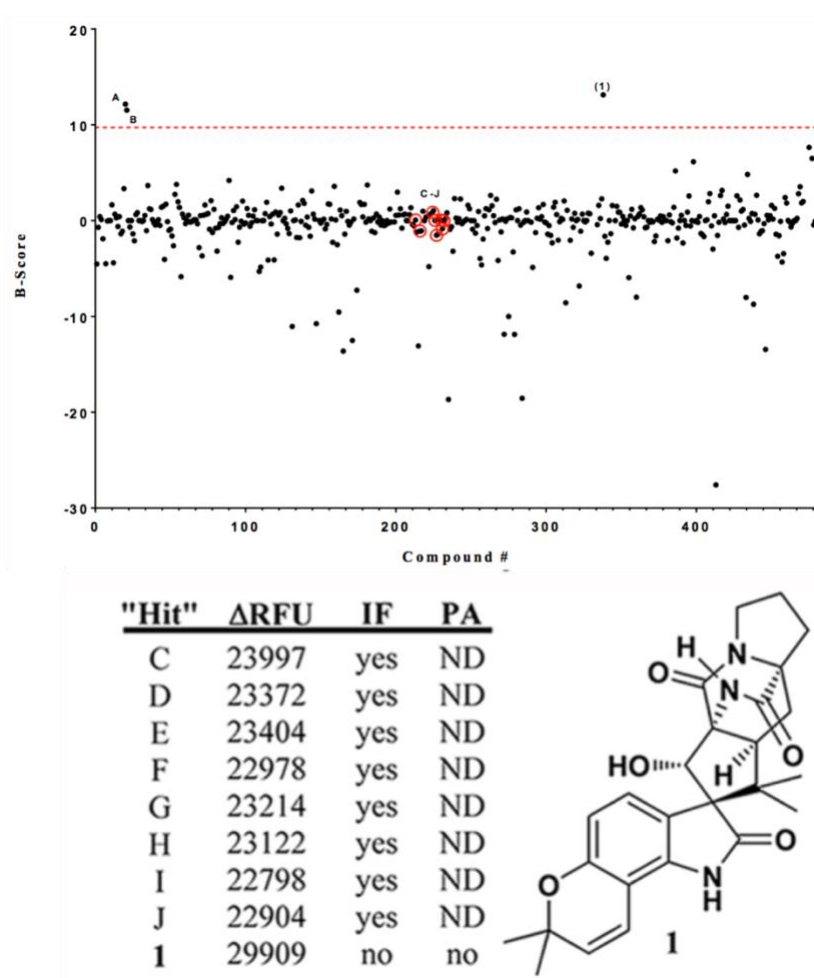
Figure 4.3 B-scored broad screen data and "hits" table
(A) Raw FITC-β-casein degradation screening results. Threshold for analysis is indicated by the red line (ΔRFU ≥ 22,500). Inset: Enlarged area of threshold exceeding "hits". (B) Fluorescence data, validation of initial "hits", and structure of sclerotiamide (1). ΔRFU = change in relative fluorescence units, IF = intrinsic compound fluorescence, PA = inherent compound proteolytic activity, ND = not determined.

For the initial screen, a fluorescence-based protease assay that utilizes a commercially available internally quenched fluorogenic ClpP substrate, FITC-β-casein, was employed.[26] Approximately 450 natural products were screened at a single concentration (50 µM) for the activation of recombinant *E. coli* ClpP (*Ec*ClpP). Enopeptin A[34,35] (25 µM) and ACP5[26] (50 µM), a natural ADEP analog and a small molecule, respectively, were implemented as positive controls. In the presence of an activating molecule, ClpP-mediated cleavage of FITC-β-casein relieves internal quenching of the substrate and yields a fluorescent output of protease activity that can be quantified with a fluorimeter (excitation/emission: 485/538 nm). In the absence of an activating molecule, ClpP is unable to proteolyze FITC-β-casein and fluorescence remains quenched.

As shown in **Figure 4.3**, a threshold of 22,500 raw ΔRFUs was set and any compound exhibiting an end-point fluorescence greater than this threshold was analyzed further. In total, 11 hits were identified, two of which were the positive controls, Enopeptin A (A, **Figure 4.3A**) and ACP5 (B, **4.3A**). The remaining nine hits were resubjected to the assay conditions to confirm the observed activity. All nine demonstrated reproducibility, which provided a respectable initial hit rate of 3.6%. To eliminate false positives, hits were evaluated for both intrinsic fluorescence and inherent proteolytic activity, which disqualified eight of the nine hits (**Figure 4.3B**). However, when the raw screening data were replotted using the B-scoring algorithm,[36,37] only a single true hit was detected. To measure intrinsic fluorescence, 538 nm emission was measured after 485 nm excitation for each compound (50 µM) in assay buffer. To measure inherent proteolytic activity, hit compounds (50 µM) were incubated with FITC-β-casein (192 µM) in assay buffer and fluorescence readings were taken to evaluate time dependent inherent proteolytic

properties. As such, sclerotiamide (**1**, **Figure 4.3B**),[38] a paraherquamide related indole alkaloid natural product, was the only hit to pass both validation filters and B-score analysis, and was evaluated further.
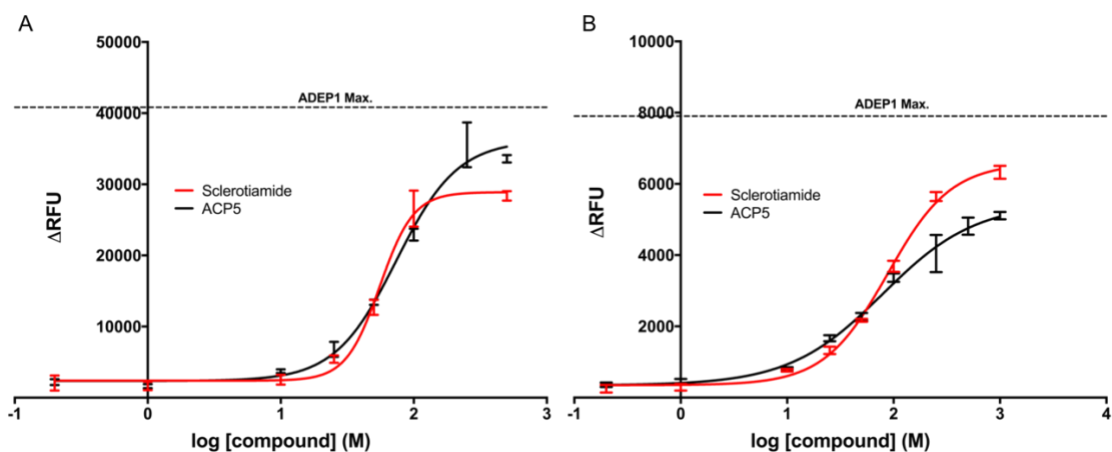
Figure 4.4 Dose dependent *Ec*ClpP activation by ACP5, and 1
(A) substrate = Abz-DFAPKMALVPY^{NO2} (B) substrate = FITC-β-casein (normalized to DMSO baseline fluorescence).

Sclerotiamide was subjected to dose-dependent peptide (Abz-DFAPKMALVPY^{NO2})[22,39] and protein (FITC-β-casein) degradation analysis. As shown in **Figure 4.4**, the potency of **1** parallels that of ACP5 and exhibits an apparent activation constant (K_{app}) of 39.6 ± 4.9 µM for decapeptide degradation and 87.5 ± 5.0 µM for FITC-β-casein degradation. It is worth noting that the consistent potency of ACP5 in these two assays differs from the trend observed for 1 and ADEP1, which also shows an increase (~10-fold) in K_{app} from decapeptide to FITC-β-casein degradation (**Table 4.1**). Hill Plot analysis of **1** demonstrates modest positive cooperativity for ClpP binding (Hill coefficient: >1.5), suggesting an ADEP-like binding process. Although the potency is modest, especially in comparison to ADEP1 (FITC-β-casein, $K_{app} = 1.6 \pm 0.4$ µM, Hill coefficient: 2.0), **1** is the first non-peptide based natural product ClpP activator discovered and thus

119

provides unique chemical space to evaluate for SAR studies. As a member of the paraherquamide family, **1** possesses a 3-dimensional bicyclo[2.2.2]diazaoctane motif that has garnered significant attention from the synthetic community,[40,41] and has recently been reported in closely related compounds that exhibit a range of biological activities.[42,43]

Compound	EC$_{50}$ (μM)		
	DFAP	FITC-Casein	Hill slope
ADEP1	0.1 ± 0.02	1.2 ± 0.1	1.6/1.5
ACP5	25.4 ± 3.6	22.2 ± 2.3	1.4/1.4
1	39.6 ± 4.9	87.5 ± 5.0	2.6/1.9

Table 4.1 Dose-Response comparison of ADEP1, ACP5, and 1 for the Decapeptide (DFAPKMALVPY^{NO2}) and unstructured protein (FITC-β-Casein) substrates.
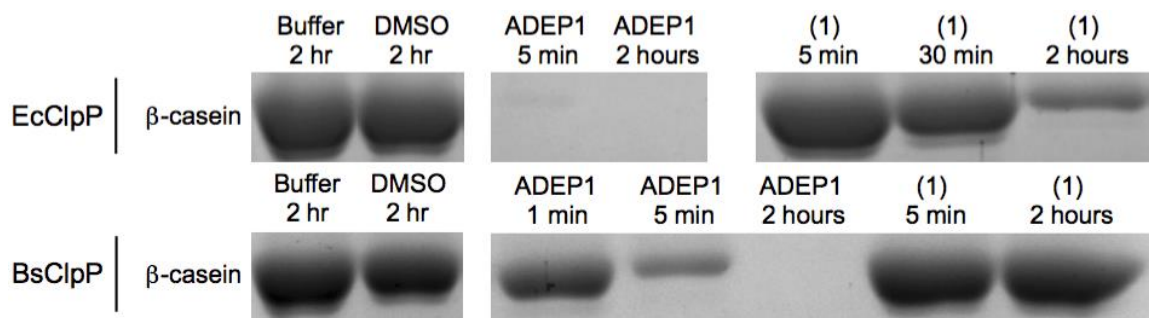
Figure 4.5 SDS-PAGE degradation of β-casein by ClpP in the presence of 1
SDS-PAGE analysis of ClpP homologue-dependent degradation of unlabeled β-casein by 1 (50 μM) in comparison to ADEP1 (1 μM).

Further validation of *Ec*ClpP activation by **1** was confirmed by SDS-PAGE analysis (**Figure 4.5**), which demonstrates dose and time dependent activation of *Ec*ClpP and subsequent degradation of unlabeled β-casein. Interestingly, when **1** was evaluated for its propensity to activate *B. subtilis* ClpP (*Bs*ClpP), no significant activation was observed

(**Figure 4.5**). This lack of *Bs*ClpP activation was noted in both fluorescence-based degradation assays and SDS-page analysis. To our knowledge, this is the first example of a ClpP activator that demonstrates a noticeable selectivity between bacterial homologs and we are currently probing the utility of this observation.
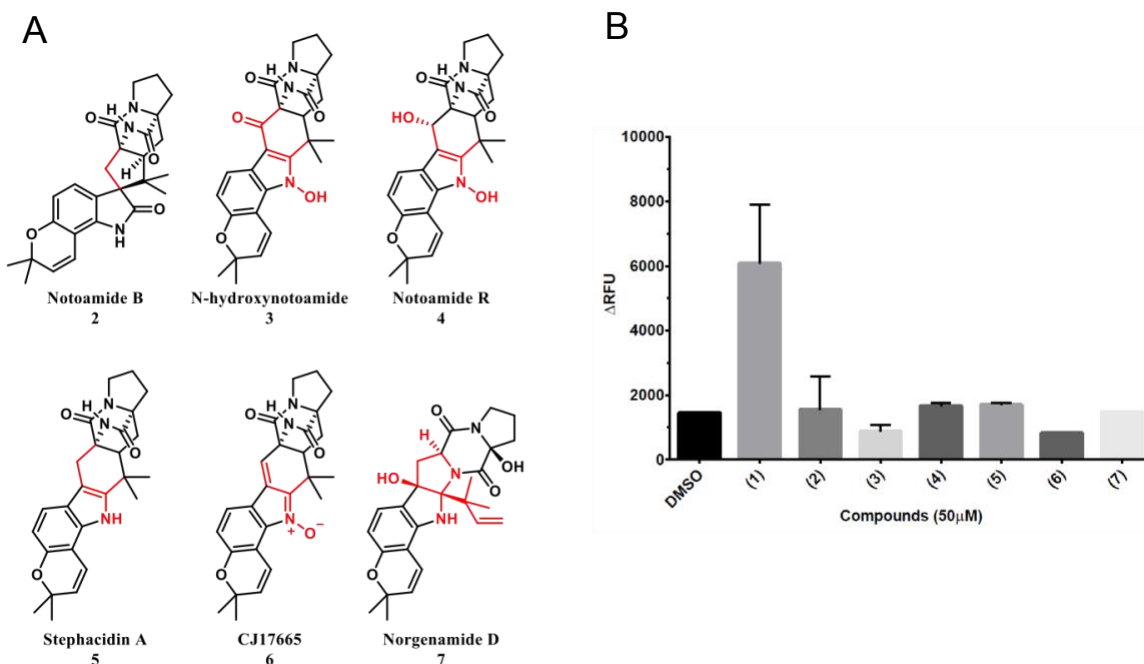
Figure 4.6 Initial paraherquamides structure-activity-relationships
(A) Additional paraherquamide related compounds present in the initial FITC-β-casein degradation screen (B) Relative ClpP activation of **1** and related compounds.

Upon reinvestigation of the screened compound set, we noted that six additional members of this family were included within the screen (**2–7**, **Figure 4.6A**). Interestingly, however, all six of these analogs fail to elicit ClpP activation to any significant extent (**Figure 4.6B**). Most notable from this group is notoamide B (**2**), which only lacks the C-10 α-oriented secondary hydroxyl group.[44] This lack of activity by **2** identifies the C-10 α-hydroxy motif as a necessary fixture in this natural product class for ClpP activation. In

addition, the 3-dimensional attributes imparted by the spiroindolinone moiety seem to be important, as all other congeners exhibit a fused architecture and fail to activate ClpP.

Indicative of its relatively modest apparent binding affinity, **1** failed to inhibit the growth (> 100 µM) of permeabilized and efflux pump deficient *E. coli* M5418 (*ΔacrB, ΔacrD, ΔacrEF::spc ΔemrB ΔemrY ΔentS::cam ΔmacB ΔmdtC ΔmdtF*)[45] and *Pseudomonas aeruginosa* PAO1116 ((Δ*mexAB-oprM*), (Δ*mexCD-oprJ*), (Δ*mexEF-oprN*), (Δ*mexJK*), (Δ*mexXY*), and (Δ*triABC*))[46] proprietary strains. These results suggest that although **1** is capable of activating recombinant *Ec*ClpP, improvement of potency is required for cellular target engagement and efficacy. Molecular dissection to identify the pharmacophore for this class of ClpP-activating natural products and X-ray cocrystallization studies are currently ongoing in our laboratory. Results from these studies will be communicated in due course and will contribute to structure-guided approaches aimed at improving upon the ClpP activation potency of this chemotype. Furthermore, the process outlined here will be expanded upon to enable the screening of natural product extracts, allowing for the interrogation of much larger chemical diversity.

4.4 Discussion

Overall, the utility of ClpP activation and inhibition has been established. To exploit ClpP as a target clinically, however, new chemical scaffolds are required. Leveraging our affiliation with the Institute of Natural Products Applications and Research Technologies (INPART) at the University of Oklahoma, we conducted the first reported natural products screen for new ClpP activators and identified the first non-peptide-based ClpP activator, sclerotiamide. While this compound lacks potency and fails to exhibit

antibacterial activity at the concentrations tested, it provides a new scaffold for medicinal chemistry interrogation. Future studies are planned to synthesize new lead analogs, and attempts to gain structural information are ongoing.

4.5 In Brief: Consequences of Depsipeptide Substitution on the ClpP Activation Activity of Antibacterial Acyldepsipeptides[4]

4.5.1 Abstract

The acyldepsipeptide (ADEP) antibiotics operate through a clinically unexploited mechanism of action and thus have attracted attention from several antibacterial development groups. The ADEP scaffold is synthetically tractable, and deep-seated modifications have produced extremely potent antibacterial leads against Gram-positive pathogens. Although newly identified ADEP analogs demonstrate remarkable antibacterial activity against bacterial isolates and in mouse models of bacterial infections, stability issues pertaining to the depsipeptide core remain. To date, no study has been reported on the natural ADEP scaffold that evaluates the sole importance of the macrocyclic linkage on target engagement, molecular conformation, and bioactivity. To address this gap in

---

ADEP structure–activity relationships, we synthesized three ADEP analogs that only differ in the linkage motif (i.e., ester, amide, and N-methyl amide) and provide a side-by-side comparison of conformational behavior and biological activity. We demonstrate that while replacement of the naturally occurring ester linkage with a secondary amide maintains in vitro biochemical activity, this simple substitution results in a significant drop in whole-cell activity. This study provides direct evidence that ester to amide linkage substitution is unlikely to provide a reasonable solution for ADEP instability.

4.5.2 Results

In addition to screening for new chemotypes, we have also attempted to address liabilities of the highly potent yet relatively unstable ADEPs. Unfortunately, we discovered that simply altering the depsipeptide linkage with a more stable amide linkage abolishes activity against bacteria, even though target-engagement seems undisturbed. We believe that this is attributed to a disruption of an intramolecular hydrogen bond, which is known to enhance molecular rigidity, a feature shown to be crucial for permeation of cyclic peptides and depsipeptides.
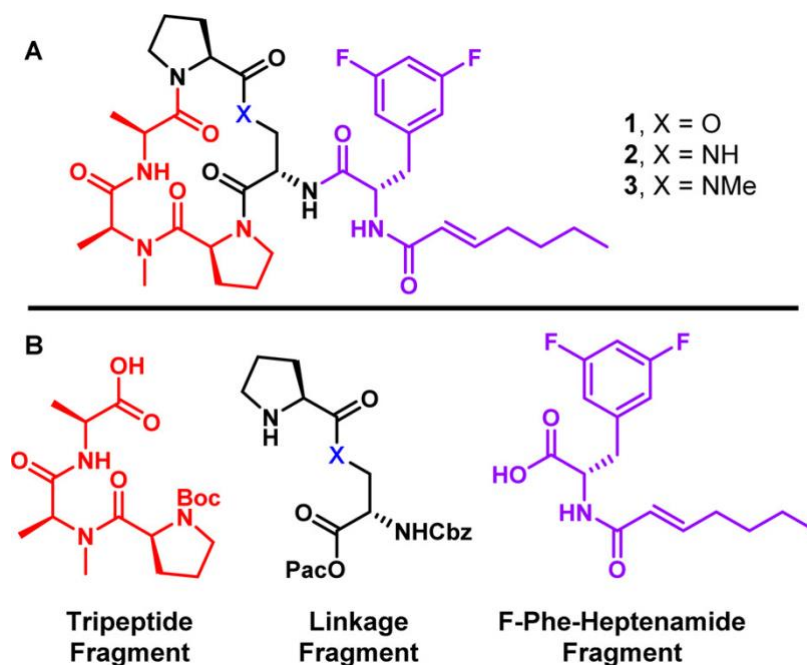
Figure 4.7 A) ADEP analogs synthesized and evaluated in this study. (B) Target fragments for the convergent synthesis of 1-3.

Specifically, hydrolysis of the ADEP depsipeptide ester under basic or acidic conditions has been a major concern regarding this natural product family.[20,47] In fact, recent studies report near total degradation of various ADEPs in Mueller–Hinton broth within 24 h; a surprising claim given the benign nature of this broth.[47] A common approach to improve the stability of ester linkages is to simply replace the ester with an amide or *N*-methyl amide. Ester to amide substitution has demonstrated utility to improve not only stability, but also to decrease off-target cytotoxicity and enhance permeability of cyclic lipodepsipeptides.[48,49] While ester to amide substitution has been investigated sporadically on ADEP analogs,[50,51] no direct systematic comparison of compounds differing in only the macrocyclic linkage type (i.e., −O−, −NH−, −NMe−) has been reported. Furthermore, all linkage substitutions reported to date have been conducted on "pre-rigidified" ADEP

analogs, in which unnatural amino acids have been introduced into the macrocyclic core to enhance structural rigidity.[50,51] Incorporation of unnatural rigidification in addition to macrocyclic linkage substitution imparts a multivariable effect, which may introduce conflicting conformational strains and make it difficult to delineate the specific effect of linkage substitution. As such, to determine the sole effect of the linker on the naturally occurring ADEP macrocyclic core, we have synthesized three ADEP analogs that differ only in the linkage type and have evaluated these analogs to provide insight regarding target engagement, molecular conformation, permeation, and antibacterial activity (**Figure 4.7**).

4.5.3 Bioactivity Evaluation

Similar to the natural cochaperones, ADEP binding results in the reorganization of ClpP and a subsequent widening of the proteolytic chamber.[52,53] Upon chemoactivation of ClpP, however, proteolysis is hyper-activated and unregulated and thus detrimental to bacterial survival. To biochemically compare the ClpP activation potential of each analog, we evaluated the ability of 1–3 to induce degradation of a self-quenching decapeptide (Abz-DFAPKMALVPY^{NO2}).[23] ClpP-induced cleavage of the decapeptide between the aminobenzoic acid fluorophore (Abz) and 2-nitrotyrosine quencher releases fluorescence, which can be quantified with a fluorimeter. Compounds 1–3 were evaluated over an 11-point dose range to determine an apparent binding constant (K_{app}) for ClpP activation. As shown in Table 1, the order of potency is 1 > 2 > 3, with a ~two-fold difference in potency between 1 and 2 and an additional ~50-fold drop between compounds 2 and 3. This demonstrates a significant SAR for the ADEP cyclic peptide linkage on ClpP activation potency. However, it also suggests that substitution may be allowable, as a respectable

level of activity is maintained, especially when comparing the ester (1) with the secondary amide (2) linkage. All three analogs exhibit a Hill Slope coefficient >1, suggesting modest positive cooperativity in ClpP binding, a phenomenon indicative of ClpP activators that bind competitively to the cochaperone IGF loop binding pocket.[14] As shown in **Table 4.2**, the ester linked ADEP (1) exhibits an improved stabilization of ClpP in melt experiments relative to both the −NH− (2) and −NMe− (3) compounds. This result is in agreement with the K_{app} values determined in the decapeptide degradation assay.

H/D exchange

Compound	K_{app} (µM)	$t_{1/2}$ (min)[a]	ΔT_m (°C)	MIC (µM:µg/mL)[c]
1 (−O−)	0.037 ± 0.005	38	29.1	0.037:0.027
2 (−NH−)	0.085 ± 0.01	<4b	22.8	6.25:4.6
3 (−NMe−)	4.39 ± 0.60	<4b	12.7	>25:>18.6

Table 4.2 Activity comparison between ADEP analogs.
[a]Amide hydrogen of the alanine residue within the cyclic peptidolactone/peptidolactam core at 40 °C in CD$_3$OD.
[b]Exchange was complete prior to the first scan.
[c]*B. subtilis* (ATCC 6051).

All three compounds were evaluated in broth microdilution minimum inhibitory concentration (MIC) assays against *B. subtilis*. As shown in **Table 4.2**, the ester exhibited the greatest whole-cell activity (37 nM) followed by the amide (6.25 µM) and then the *N*-methyl amide (>25 µM). Therefore, while the biochemical activity and thermal stabilization studies suggest −NH− macrocyclic substitution to be commensurate with the natural depsipeptide (~two-fold difference), the whole-cell activity demonstrates a significant difference in efficacy (>150-fold difference), presumably due to a decrease in the efficiency of membrane permeation.[54,55]

Inspection of the published ADEP1·ClpP (PDB ID: 3KTI) and ADEP2·ClpP (PDB ID: 3KTK) cocrystal structures reveals that the oxygen comprising the ester linkage of the depsipeptide is not involved in either intramolecular or intermolecular interactions when bound to ClpP.[20,53] As such, we hypothesized that any observed differences in biological activity, especially between the −O− and −NH− linkages likely arises from conformational differences. To evaluate the effect of linkage substitution on the conformational dynamics of the cyclic peptidolactone/peptidolactam cores, we conducted hydrogen–deuterium exchange experiments. Specifically of interest were the H/D exchange properties of the alanine residue within the cyclic peptidolactone/peptidolactam cores. Intramolecular hydrogen bonding of the alanine −NH− and the extracyclic 3,5-difluorophenylalanine carbonyl is observed in ADEP·ClpP cocrystal structures and thus has been postulated as an important feature in ADEP binding.[20,23] Strengthening this intramolecular hydrogen bond interaction can be accomplished by incorporation of a pipecolate residue in the depsipeptide core.[23] This structural modification leads to more rigidified analogs that mimic the bound conformation and thus reduces entropic binding penalties, resulting in the observed improvement in potency for rigidified ADEPs.[23]

The −O-linked compound (1) exhibited a much longer H/D exchange rate ($t_{1/2} = 38$ min) than the −NH− (2) and −NMe− (3) compounds, both of which revealed complete H/D exchange within the time required to setup the experiment ($t_{1/2} < 4$ min). This suggests that both the −NH− and −NMe− linkages perturb the macrocyclic conformation enough to disrupt the important intramolecular hydrogen bonding interaction between the alanine −NH− and the carbonyl of the 3,5-difluorophenylalanine. This is noteworthy in regards to the whole-cell activity, as intramolecular hydrogen bonding of macrocycles has been

shown to enhance permeation through lipid bilayers, presumably by decreasing energetic penalties for desolvation of hydrogen bond donors, especially NH groups.[54,55] Thus, although the overall effect of macrocyclic conformation for −O− to −NH− substitution in the linker is relatively small and can be easily overcome in the biochemical assay, it is plausible that the disruption of this intramolecular hydrogen bond negatively affects permeation and contributes significantly to the decreased whole-cell activity of 2.

Not surprisingly, the −NMe− linkage results in more drastic deviations from the optimal macrocyclic conformation, disrupting the intramolecular hydrogen bonding and likely producing a large amount of *cis* amide conformer. This cannot easily be overcome during binding, thus resulting in significant decreases in both potency and whole-cell activity. Indeed, our NMR analysis strongly indicates a conformational mixture of multiple highly populated conformations for 3.

4.5.4 Conclusion

In summary, we have synthesized and biochemically evaluated three ADEP analogs that only differ in the type of linkage (i.e., −O−, −NH−, and −NMe−). This systematic study allowed for the direct comparison of linkage substitution on target engagement, conformation, and whole-cell activity. In biochemical activity assays, the −O-linked analog (**1**) exhibits ~two-fold and ~100-fold better potency than the −NH− (**2**) and −NMe− (**3**) analogs, respectively. In MIC experiments against *B. subtilis*, **1** is ~170-fold and >650-fold more active than **2** and **3**, respectively. In all biochemical assays in which these derivatives were evaluated, this **1** > **2** > **3** trend of activity was observed. Computational and spectroscopic analyses revealed that conformation is likely the key factor in differentiating target engagement and whole-cell activity. We demonstrate that

simple replacement of the naturally occurring ester linkage with a secondary amide may not severely compromise the *in vitro* biochemical activity (target engagement), but results in a significant drop in whole-cell activity, presumably due to a disruption of a key hydrogen bonding interaction that is critical to cell permeation. As such, the excellent potency exhibited by rigidified ADEPs may not only arise from the preorganization of the depsipeptide core into a conformation optimized for ClpP binding, but also from an enhanced permeation profile. This study provides direct evidence that ester to amide linkage substitution is unlikely to yield a solution to ADEP instability and further highlights the need to continue the exploration for new ClpP activating chemotypes.

4.6 Materials and Methods

4.6.1 General Experimental Procedures

Positive controls were purchased from commercial sources and include enopeptin A (Santa Cruz Biotechnology, #sc-397311A), ADEP1 (Cayman Chemical, #15305), and ACP5 (Chembridge #5107473). ClpP substrates were purchased from commercial vendors and include FITC-β-casein (Sigma-Aldrich, C3777, 20−50 µg FITC per mg solid) and Abz-DFAPKMALVPY^{NO2} (Biomatik). Fluorescence readings were recorded on an i-TECAN Infinite M200 plate reader. Gel images were acquired on a Bio-Rad ChemiDoc MP CCD imaging system. All data analyses were performed with GraphPad Prism.

4.6.2 Protein Purification

Two different E. coli cell strains were used for overexpression. *Ec*ClpP was overexpressed in BLR (DE3) from Novagen and *Bs*ClpP in BL21 (DE3) from New England Biolabs. Overexpression and purification conditions for both proteins were

similar. Cell strains transformed with the relevant plasmids were grown at 37 °C to an OD600 of 0.7 followed by induction with 1 mM isopropyl β-D-thiogalactopyranoside and overnight overexpression at 25 °C. Cell pellets were resuspended in 20 mM Tris and 150 mM NaCl (pH 8.0) and lysed using an Avestin C3 Emulsiflex. Lysates were clarified by centrifugation at 12 000 rpm for 30 min and incubated with Ni-NTA (Qiagen) resin pre-equilibrated with 20 mM Tris and 150 mM NaCl (pH 8.0). Protein was eluted from Ni-NTA resin with 20 mM Tris, 150 mM NaCl, and 500 mM imidazole (pH 8.0) and concentrated. Gel filtration, using a Superdex 200 Increase size exclusion column (GE Healthcare), was used as a final purification step for both proteins. Gel filtration buffer conditions were 25 mM Tris, 100 mM KCl, and 10% glycerol (pH 7.5)[56] for *Ec*ClpP and 25 mM HEPES, 100 mM KCl, 20 mM MgCl2, 1 mM EDTA, and 10% glycerol (pH 7.6)[57] for *Bs*ClpP. Protein concentrations were determined using the calculated molar extinction coefficient in 6 M guanidinium hydrochloride.[58]

4.6.3 FITC-Casein Screening Assay

300 nM tetradecameric *Ec*ClpP in buffer A (25 mM Tris-HCl, pH 7.5, and 100 mM KCl) was incubated with compounds (50 µM) at 37 °C for 15 minutes in flat bottom, non-binding, non-sterile, white polystyrene 96-well plates (Corning 3990). After the pre-incubation period, 1 µL of a 19.2 mM FITC-β-casein solution (Sigma-Aldrich, C3777, 20-50 µg FITC per mg solid) in buffer A, was added to each assay well to give a final assay concentration of 192 µM FITC-β-casein and final assay volume of 100 µL. Assay plates were incubated at 37 °C and hydrolysis of the fluorogenic peptide was monitored via a TECAN Infinite M200 plate reader (excitation: 485 nm; emission: 538 nm). Readings were taken every 30 minutes for 6 hours. All compounds, along with Enopeptin A (25 µM,

positive control) and 1% DMSO (negative control) were normalized relative to background FITC-β-casein fluorescence. Data analysis was executed with GraphPad Prism.

4.6.4 Decapeptide Degradation Assay

As described previously,[22] 25 nM tetradecameric *Ec*ClpP in buffer B (25 mM HEPES, pH 7.5, 100 mM KCl, 5 mM MgCl$_2$, 10% glycerol, and 1 mM DTT) was incubated with the compound of interest over a range of concentrations at 30 °C for 15 minutes in flat bottom, non-binding, non-sterile, white polystyrene 96-well plate (Corning 3990). After the pre-incubation period 1µL of a 1.5 mM Abz-DFAPKMALVPY^{NO2} (Biomatik) solution was added to each assay well to give a final assay concentration of 15 µM fluorogenic decapeptide and final assay volume of 100 µL. Assay plates were incubated at 30 °C and hydrolysis of the fluorogenic peptide was monitored via an TECAN Infinite M200 plate reader (excitation: 320 nm; emission: 420 nm). Readings were taken every 30 minutes for 2 hours. All compounds, along with ADEP1 (positive control) and 1% DMSO (negative control) were normalized relative to background Abz-DFAPKMALVPY^{NO2} fluorescence. Data analysis was executed with GraphPad Prism.

4.6.5 FITC-Casein Degradation Assay

257 nM tetradecameric *Ec*ClpP in buffer A (25 mM Tris-HCl, pH 7.5, and 100 mM KCl) was incubated with the compound of interest over a range of concentrations at 37 °C for 15 minutes in flat bottom, non-binding, non-sterile, white polystyrene 96-well plate (Corning 3990). After the pre-incubation period 1 µL of a 0.45 mM FITC-β-casein (Sigma-Aldrich, C3777, 20-50 µg FITC per mg solid) solution in buffer A was added to each assay well to give a final assay concentration of 4.5 µM fluorogenic decapeptide and final assay volume of 100 µL. Assay plates were incubated at 37 °C and hydrolysis of the fluorogenic

peptide was monitored via an TECAN Infinite M200 plate reader (excitation: 485 nm; emission: 538 nm). Readings were taken every 30 minutes for 6 hours. All compounds, along with ADEP1 (positive control) and 1% DMSO (negative control) were normalized relative to background FITC-β-casein fluorescence. Data analysis was executed with GraphPad Prism.

4.6.6 SDS-PAGE Analysis

420 nM tetradecameric *Ec*ClpP or *Bs*ClpP in buffer A (59 µL) was incubated with the compound of interest at the desired concentration for 15 minutes at 37 °C in Eppendorf tubes. 16 µL of a bovine β-casein (Sigma-Aldrich C6905, Bio-Ultra ≥ 98%) solution in buffer A was then added for a final substrate concentration of 7.5 µM and a final assay volume of 75 µL. The reaction was quenched with 25 µL of Laemmli loading buffer (Alfa Aesar J60015) at 80 °C. Individual reactions were quenched after 5 m, 30 m, 1 h, and/or 2 h depending on the compound. The samples were then boiled for approximately 1 minute prior to loading. Time-dependent degradation of the β-casein band visualized using SDS-PAGE performed on a 10% acrylamide Bis-Tris gel.

4.5.7 MIC Determination

Using the 2-fold dilution technique in 96-well microtiter plates, cells were subcultured (1:100 dilution) in fresh LB media (tryptone 10 g/L, yeast extract 5 g/L, and NaCl 5 g/L) and grown to an OD600 of ~1.0. Cells were inoculated at a density of 105 cells per mL into LB media in the presence of 2-fold increasing concentrations of 1. MIC values were determined visually after incubation of the microtiter plates at 37 °C for 18 h.

4.6.8 Thermal Shift Assay

All compounds were evaluated at a final assay concentration of 50 µM. 1 µM *Bs*ClpP monomer (71.4 nM tetradecamer) and 2 µL of 5 mM compound of interest prepared in activity buffer 2 (20 mM HEPES pH = 7.0, 100 mM NaCl) in 1.5 mL Eppendorf tubes. SYPRO baseline control and DMSO negative control were prepared similarly. Protein and controls were pre-incubated for 30 min at 25 °C. After pre-incubation, 2 µL of 100X SYPRO Orange Protein Gel Stain, prepared in 100% DMSO and stored in light-free desiccator at 25 °C, was added to the samples and mixed thoroughly for a total volume of 200 µL. The large 200 µL samples were split into 3 x 50 µL wells in 96-well, Hard Shell®, thin-wall PCR Plates (BioRad HSP9601) sealed with optically clear Microseal® 'B' adhesive seals (BioRad MSB1001). The resulting plates were spun in a tabletop PCR plate spinner (VWR 89184-608) in 15 sec intervals until all bubbles were removed. Samples rested in the dark for 10 min and were then evaluated using BioRad CFX96 TM Real-Time System. Melt curves were prepared in increments of 0.3 °C per minute over a range of 25 °C to 85 °C, with FRET readings taken after a 1-minute hold at each temperature. Melting temperatures were determined by nonlinear fitting to a Boltzmann Sigmoidal Curve using GraphPad Prism.

4.6.9 MIC Determination

B. subtilis ATCC 6051 was streaked onto an LB agar plate and grown overnight at 37 °C. Pre-warmed (37 °C) Mueller–Hinton broth (5 mL) was inoculated with 3–5 colonies of *B. subtilis*. The culture was incubated at 37 °C shaking at 250 rpm overnight. The resulting overnight stock solution of *B. subtilis* was diluted 1:100 to provide the assay stock solution. Following standard microdilution protocol1 compounds 1–3 were serially diluted

to provide a final well volume of 200 µL. Briefly, 2 µL of compound stock was added to 198 µL of Mueller-Hinton broth. This was then serially diluted 2-fold down the plate by taking 100 µL and transferring to the subsequent well that contained 100 µL of Mueller–Hinton broth. To each well was then added 100 µL of the 1:100 dilution *B. subtilis* assay culture to obtain a final well volume of 200 µL. Plates were incubated overnight at 37 °C and after 16 h, MIC values were determined by visual inspection. Reported MIC values indicate the concentration of the last well containing no visible cell growth. Ampicillin and Kanamycin were used as positive controls. DMSO treatment was used as a negative control. Buffer only wells were included as a control/indicator of bacterial contamination. Each compound was tested in triplicate. Top concentrations for each compound evaluated: Ampicillin (125 µg/mL, 357.7 µM), Kanamycin (125 µg/mL, 258.0 µM), 1 (0.183 µg/mL, 250 nM). 2 (18.25 µg/mL, 25 µM), 3 (18.60 µg/mL, 25 µM). Stock solutions for each compound evaluated: Ampicillin (71.5 mM), Kanamycin (51.6 mM), 1 (50 µM), 2 (5 mM), and 3 (5 mM).

4.6.10 Hydrogen-Deuterium Exchange

Purified ADEPs 1 and 2 were stored in a desiccator for one week at 25 °C prior to H/D exchange experiments. The NMR probe was pre-equilibrated to either 25 °C or 40 °C before introduction of the NMR sample. NMR samples were prepared by dissolving compound 1 or 2 in ampule sealed CD_3OD at a concentration of 2 mM. The samples were mixed and promptly transferred to a clean NMR tube. 1H-NMR spectra were acquired at 500 MHz with 8 scans, 1 second delay, sweep width of 8012.8 Hz and 16384 complex points. Timing of each kinetic run was carefully started upon sample mixing. The time of the first collected spectra was designated as t1. Subsequent spectra were collected at 300

second intervals with a 24 second acquisition time. The kinetic runs were terminated when the amide peaks were completely exchanged and no longer visible. The data was processed in MestReNova software. The data was zero filled to 65536 points with a 0.70 Hz exponential function and baseline correction applied upon processing. The integration of the exchanging amide signal of interest was calibrated to a non-exchanging reference peak and converted to concentration. The concentration versus time data was analyzed using PRISM software.

4.7 References

1. Gersch, M. *et al.* AAA+ chaperones and acyldepsipeptides activate the ClpP protease via conformational control. *Nat. Commun.* **6,** 6320 (2015).

2. Bhandari, V. *et al.* The role of ClpP protease in bacterial pathogenesis and human diseases. *ACS Chem. Biol.* **13,** 1413–1425 (2018).

3. Böttcher, T. & Sieber, S. A. Beta-lactones as specific inhibitors of ClpP attenuate the production of extracellular virulence factors of *Staphylococcus aureus*. *J. Am. Chem. Soc.* **130,** 14400–14401 (2008).

4. Gersch, M. *et al.* The mechanism of caseinolytic protease (ClpP) inhibition. *Angew. Chem. Int. Ed. Engl.* **52,** 3009–3014 (2013).

5. Böttcher, T. & Sieber, S. A. Beta-lactones as specific inhibitors of ClpP attenuate the production of extracellular virulence factors of *Staphylococcus aureus*. *J. Am. Chem. Soc.* **130,** 14400–14401 (2008).

6. Ollinger, J., O'Malley, T., Kesicki, E. A., Odingo, J. & Parish, T. Validation of the essential ClpP protease in *Mycobacterium tuberculosis* as a novel drug target. *J.*

Bacteriol. **194,** 663–668 (2012).

7.   Compton, C. L., Schmitz, K. R., Sauer, R. T. & Sello, J. K. Antibacterial activity of and resistance to small molecule inhibitors of the ClpP peptidase. *ACS Chem. Biol.* **8,** 2669–2677 (2013).

8.   Hackl, M. W. *et al.* Phenyl esters are potent inhibitors of caseinolytic protease P and reveal a stereogenic switch for deoligomerization. *J. Am. Chem. Soc.* **137,** 8475–8483 (2015).

9.   Cole, A. *et al.* Inhibition of the mitochondrial protease clpp as a therapeutic strategy for human acute myeloid leukemia. *Cancer Cell* **27,** 864–876 (2015).

10. Evans, M. J. & Cravatt, B. F. Mechanism-based profiling of enzyme families. *Chem. Rev.* **106,** 3279–3301 (2006).

11. Brötz-Oesterhelt, H. *et al.* Dysregulation of bacterial proteolytic machinery by a new class of antibiotics. *Nat. Med.* **11,** 1082–1087 (2005).

12. Michel, K. H. & Kastner, R. E. A54556 antibiotics and process for production thereof. *US Patent 4* (492AD).

13. Bewley, M. C., Graziano, V., Griffin, K. & Flanagan, J. M. Turned on for degradation: ATPase-independent degradation by ClpP. *J. Struct. Biol.* **165,** 118–125 (2009).

14. Li, D. H. S. *et al.* Acyldepsipeptide antibiotics induce the formation of a structured axial channel in ClpP: A model for the ClpX/ClpA-bound state of ClpP. *Chem. Biol.* **17,** 959–969 (2010).

15. Lee, B.-G., Kim, M. K. & Song, H. K. Structural insights into the conformational diversity of ClpP from *Bacillus subtilis*. *Mol. Cells* **32,** 589–595 (2011).

16. Joshi, S. A., Hersch, G. L., Baker, T. A. & Sauer, R. T. Communication between ClpX and ClpP during substrate processing and degradation. *Nat. Struct. Mol. Biol.* **11,** 404–411 (2004).

17. Lee, M. E., Baker, T. A. & Sauer, R. T. Control of substrate gating and translocation into ClpP by channel residues and ClpX binding. *J. Mol. Biol.* **399,** 707–718 (2010).

18. Carney, D. W., Schmitz, K. R., Scruse, A. C., Sauer, R. T. & Sello, J. K. Examination of a Structural Model of Peptidomimicry by Cyclic Acyldepsipeptide Antibiotics in Their Interaction with the ClpP Peptidase. *Chembiochem* **16,** 1875–1879 (2015).

19. Gominet, M., Seghezzi, N. & Mazodier, P. Acyl depsipeptide (ADEP) resistance in *Streptomyces*. *Microbiology (Reading, Engl.)* **157,** 2226–2234 (2011).

20. Hinzen, B. *et al.* Medicinal chemistry optimization of acyldepsipeptides of the enopeptin class antibiotics. *ChemMedChem* **1,** 689–693 (2006).

21. Conlon, B. P. *et al.* Activated ClpP kills persisters and eradicates a chronic biofilm infection. *Nature* **503,** 365–370 (2013).

22. Carney, D. W. *et al.* A simple fragment of cyclic acyldepsipeptides is necessary and sufficient for ClpP activation and antibacterial activity. *Chembiochem* **15,** 2216–2220 (2014).

23. Carney, D. W., Schmitz, K. R., Truong, J. V., Sauer, R. T. & Sello, J. K. Restriction of the conformational dynamics of the cyclic acyldepsipeptide antibiotics improves their antibacterial activity. *J. Am. Chem. Soc.* **136,** 1922–1929 (2014).

24. Socha, A. M., Tan, N. Y., LaPlante, K. L. & Sello, J. K. Diversity-oriented synthesis of cyclic acyldepsipeptides leads to the discovery of a potent antibacterial agent. *Bioorg. Med. Chem.* **18,** 7193–7202 (2010).

25. Brötz, H. Dysregulation of bacterial proteolytic machinery by a new class of antibiotics. *Oesterhelt*

26. Leung, E. *et al.* Activators of cylindrical proteases as antimicrobials: identification and development of small molecule activators of ClpP protease. *Chem. Biol.* **18,** 1167–1178 (2011).

27. Gottesman, S., Roche, E., Zhou, Y. & Sauer, R. T. The ClpXP and ClpAP proteases degrade proteins with carboxy-terminal peptide tails added by the SsrA-tagging system. *Genes Dev.* **12,** 1338–1347 (1998).

28. Lavey, N. P., Coker, J. A., Ruben, E. A. & Duerfeldt, A. S. Sclerotiamide: The First Non-Peptide-Based Natural Product Activator of Bacterial Caseinolytic Protease P. *J. Nat. Prod.* **79,** 1193–1197 (2016).

29. Du, L. *et al.* Crowdsourcing Natural Products Discovery to Access Uncharted Dimensions of Fungal Metabolite Diversity. *Angew. Chem. Int. Ed. Engl.* (2013). doi:10.1002/anie.201306549

30. Niu, G. *et al.* Targeting mosquito FREP1 with a fungal metabolite blocks malaria transmission. *Sci. Rep.* **5,** 14694 (2015).

31. Wang, B., You, J., King, J. B., Cai, S. & Park, E. Polyketide Glycosides from Bionectria ochroleuca Inhibit Candida albicans Biofilm Formation. *Journal of natural ...* (2014).

32. Du, L., Risinger, A. L., King, J. B., Powell, D. R. & Cichewicz, R. H. A potent HDAC inhibitor, 1-alaninechlamydocin, from a Tolypocladium sp. induces G2/M cell cycle arrest and apoptosis in MIA PaCa-2 cells. *J. Nat. Prod.* **77,** 1753–1757 (2014).

33. Du, L., Robles, A. J., King, J. B., Mooberry, S. L. & Cichewicz, R. H. Cytotoxic

dimeric epipolythiodiketopiperazines from the ascomycetous fungus Preussia typharum. *J. Nat. Prod.* **77,** 1459–1466 (2014).

34. Osada, H., Yano, T. & Koshino, H. Enopeptin A, a novel depsipeptide antibiotic with anti-bacteriophage activity. *The Journal of …* (1991).

35. Koshino, H., Osada, H., Yano, T., Uzawa, J. & Isono, K. The structure of enopeptins A and B, novel depsipeptide antibiotics. *Tetrahedron Lett.* **32,** 7707–7710 (1991).

36. Brideau, C., Gunter, B., Pikounis, B. & Liaw, A. Improved statistical methods for hit selection in high-throughput screening. *J. Biomol. Screen.* **8,** 634–647 (2003).

37. Pelz, O., Gilsdorf, M. & Boutros, M. web cellHTS2: a web-application for the analysis of high-throughput screening data. *BMC Bioinformatics* **11,** 185 (2010).

38. Whyte, A. C., Gloer, J. B., Wicklow, D. T. & Dowdw, P. F. Sclerotiamide: a new member of the paraherquamide class with potent antiinsectan activity from the sclerotia of *Aspergillus sclerotiorum*. *J. Nat. Prod.* **59,** 1093–1095 (1996).

39. Thompson, M. W. & Maurizi, M. R. Activity and specificity of *Escherichia coli* ClpAP protease in cleaving model peptide substrates. *J. Biol. Chem.* **269,** 18201–18208 (1994).

40. Finefield, J. M. *et al.* Biosynthetic studies of the notoamides: isotopic synthesis of stephacidin A and incorporation into notoamide B and sclerotiamide. *Org. Lett.* **13,** 3802–3805 (2011).

41. Mercado, E. V. Total synthesis and isolation of citrinalin and cyclopiamine congeners. *Marin*

42. Finefield, J. M., Frisvad, J. C., Sherman, D. H. & Williams, R. M. Fungal origins of the bicyclo[2.2.2]diazaoctane ring system of prenylated indole alkaloids. *J. Nat.*

Prod. **75,** 812–833 (2012).

43. Peng, J., Zhang, X.-Y., Tu, Z.-C., Xu, X.-Y. & Qi, S.-H. Alkaloids from the deep-sea-derived fungus *Aspergillus westerdijkiae* DFFSCS013. *J. Nat. Prod.* **76,** 983–987 (2013).

44. Kato, H. *et al.* Notoamides A-D: prenylated indole alkaloids isolated from a marine-derived fungus, *Aspergillus* sp. *Angew. Chem. Int. Ed. Engl.* **46,** 2254–2256 (2007).

45. Rosner, J. L. & Martin, R. G. Reduction of cellular stress by TolC-dependent efflux pumps in *Escherichia coli* indicated by BaeSR and CpxARP activation of spy in efflux mutants. *J. Bacteriol.* **195,** 1042–1050 (2013).

46. Mima, T., Joshi, S. & Gomez, M. Identification and characterization of TriABC-OpmH, a triclosan efflux pump of *Pseudomonas aeruginosa* requiring two membrane fusion proteins. *Escalada…*

47. Famulla, K. *et al.* Acyldepsipeptide antibiotics kill mycobacteria by preventing the physiological functions of the ClpP1P2 protease. *Mol. Microbiol.* **101,** 194–209 (2016).

48. Bionda, N., Fleeman, R. M., Shaw, L. N. & Cudic, P. Effect of Ester to Amide or N-Methylamide Substitution on Bacterial Membrane Depolarization and Antibacterial Activity of Novel Cyclic Lipopeptides. *ChemMedChem* (2013). doi:10.1002/cmdc.201300173

49. Bionda, N., Stawikowski, M. & Stawikowska, R. Effects of cyclic lipodepsipeptide structural modulation on stability, antibacterial activity, and human cell toxicity. … (2012).

50. Goodreid, J. D. *et al.* Development and Characterization of Potent Cyclic

Acyldepsipeptide Analogues with Increased Antimicrobial Activity. *J. Med. Chem.* **59,** 624–646 (2016).

51. Lewis, K., Conlon, B. & Nelson, M. L. Methods of eradicating bacterial cell populations. *US Patent App. 14 …* (2014).

52. Brötz, H. Dysregulation of bacterial proteolytic machinery by a new class of antibiotics. *Oesterhelt*

53. Lee, B.-G. *et al.* Structures of ClpP in complex with acyldepsipeptide antibiotics reveal its activation mechanism. *Nat. Struct. Mol. Biol.* **17,** 471–478 (2010).

54. Rezai, T. *et al.* Conformational flexibility, internal hydrogen bonding, and passive membrane permeability: successful in silico prediction of the relative permeabilities of cyclic peptides. *J. Am. Chem. Soc.* **128,** 14073–14080 (2006).

55. Rezai, T., Yu, B., Millhauser, G. L., Jacobson, M. P. & Lokey, R. S. Testing the conformational hypothesis of passive membrane permeability using synthetic cyclic peptide diastereomers. *J. Am. Chem. Soc.* **128,** 2510–2511 (2006).

56. Flanagan, J. M., Wall, J. S., Capel, M. S., Schneider, D. K. & Shanklin, J. Scanning transmission electron microscopy and small-angle scattering provide evidence that native *Escherichia coli* ClpP is a tetradecamer with an axial pore. *Biochemistry* **34,** 10910–10917 (1995).

57. Martin, A., Baker, T. A. & Sauer, R. T. Distinct static and dynamic interactions control ATPase-peptidase communication in a AAA+ protease. *Mol. Cell* **27,** 41–52 (2007).

58. Gill, S. C. & von Hippel, P. H. Calculation of protein extinction coefficients from amino acid sequence data. *Anal. Biochem.* **182,** 319–326 (1989)

Chapter 5

The Crystallographic Structure of Caseinolytic Protease P1 from

Clostridium difficile 630[5]

5.1 Abstract

We sought to determine the structure of each caseinolytic protease P (ClpP) isoform in *Clostridium difficile* to provide structural evidence to better understand why ClpP1 is susceptible to acyldepsipeptide activation, while ClpP2 was not. Furthermore, the structural information obtained would allow us to tailor chemical modulators to each isoform. Our efforts resulted in producing crystals of each isoform, eventually yielding the crystallographic structure of ClpP1 at 2.5Å resolution. Herein, the crystallization and structural solution of ClpP1 will be discussed.

---

[5] N.P.L. conducted the crystallization, collected the datasets, and provided initial structural solutions. Leonard Thomas from the Macromolecular Core Laboratory provided the final refined structural solution, and validated the ClpP1 structure for Protein Database submission. All datasets were collected at the Stanford Synchrotron Radiation Lightsource.

5.2 Results

Broad screen crystallization trials were performed in order to find suitable crystallization conditions that would yield large, high quality crystals of each ClpP isoform (Appendix C). ClpP1 was overexpressed in JK10 cells and purified as described in Chapter 2. Sitting drop crystallization experiments were conducted with ClpP1 at a concentration of 4.5 mg/mL, aliquoted into 96-well plates in 1:1 or 2:1 to crystallization buffer. ClpP1 readily crystallized in several different conditions at room temperature, with 2.6M sodium malonate at pH 7.0 providing large crystals in a relatively short period of time (<4 days). We chose sodium malonate as our primary condition to optimize because sodium malonate is an excellent cryoprotectant, making this step much easier in the future.[1] To optimize this condition, we performed hanging drop crystallization experiments in 24-well plates over a range of sodium malonate concentrations, and varying pH. 2.4M sodium malonate at pH 6.0 yielded the largest crystals in approximately 2 days, and this was routinely reproduced successfully. These crystals were then screened for diffraction at the Macromolecular Core Laboratory (MCL) before being sent to the Stanford Synchrotron Radiation Lightsource (SSRL).

The ClpP1 crystals provided diffraction patterns of sufficient quality which were processed in HKL2000 for scaling and merging. These datasets were then processed in PHENIX with Molecular Replacement (MR) to provide the initial structural solution.[2] The individual datasets lacked sufficient completeness (>95%), requiring two datasets in the P1 space group to be combined with BLEND.[3,4] After the datasets were combined, scaled, and merged, the structural solution via MR yielded the structure of ClpP1 in the active extended conformation (**Figure 5.1**).
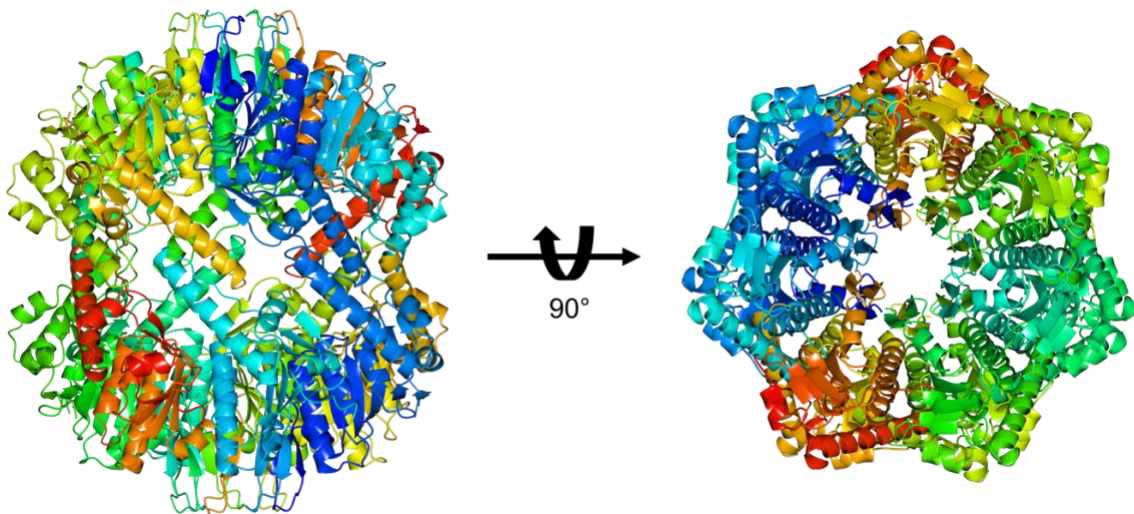
Figure 5.5 - Structure of ClpP1 in the Active Extended Conformation
The structure of ClpP1 in the active extended conformation was solved via MR, and further refined in PHENIX before deposition in the Protein Database (PDB) under 6MX2. The biological unit is shown above in the side pose (left) and the top pose (right). The data collection and refinement statistics are listed in **Appendix C.2**.

The structure of ClpP1 from *C. difficile* possessed no obvious differences from other known structures of ClpP listed in the PDB. This was anticipated as the structure of ClpP is highly conserved, even when compared to other isoforms with low sequence similarity. By itself, the structure of ClpP1 is not particularly useful nor impactful to report within the field. The structure serves to confirm our initial results in Chapter 2, in that ClpP1 forms a stable tetradecameric complex that is not contaminated with *E. coli* ClpP.

5.3 Future Directions

Our future directions are immediately concerned with obtaining the crystal structure of ClpP2 in the active extended conformation. Currently, we are able to produce crystals of ClpP2 in several different conditions that successfully diffract. Unfortunately, these datasets severely lack completeness and are poor in quality. Optimizing our initial

crystallization conditions will aid in obtaining higher quality datasets for ClpP2, and these experiments are currently underway. As stated initially, obtaining a crystallographic structure of ClpP2 will provide the structural evidence for why ClpP1 and ClpP2 differ in susceptibility to ADEPs and aid in structure guided optimization of future chemical modulators.

5.4 Materials and Methods

5.4.1 Protein Production and Purification

ClpP1 and ClpP2 were overexpressed and purified as described in Chapter 2 of this dissertation, and were similarly kept in activity buffer for crystallization. We found that transferring to a simple crystallization buffer (50mM Tris pH 7.6, 100mM NaCl, 10% glycerol) triggered rapid precipitation of the protein.

5.4.2 Crystallization and Structure Solution

ClpP1 and ClpP2 were each subjected to several commercial broad screen crystallization kits in a 96-well format at room temperature (**Appendix C.1**). Prior to any crystallization experiment, the protein was spun at 12,000 rcf for 8 minutes to ensure any precipitated protein was pelleted and discarded. A Mosquito liquid handler was used to dispense aliquots of ClpP1 and ClpP2 at 4.5 mg/mL into 96-well plates for sitting drop crystallization in 1:1 and 2:1 ratio against precipitation buffers, to a total volume of 300 nL. Plates were then sealed with optically clear tape and allowed to crystallize at room temperature. Optimization of broad screen hits were formed in hanging drop experiments on silicon wafers, which were sealed with vacuum grease above wells in a 24-well plate.

Each well contained 500 μL of precipitation buffer to which hanging drops were mixed with in 1:1, 2:1, and 1:3 ratios.

For ClpP1, crystals formed after 1-2d at room temperature in 2.6M sodium malonate at pH 6.0. These crystals were sufficiently cryoprotected, but sometimes were further cryoprotected by addition 3.2M sodium malonate at pH 6.0 directly to the hanging drop. Crystals were flash frozen in liquid N_2 and shipped to the SSRL beamline 9-2 for remote data collection. These datasets were initially processed in HKL3000 for integration, merging, and scaling. The resulting dataset was then processed in PHENIX with MR to solve the structure against 3KTH. Phenix.refine was then used to refine the resulting structure, after manual refinement and residue correction via COOT. A final round of refinement was performed by PDB-REDO before submitting to the MCL for final structure refinement and validation.

5.5 References

1. Holyoak, T. *et al.* Malonate: a versatile cryoprotectant and stabilizing solution for salt-grown macromolecular crystals. *Acta Crystallogr. Sect. D, Biol. Crystallogr.* **59,** 2356–2358 (2003).

2. Adams, P. D. *et al.* PHENIX: a comprehensive Python-based system for macromolecular structure solution. *Acta Crystallogr. Sect. D, Biol. Crystallogr.* **66,** 213–221 (2010).

3. Mylona, A. *et al.* A Novel Approach to Data Collection for Difficult Structures: Data Management for Large Numbers of Crystals with the BLEND Software. *Crystals* **7,** 242 (2017).

4. Winn, M. D. *et al.* Overview of the CCP4 suite and current developments. *Acta Crystallogr. Sect. D, Biol. Crystallogr.* **67,** 235–242 (2011).

Epilogue

This body of work biochemically and phenotypically describes the ClpP system in *C. difficile*. Our long-term goal for this project was to show the biological significance of targeting ClpP, in order to introduce ClpP as a new target against CDI. To do so, we wanted to directly address the current challenges facing the development of therapeutics for treating CDI. We first set out to understand what the operative ClpP system was before we moved into the pathogen itself. This included understanding how each ClpP isoform assembled, how they behaved *in vitro*, and what the structures were. We accomplished this initial goal, both biochemically and structurally characterizing the ClpP system in *C. difficile*. Those results laid the groundwork for pursuing the biological significance of the ClpP system in *C. difficile* 630.

Future experiments will build upon the work described throughout this dissertation that will be concentrated on sporulation, virulence, and nutrient response regulation. Our immediate attention will be focused towards completing the work described in Chapter 3, as many of these studies are currently underway. The most critical gaps are: 1) generating complements for *clpP1*, *clpP2*, and *clpP1P2*, 2) quantifying sporulation regulatory factor transcripts via qRTPCR in *clpP* mutants, and 3) obtaining *spo0A* mutants as our sporulation negative control. The complements will be necessary in order to show that loss of ClpP function is responsible for the asporogenic phenotype, and not a consequence of our mutagenesis.

Broader future directions related to the work described in this dissertation are: 1) Replicating the asporogenic phenotype in *C. difficile* through chemo-modulation of ClpP, and 2) completing RNAseq in *clpP* mutants to globally monitor sporulation regulatory

signals after loss of ClpP function. ClpP inhibitors already exist which have not yet been assayed for activity against either ClpP1 or ClpP2. In order to assess ClpP inhibition as a viable therapeutic strategy to combat CDI, *in vitro* activity assays are planned to determine whether known ClpP inhibitors are active against *C. difficile* ClpP isoforms. More broad-spectrum inhibitors such as phenylmethylsulfonyl fluoride are commercially available and broadly inhibit serine proteases which could be used in the event ClpP inhibitors are ineffective. RNAseq experiments are currently being planned which will help define the role each ClpP isoform maintains in regulating sporulation. For example, ClpP1 and ClpP2 maintain specific roles in processing the engulfment machinery protein SpoIIP. RNAseq would help to differentiate ClpP1 from ClpP2 by understanding the overarching regulation of sporulation which may contribute to the processing of SpoIIP which would be highly impactful to *C. difficile* sporulation research as SpoIIP processing is currently not understood.

Advancing our understanding of these fundamental processes critical to sporulation may reveal new therapeutic targets that are more tractable, or easier to target. Results from these studies could eventually aid in the design of new chemical probes and antibiotics to better understand sporulation and translate into real therapeutics to combat the transmission and spread of CDI.

Appendix A: Sequences and supporting data for *Clostridium difficile* ClpP Homologs are Capable of Uncoupled Activity and Exhibit Different Levels of Susceptibility to Acyldepsipeptide Modulation

Primer ID	Primer Sequence (5'-3')
rpoB_F	AACTAGGGCCAGAGGAAATAAC
rpoB_R	CTGAGTCTACTTCTGCACCTATTC
clpP1_F	GCTGAAGACCCAGACAAAGATA
clpP1_R	CTCCCATAGAAGCAGCCATAC
clpP2_F	GGCTCTGCTACATCAGGATTTG
clpP2_R	CATGTGTTCCTCCTGCAAGTAA

Table A.1 qRTPCR Primers.
Integrated DNA Technologies (IDT) PrimerQuest tool was used to pick primer pairs for *clpP1* and *clpP2*. *rpoB*, the gene that encodes the β-subunit of bacterial RNA polymerase, was used as the reference gene.

	clpP1	*clpP2*	*rpoB*
Log	14.80 ± 0.02	20.88 ± 0.02	16.81 ± 0.00
Stationary	17.34 ± 0.01	22.68 ± 0.02	19.89 ± 0.02

Table A.2 C_t counts for qRT-PCR Individual C_t values for each transcript quantified
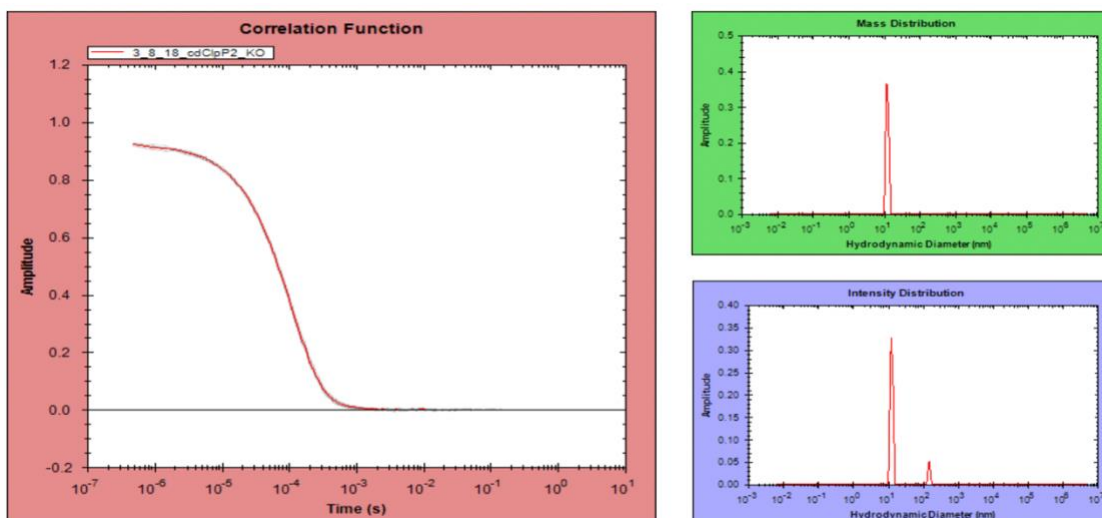Raw C_t counts for qRT-PCR experiments performed in Chapter 2.

```
A0A125YDM9_CLODI  MSLVPHVIEQTGQGERSYDIYSKLLKDRIIFIGEEINDAIASLVVAQLLFLESEDPDSDI  60
U3V0G5_CLODI      MALVPVVVEQTGRGERSYDIFSRLLKDRIIFLGDQVNDATAGLIVAQLLFLEAEDPDKDI  60
                  *:*** *:****:*******:*:*******:*::*** *.*:********:****.**

A0A125YDM9_CLODI  IIYINSPGGSATSGFAIYDTMNYVRCDVSTICIGMAASMSAFLLAGGTHGKRCALPNSEI  120
U3V0G5_CLODI      HLYINSPGGSITSGMAIYDTMQYIKPDVSTICIGMAASMGAFLLAAGAKGKRLALPNSEI  120
                  :********  ***:******:*:: *************.*****.*::*** *******

A0A125YDM9_CLODI  MIHQPMGGAKGQATDVKIAVDNILKIKERLDKILSENTGKSIEDIRRDTDRDNFMTALEA  180
U3V0G5_CLODI      MIHQPLGGAQGQATDIEIHAKRILKIKETLNEILSERTGQPLEKIKMDTERDNFMSALEA  180
                  *****:***:*****::*  ...******  *::****.**:  :*.*:  **:*****:****

A0A125YDM9_CLODI  KEYGLIDYIMNRNE  194
U3V0G5_CLODI      KEYGLIDEVFTKRP  194
                  ******* ::.:.
```

Figure A.1 HR-ESIMS peptide digest and sequencing results.
Combined sequence coverage of ClpP1 (bottom) and ClpP2 (top) prepared from Δ*Ec*ClpP. Coverage obtained following data merging after trypsin and chymotrypsin digest. Bold underline: identified sequence; green: amino acids differing between the two isoforms.

Figure A.2 pUNK DLS results for ClpP1 prepared from Δ*Ec*ClpP cells.
DLS measurements were performed in order to demonstrate monodispersity of the ClpP1 sample, and understand if multiple complexes were being performed.

Figure A.3 pUNK DLS results for ClpP2 prepared from ΔEcClpP cells.
DLS measurements were performed in order to demonstrate monodispersity of the ClpP2 sample, and understand if multiple complexes were being performed.

Figure A.4 Predicted ClpP2 disulfides predicted by DiANNA.
DiANNA webserver can predict potential disulfide bond interactions given the primary sequence of the protein of interest. This was performed in order to understand the potential for ClpP2 to form disulfide bonds which may have explained the lack of peptidolytic or proteolytic activity in our initial activity experiments.
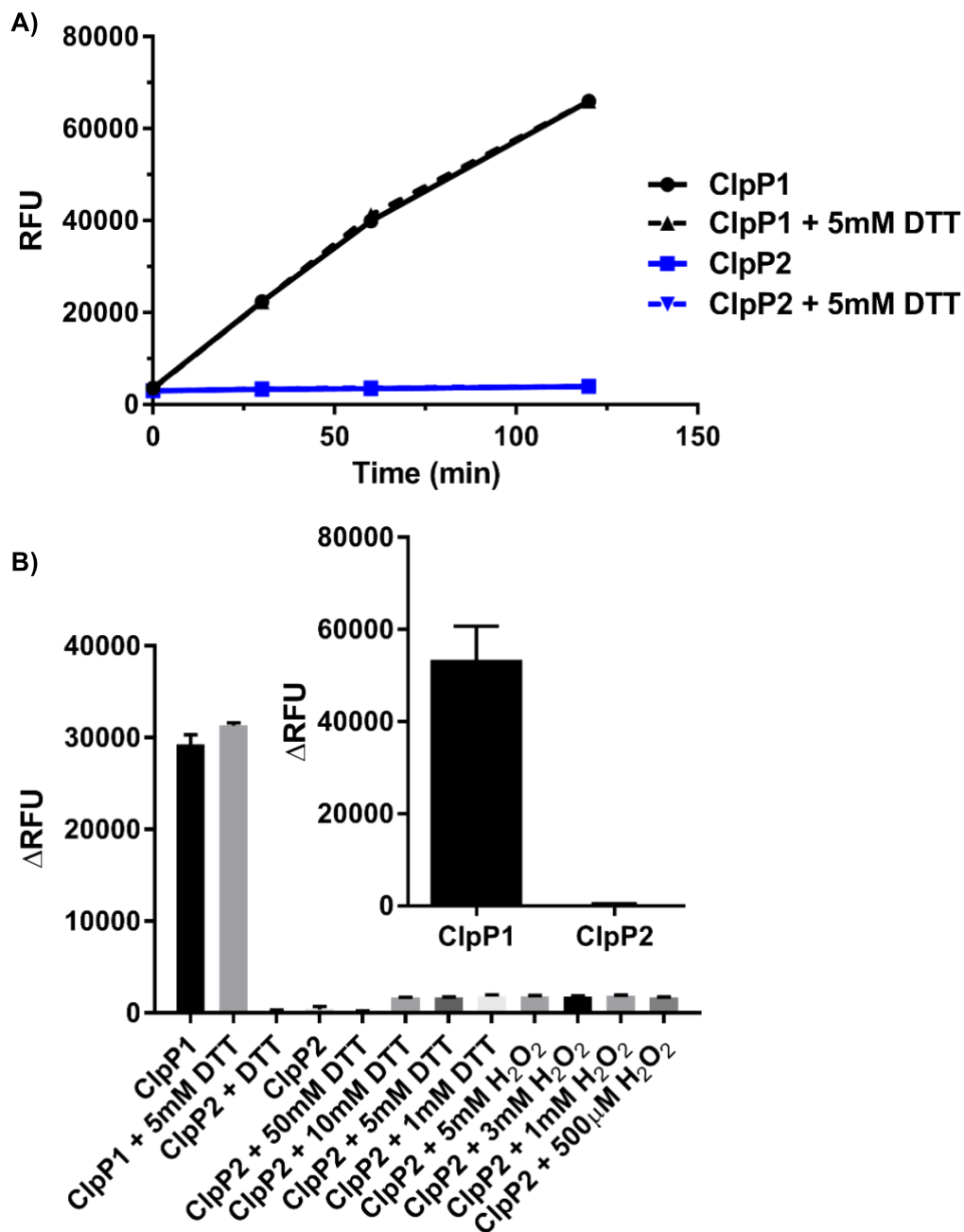
Figure A.5 Reduction or oxidation of ClpP2 has no consequences on proteolytic activity.
A) SLY-AMC peptidolytic assay over 2h, fluorescence measurements taken 30 m, 60 m, and 120 m with and without 5 mM DTT. B) SLY-AMC peptidolytic assay with reducing (DTT) and oxidizing (H_2O_2) conditions had no effect on proteolytic activity of ClpP2. Inset, Aliquots from GFP-ssrA degradation assays were diluted 10-fold into 100 μL activity buffer containing 5 mM DTT and pipetted in triplicate into a black 96-well flat bottom

plate. SLY-AMC was added, and the reaction was allowed to proceed for ~48h before reading.
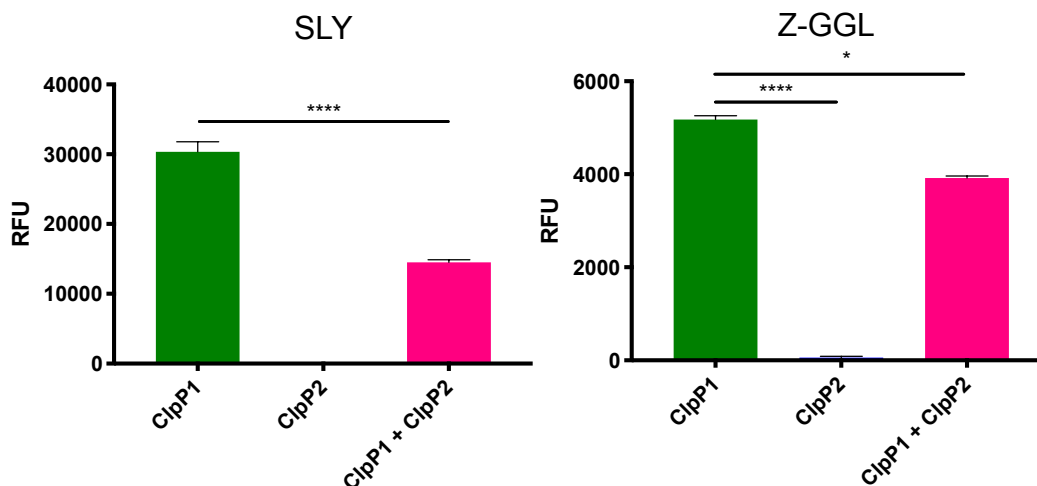
Rate of Degradation (ΔRFU, min^-1)

	SLY	Rel. ClpP1	Z-GGL	Rel. ClpP1
ClpP1	1944	n/a	540.6	n/a
ClpP2	21.1	1.1	8.0	1.5
ClpP1 + ClpP2	899.8	46.3	306	56.6

Figure A.6 Peptidolytic activity of mixed solutions of ClpP1 and ClpP2 compared to homogenous solutions.

An attempt to assess whether or not ClpP1 and ClpP2 could form a heteromeric complex *in vitro*. When mixed in equal concentrations, the relative intensities generated by the mixture is approximately half of the relative intensity observed in ClpP1 alone. In this manner, it appears that ClpP1 is chiefly responsible for the majority of observed fluorescence.
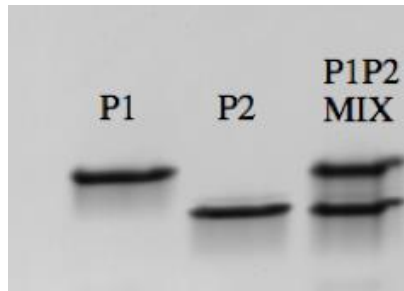
Figure A.7 Non-denaturing PAGE gel (7-15%) of mixed ClpP1 and ClpP2 homotetradecamers after 2 h.

As shown by native PAGE, mixing the two homogenous assemblies of tetradecameric ClpP was unable to produce a heteromeric complex.
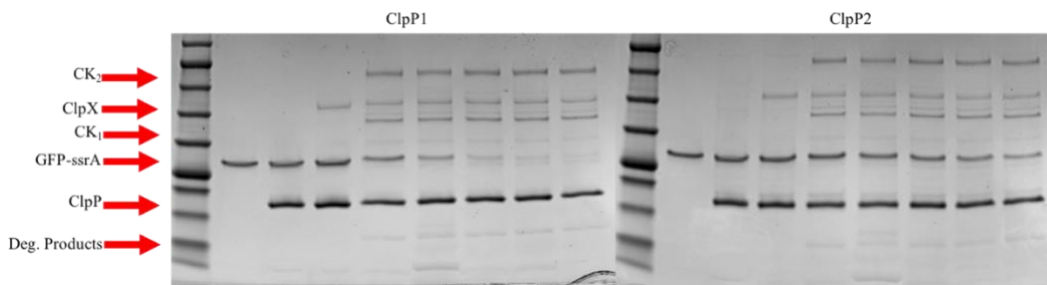
Lane	Contents
1	**GoldBio BlueStain Protein Marker**
2	**ssrA-GFP**
3	**ssrA-GFP + ClpP**
4	**ssrA-GFP, ClpP, ClpX, no ATP 5 h**
5	**ssrA-GFP, ClpP, ClpX, + 4 mM ATP 1 h**
6	**ssrA-GFP, ClpP, ClpX, + 4 mM ATP 2 h**
7	**ssrA-GFP, ClpP, ClpX, + 4 mM ATP 3 h**
8	**ssrA-GFP, ClpP, ClpX, + 4 mM ATP 4 h**
9	**ssrA-GFP, ClpP, ClpX, + 4 mM ATP 5 h**

Figure A.8 SDS-PAGE visualization of ssrA-GFP degradation over time via ClpXP in the presence of 4 mM ATP.
Individual lane assignments are the same between both ClpP1 and ClpP2 SDS-PAGE gels, as listed in the table above.
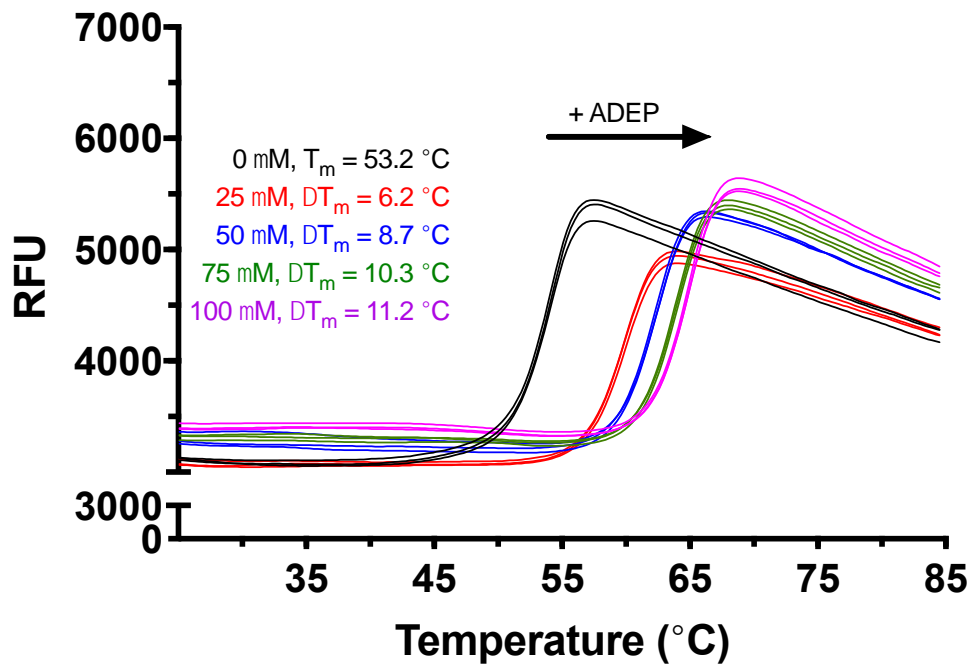
Figure A.9 Raw data replicates of ClpP1 + ADEP thermal shift experiments.
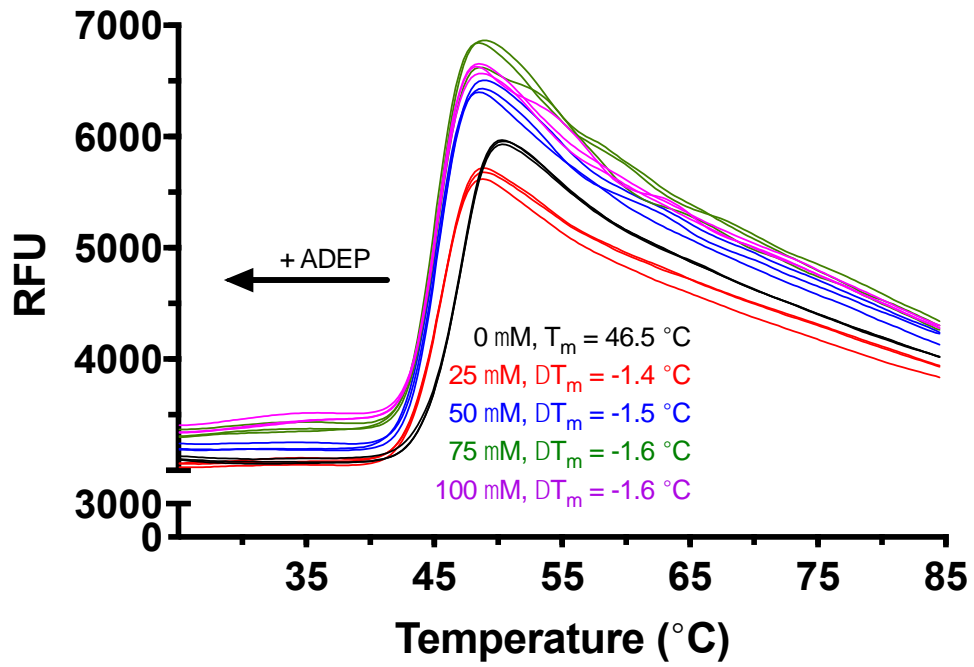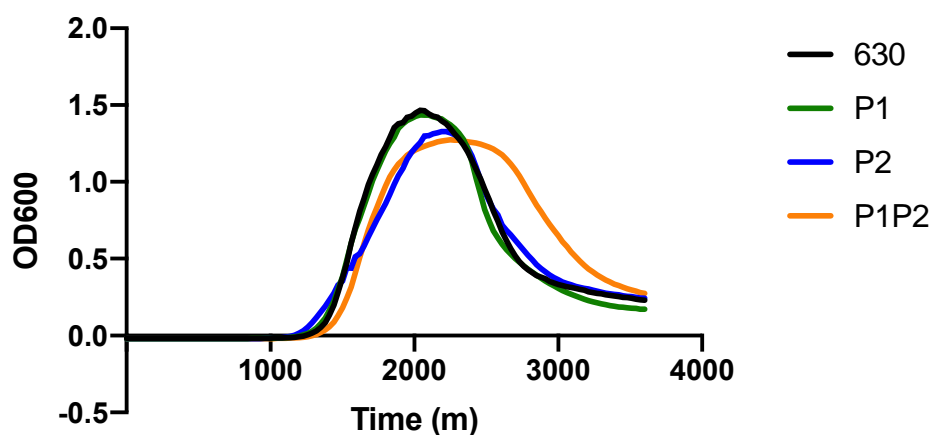
Figure A.10 Raw data replicates of ClpP2 + ADEP thermal shift experiments.

Appendix B: Phenotypic Response from the Loss of ClpP Function in

Clostridium difficile

37C GC MM

42C Minimal Media
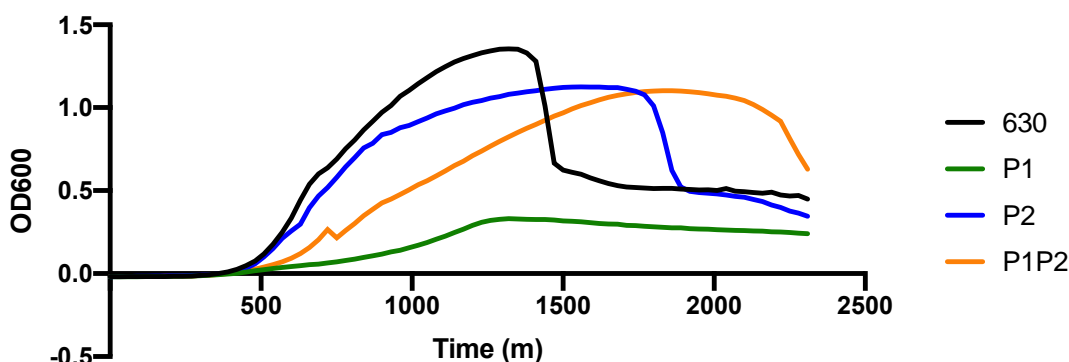
Figure B.1 All *C. difficile* strains grown anaerobically in minimal defined media supplemented with glucose at 37 ºC and 42 ºC.
Minimal defined media was used in order to assay potential differences in nutrient response regulation. Clear differences emerge under heat-shock conditions, where ΔP1 and ΔP2 differ from the WT in significant ways. ΔP1P2 appears to grow while ΔP1 mutants appears to be unable to grow. This suggests that ClpP1 may function to directly or indirectly regulate a nutrient response regulator, while it is less obvious if ClpP2 plays an important role in regulation and nutrient response regulator.

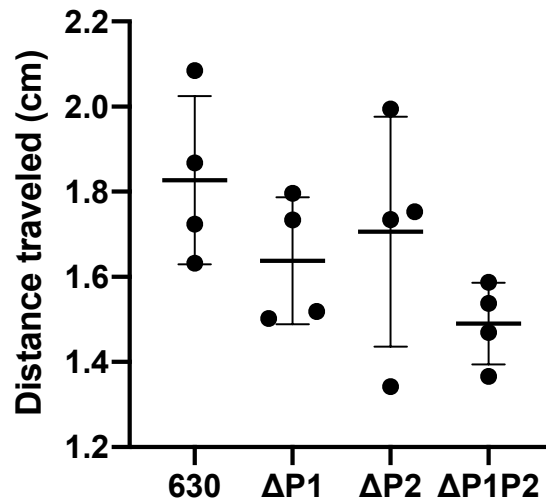## Distance traveled in 50% BHIS after 72h

Figure B.2 Motility assays were performed in 50% BHIS media (0.3% agar)
Motility was not significantly reduced in any of the knockout mutants. Statistical significance was assessed via One-way RM ANOVA using Dunnet's test to correct for multiple comparisons.
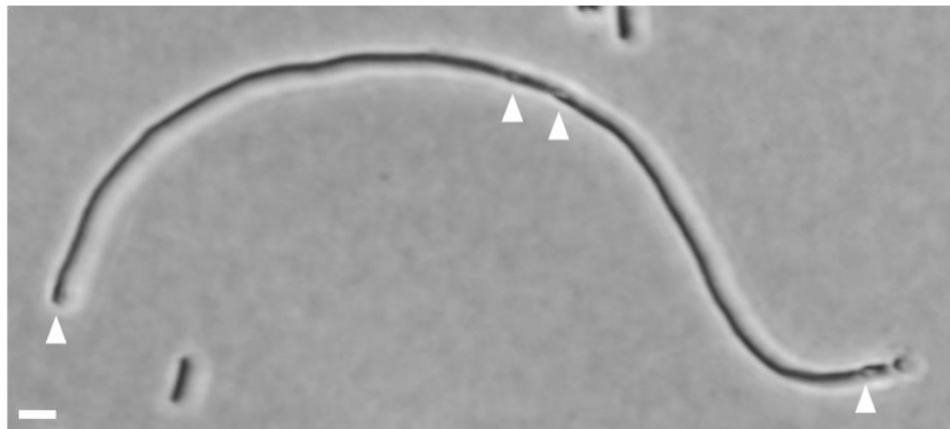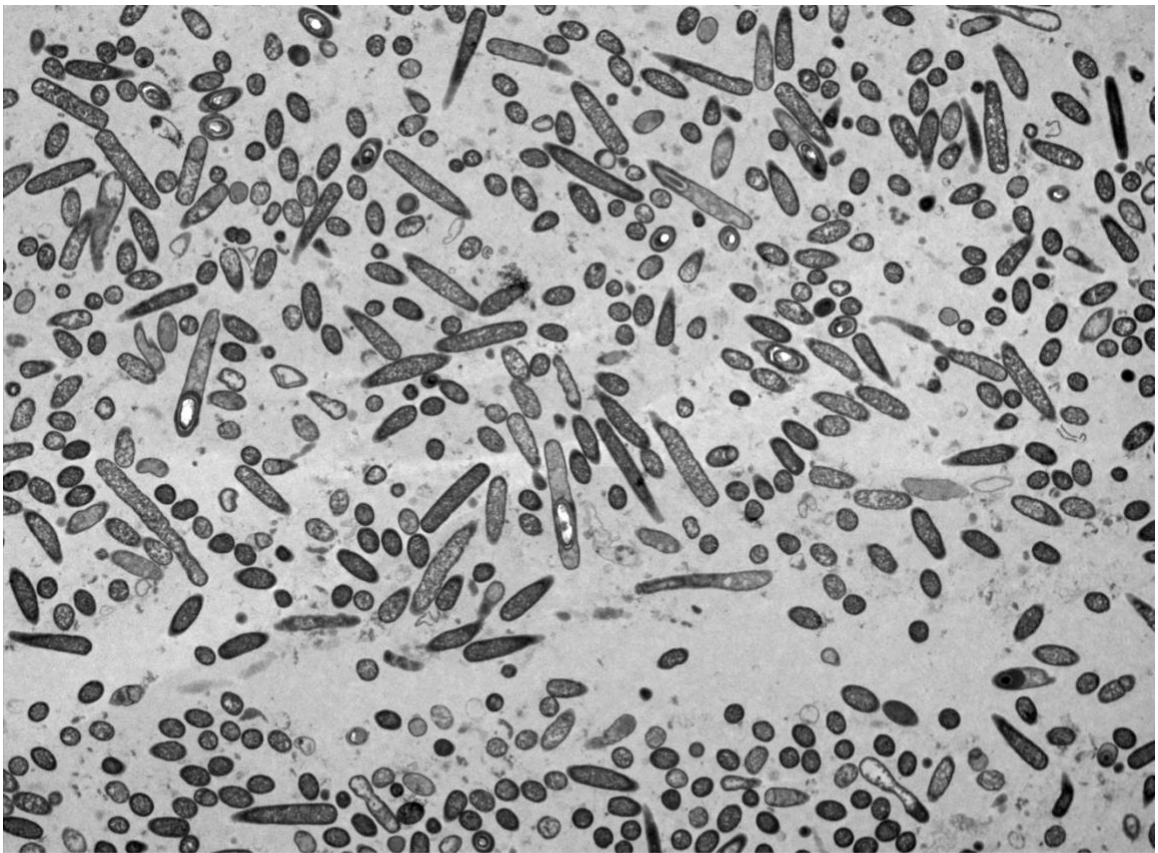

Figure B.3 Bright field microscopy of elongated ΔP1P2 cell phenotype
harvested from BHIS cultures and immobilized on 1% agarose pads, observed via 100x oil-immersion under a Ph3 filter. White arrows denote apparent phase-bright spores. Scale bar represents 5 µm.
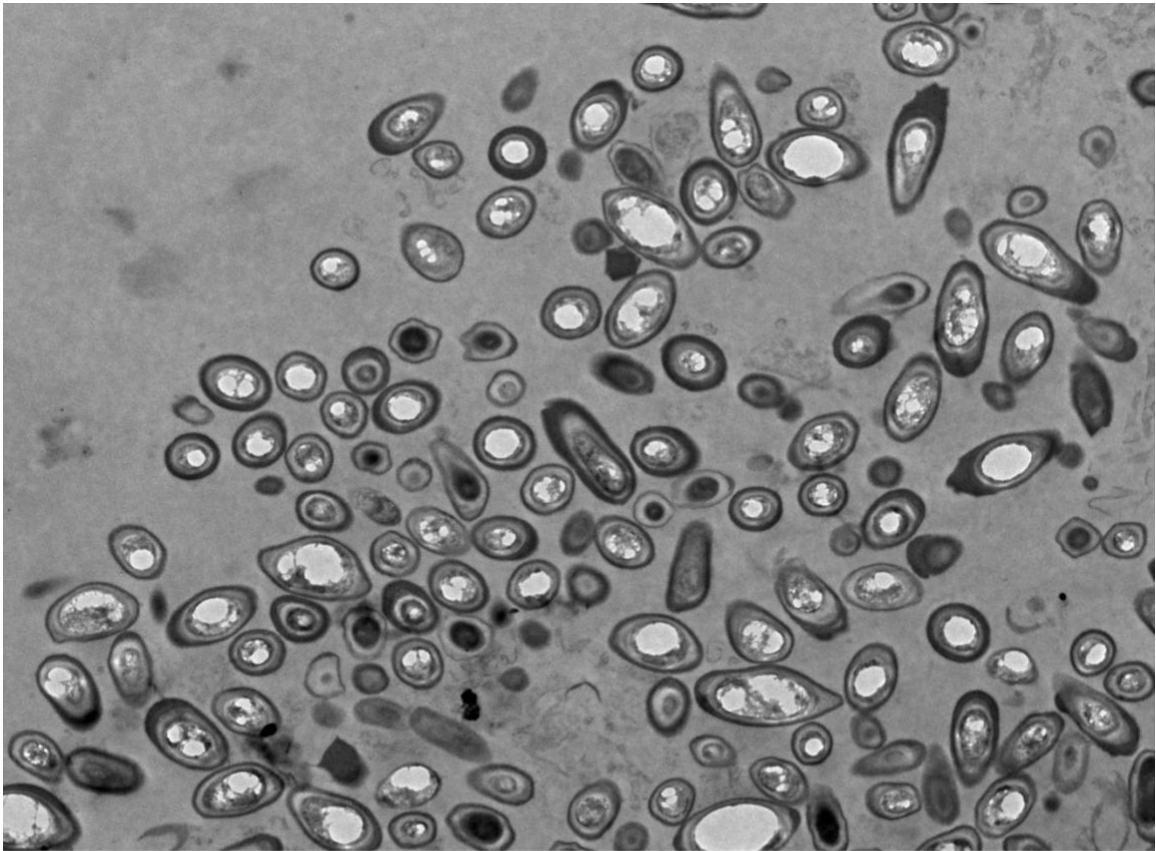
9A_630_1.tif
Cal: 0.011204 µm/pix
13:54 1/17/2019

4 µm
HV=80kV
Direct Mag: 500 x
Oklahoma Medical Research Facility

Camera: NANOSPRT12, Exposure: 800 (ms) x 4 drift frames, Gain: 1, Bin: 1
Gamma: 1.00, No Sharpening, Normal Contrast

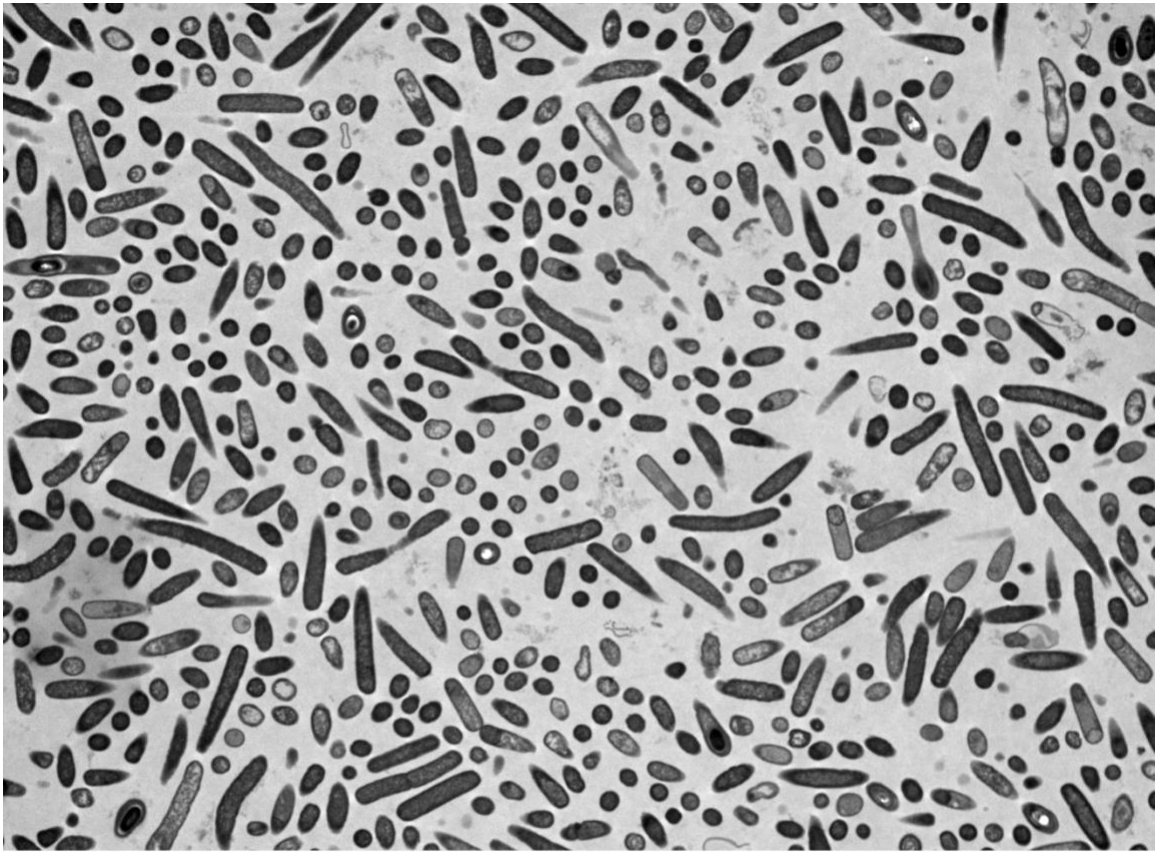**Figure B.4 TEM overview image of WT harvested from 70:30 plate media**

630_13A_1.tif
Cal: 0.004599 µm/pix
13:57 3/13/2019

2 µm
HV=80kV
Direct Mag: 1200 x
Oklahoma Medical Research Facility

Camera: NANOSPRT12, Exposure: 800 (ms) x 4 drift frames, Gain: 1, Bin: 1
Gamma: 1.00, No Sharpening, Normal Contrast

Figure B.5 TEM overview image of purified WT spores harvested from 70:30 plate media

5B_P1_01.tif
Cal: 0.011204 µm/pix
13:03 1/18/2019

4 µm

HV=80kV
Direct Mag: 500 x
Oklahoma Medical Research Facility

Camera: NANOSPRT12, Exposure: 800 (ms) x 4 drift frames, Gain: 1, Bin: 1
Gamma: 1.00, No Sharpening, Normal Contrast

Figure B.6 TEM overview image of ΔP1 harvested from 70:30 plate media

P1_17A_01.tif
Cal: 0.004599 µm/pix
15:20 3/13/2019

2 µm
HV=80kV
Direct Mag: 1200 x
Oklahoma Medical Research Facility

Camera: NANOSPRT12, Exposure: 800 (ms) x 4 drift frames, Gain: 1, Bin: 1
Gamma: 1.00, No Sharpening, Normal Contrast

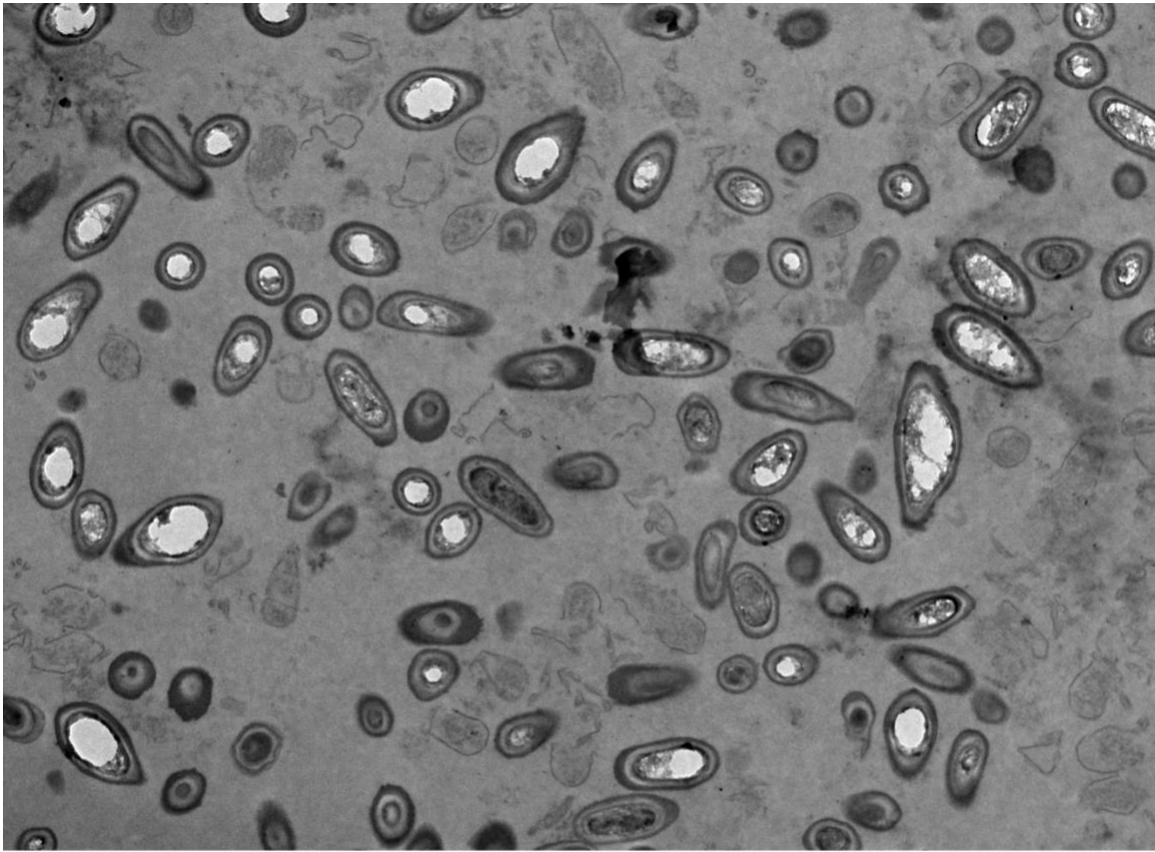**Figure B.7 TEM overview image of purified ΔP1 spores harvested from 70:30 plate media**

7A_P2_01.tif
Cal: 0.005472 µm/pix
10:15 1/18/2019

2 µm
HV=80kV
Direct Mag: 1000 x
Oklahoma Medical Research Facility

Camera: NANOSPRT12, Exposure: 800 (ms) x 4 std. frames, Gain: 1, Bin: 1
Gamma: 1.00, No Sharpening, Normal Contrast

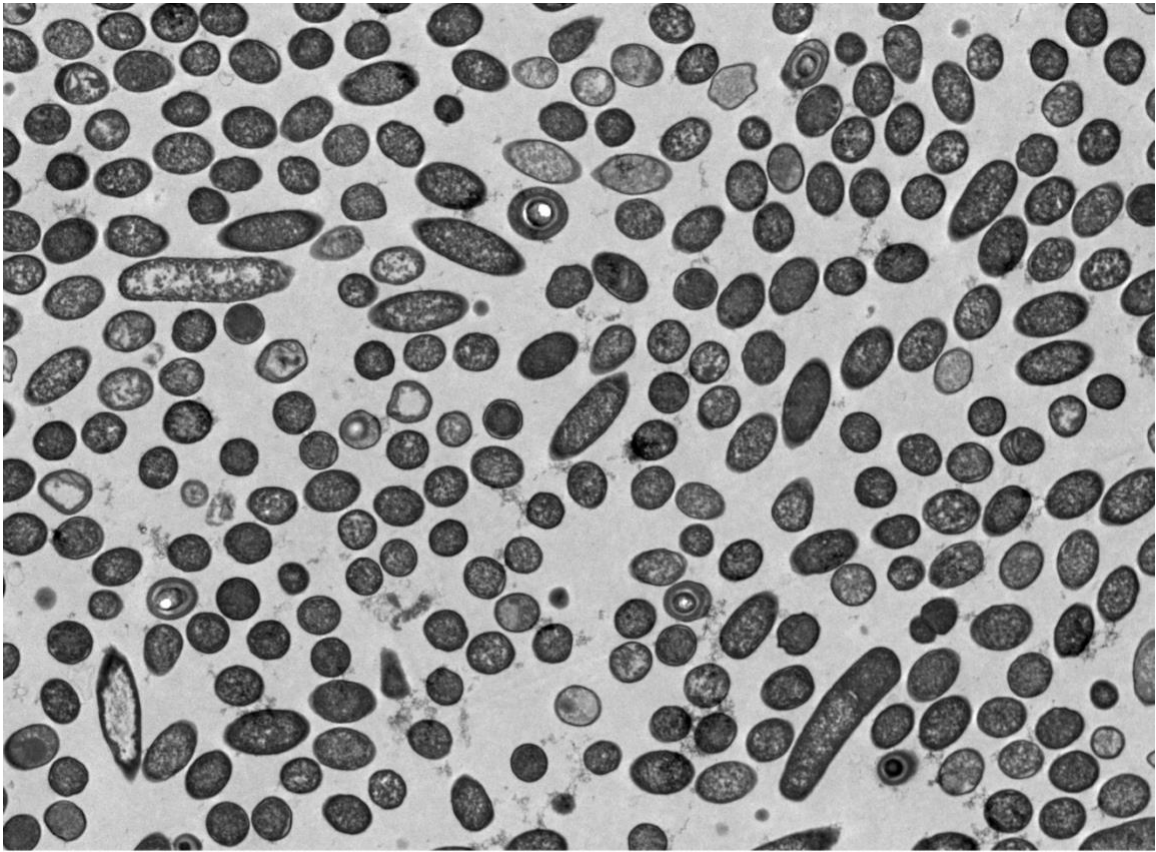**Figure B.8 TEM overview image of ΔP2 harvested from 70:30 plate media**

P2_19A_05.tif
Cal: 0.003390 μm/pix
16:32 3/13/2019

1 μm
HV=80kV
Direct Mag: 1500 x
Oklahoma Medical Research Facility

Camera: NANOSPRT12, Exposure: 800 (ms) x 4 drift frames, Gain: 1, Bin: 1
Gamma: 1.00, No Sharpening, Normal Contrast

Figure B.9 TEM overview image of purified ΔP2 spores harvested from 70:30 plate media
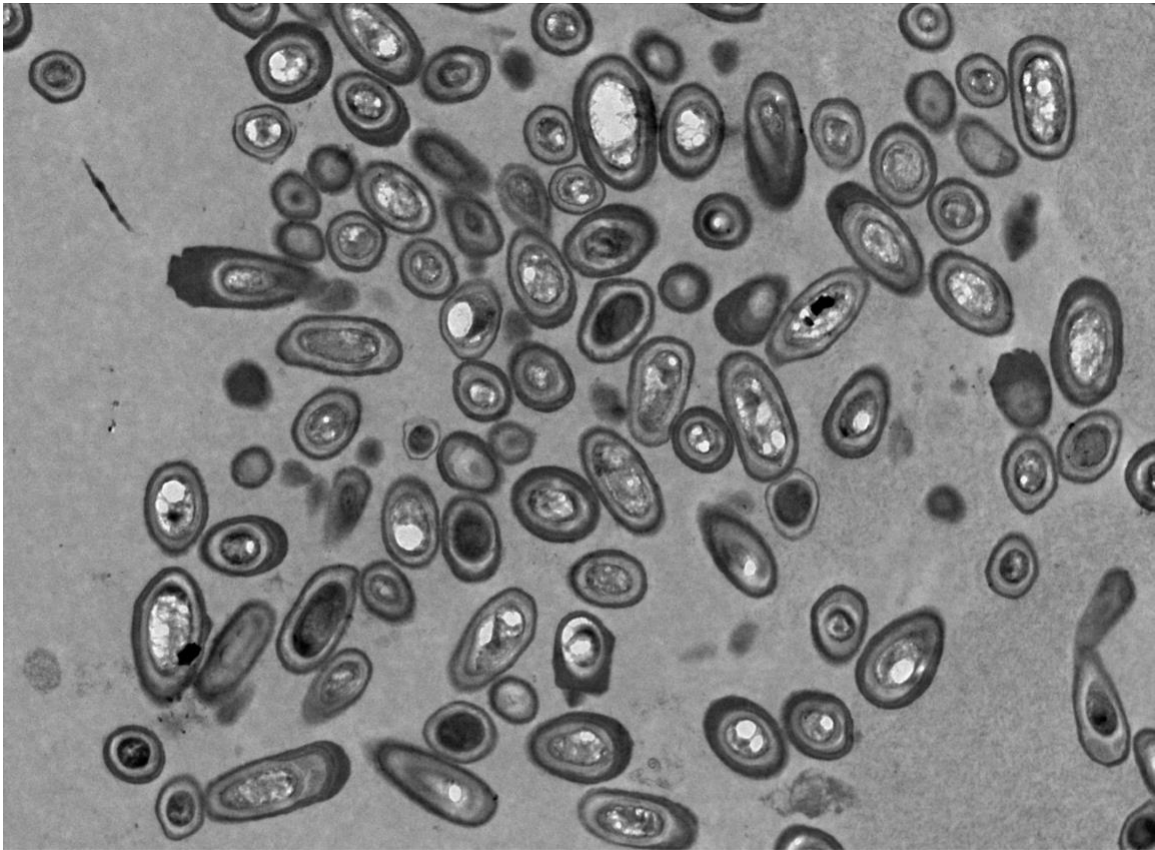
11A_P1P2_06.tif
Cal: 0.011204 µm/pix
12:06 1/18/2019

4 µm
HV=80kV
Direct Mag: 500 x
Oklahoma Medical Research Facility

Camera: NANOSPRT12, Exposure: 800 (ms) x 4 drift frames, Gain: 1, Bin: 1
Gamma: 1.00, No Sharpening, Normal Contrast

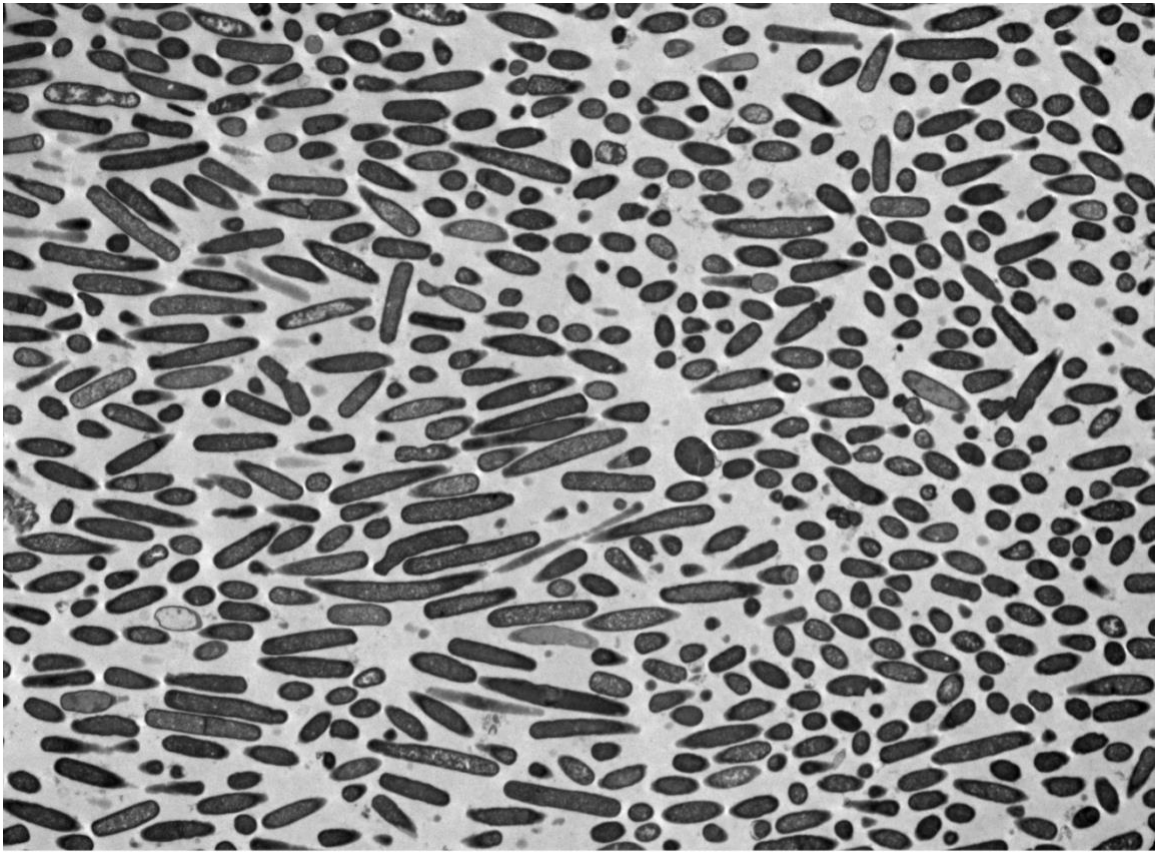**Figure B.10 TEM overview image of ΔP1P2 harvested from 70:30 plate media**

P1P2_15A_02.tif
Cal: 0.008003 µm/pix
14:34 3/14/2019

4 µm
HV=80kV
Direct Mag: 700 x
Oklahoma Medical Research Facility

Camera: NANOSPRT12, Exposure: 800 (ms) x 4 drift frames, Gain: 1, Bin: 1
Gamma: 1.00, No Sharpening, Normal Contrast

Figure B.11 TEM overview image of purified ΔP1P2 spores harvested from 70:30 plate media
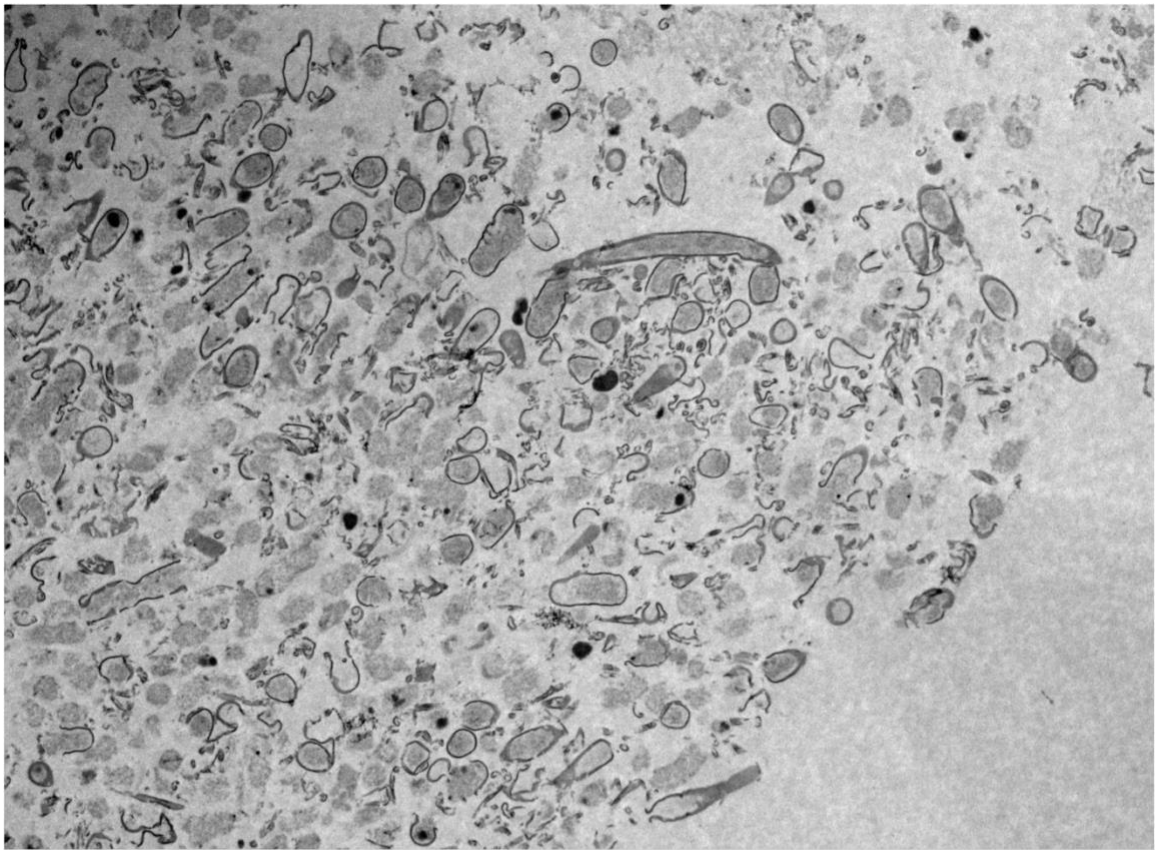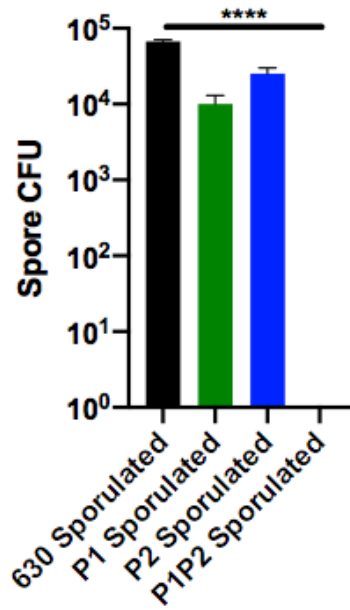
Figure B.12 Spore production is significantly lower in BHIS liquid media for all mutants with comparison to WT after 2 days
Spores were enumerated with BHIS media + 0.1% taurocholate plate media post 70 °C heat shock for 30 min. Plates were grown for at least 24h prior to colony counts.
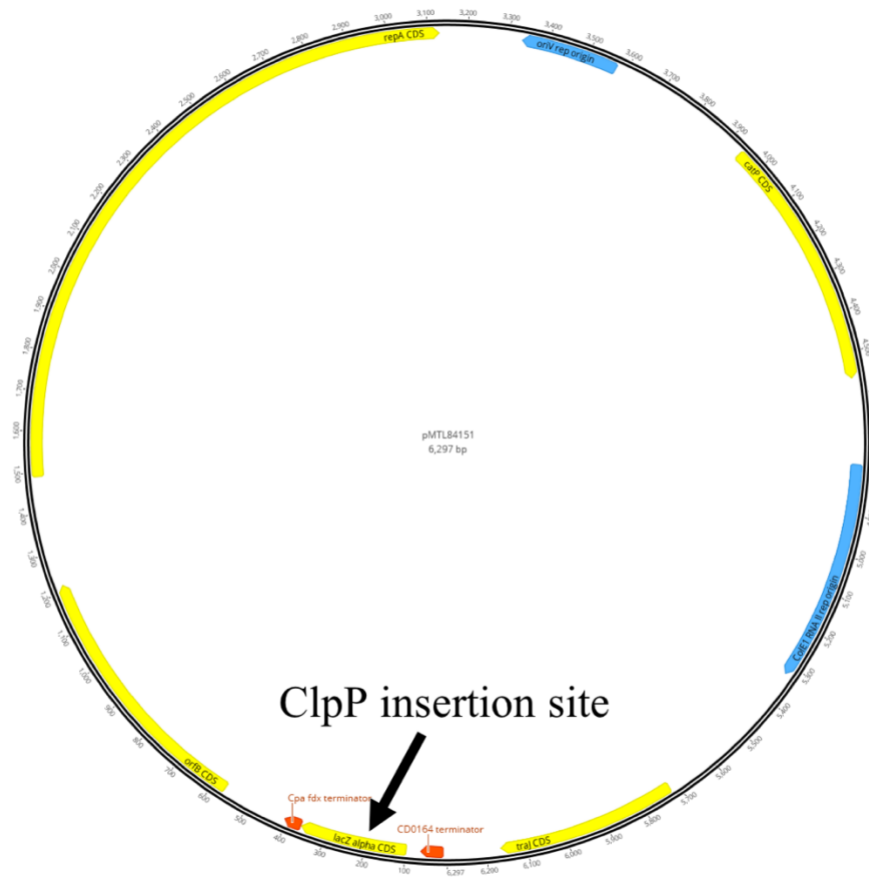
Figure B.13 pMTL84151 plasmid map

The plasmid map for pMTL84151 that was used to create *clpP* mutants using CRISPR/Cas9 mutagenesis. Each *clpP1* and *clpP2* were separately inserted into the *lacZ* operon along with 100 bp upstream from the *clpP* gene. The native expression of each ClpP isoform was used to complement the single mutants.

Appendix C: The Structure of ClpP1 from *Clostridium difficile*

| Condition	Time To Crystallize (days)	Morphology
ClpP1		
0.1M Tris-base pH 8.5, 2.0M ammonium sulfate	2	small plates
0.1M sodium acetate pH 4.5, 2.0M sodium chloride	4	needles
0.1M Tris-base pH 8.5, 2.0M ammonium sulfate	2	small plates
0.1M HEPES pH 7.5, 1.4M tri-sodium citrate	1	large plates/cubes
0.1M HEPES pH 7.5, 1.4M tri-sodium citrate	1	large plates/cubes
0.2M ammonium acetate, 0.1M Bis-tris pH 5.5, 45% v/v MPD	>21	large plates/cubes
0.2M ammonium acetate, 0.1M Bis-tris pH 6.5, 45% v/v MPD	>28	large plates/cubes
0.2M ammonium acetate, 0.1M Bis-tris pH 6.5, 45% v/v MPD	>28	large plates/cubes
0.2M lithium sulfate, 0.1M Tris-base pH 8.5, 25% w/v PEG 3350	>35	small plates
0.16M MgCl2, 24% w/v PEG 4k, 0.08M Tris pH 8.5, 20% w/v glycerol	4	small plates
0.16M MgCl2, 24% w/v PEG 4k, 0.08M Tris pH 8.5, 20% w/v glycerol	4	medium plates
0.2M potassium sulfate, 20% w/v PEG 3350	8	small cubes
2.0M ammonium sulfate 0.1M HEPES pH 7.5	1	small rectangular plates
0.2M sodium formate pH 7.3, 20% w/v PEG 3350	14	small cubes
0.2M lithium chloride, 20% w/v PEG 3350	14	small cubes
60% v/v Tacsimate pH 7.0	>30	large plates/cubes
0.2M sodium fluoride, 20% w/v PEG 3350	>21	small cubes
1.4M di-ammonium tartrate, 0.1M Tris pH 8.5	1	large plates/cubes
2.8M sodium acetate pH 7.0	1	small cubes
0.2M lithium sulfate, 2.0M ammonium sulfate, 0.1M CAPS	1	small plates
2.8M sodium acetate pH 7.0	1	small cubes
0.2M lithium citrate, 20% w/v PEG 3350	1	small rectangular plates
ClpP2		
0.1M HEPES pH 7.5, 1.4 tri-sodium citrate	1	small cubes
2.1M Malic acid, pH 7.0	1	small plates
2.4M sodium malonate, pH 7.0	1	small plates
0.1M Bis-tris pH 6.5, 28% w/v PEG MME 2k	>30	small plates
0.1M HEPES pH 7.5, 25% w/v PEG 3350	>30	small plates
0.2M ammonium sulfate, 0.1M Bis-tris pH 6.5, 25% w/v PEG 3350	>14	small plates

0.2M sodium chloride, 0.1M Tris-base pH 8.5, 25% w/v PEG 3350	10	small hexagonal plates
0.2M lithium sulfate, 0.1M HEPES pH 7.5, 25% w/v PEG 3350	>21	small plates
0.2M sodium formate, 20% w/v PEG 3350	>28	large cylinders
0.1M potassium thiocyanate, 30% w/v PEG MME 2k	>21	large rectangle
0.15M potassium bromide, 30% w/v PEG MME 2k	>37	large rectangle
0.1M Bis-tris pH 6.5, 28% w/v PEG MME 2k	>12	small cylinders
0.1M Bis-tris pH 6.5, 25% PEG 3350	>28	small cylinders
0.2M sodium thiocyanate pH 6.9, 20% w/v PEG 3350	>21	large cylinders
0.2M $MgCl_2$, 30% v/v PEG 400, 0.1M Tris pH 8.5	4	medium plates
0.2M sodium thiocyanate pH 6.9, 20% w/v PEG 3350	>21	cylinders/plates/cubes
0.2M potassium sulfate, 20% w/v PEG 3350	>28	small cubes
2.4M sodium malonate pH 7.0	1	small cubes
0.2M di-ammonium hydrogen citrate pH 5.0, 20% w/v PEG 3350	4	needles
0.2M potassium iodide, 20% w/v PEG 3350	>28	medium cubes

Table C.1 Crystallization conditions for ClpP1 and ClpP2

Wavelength	0.98 Å
Resolution range	34.06 - 2.498 (2.587 - 2.498)
Space group	P 1
Unit cell	97.328 97.372 106.494 113.149 104.562 103.213
Total reflections	460673 (45316)
Unique reflections	109963 (10507)
Multiplicity	4.2 (4.3)
Completeness (%)	98.01 (94.19)
Mean I/sigma(I)	5.46 (1.79)
Wilson B_{Factor}	27.6
R_{merge}	0.2181 (0.5619)
R_{meas}	0.2484 (0.6379)
R_{pim}	0.1176 (0.2989)
$CC^{1/2}$	0.935 (0.715)
CC^*	0.983 (0.913)
Reflections used in refinement	109922 (10505)
Reflections used for R_{Free}	5435 (523)
R_{Work}	0.1917 (0.2305)
R_{Free}	0.2436 (0.3085)
CC_{Work}	0.944 (0.849)

CC$_{Free}$	0.925 (0.712)
Number of non-hydrogen atoms	20431
macromolecules	19627
ligands	23
solvent	781
Protein residues	2551
RMS(bonds)	0.003
RMS(angles)	0.48
Ramachandran favored (%)	96.95
Ramachandran allowed (%)	3.05
Ramachandran outliers (%)	0
Rotamer outliers (%)	0
Clashscore	3.85
Average B-factor (Å^2)	30.54
macromolecules	30.54
ligands	29.25
solvent	30.56

Table C.2 The data collection and refinement statistics for the crystal structure of ClpP1